Characterization and Modeling of Natural-Fibres-Reinforced composites (Moisture Absorption Kinetics, Monotonic Behaviour and Cyclic Behaviour)

by

Ahmed Fotouh

A thesis submitted in partial fulfillment of the requirements for the degree of

Doctor of Philosophy

Department of Mechanical Engineering
University of Alberta

ABSTRACT

Natural fibres have been shown to offer a good potential in replacing or supplementing synthetic fibres in composite material applications. To fully utilize these new materials in design, however, engineering models of the mechanical behaviour need to be developed and validated. In this research, the moisture absorption and mechanical behaviour of hemp-fibre-reinforced polyethylene composites at various fibre volume fractions were investigated and modelled. In terms of environmental exposure, the effects of fibre volume fraction (v_f) and matrix crystallinity along with matrix stiffness and contraction on the mechanisms of moisture sorption were investigated. The maximum amount of absorbed moisture (M_{tmax}) was determined for each fibre volume fraction. The composite diffusion coefficient (D) was measured to distinguish the ability of water molecules to diffuse into the biocomposite. The increase in the matrix crystallinity level in addition v_f of the tested composites increased the moisture absorption rate. Fickian diffusion was found to be the dominant moisture diffusion behaviour. The stress-strain behaviour of the hemp fibre composites were analyzed and modelled for both monotonic (rate dependent) and cyclic loading conditions. An exponential model was developed to simulate the monotonic stress-strain uniaxial behaviour. A strain rate hardening detected and a model was developed by applying the nonlinear form of Norton-Hoff rheology model for viscoplastic material to simulate the relationship between the strain rate ($\dot{\varepsilon}$) and each mechanical property of the tested composites. The strain rate hardening model was later incorporated with an exponential model to develop a new general

stress-strain model to simulate the monotonic tensile behaviour of the tested natural-fiber-reinforced composites. The developed new model took into account the effect of $\dot{\varepsilon}$ and v_f of the composite as well as the effect of moisture absorption. Fatigue tests were also performed at two fibre volume fractions as well as the reinforced polymer under both wet and dry conditions. The fatigue strength of the polymer was slightly improved by addition of hemp fibers; though, the sensitivity of the developed fatigue life curves did not change. A generalized model was developed using the normalized fatigue life diagrams. These diagrams were normalized by a new developed modified stress level (S_m). The previously developed strain rate hardening model was then incorporated into the fatigue model to capture the effect of the changes in the loading rate. The new fatigue model was capable of predicting the fatigue life at different frequencies (f), fatigue stress ratios (R), fatigue stress amplitudes ($\Delta\sigma$) and v_f. Additionally, the fatigue model succeeded to simulate the degradation effect of moisture absorption on the fatigue strength. The new developed models provide essential tools for designers to incorporate this new material into a new generation of reliable products.

PREFACE

This work was funded by the Government of Alberta through the Unleashing Innovation Program (project IP-07-002-UI).

Chapter 2 is a modified version of a paper that was published as Ahmed Fotouh, J. D. Wolodko, M. Lipsett, "A Review of Aspects Affecting Performance and Modeling of Short-Natural-Fiber-Reinforced Polymers under Monotonic and Cyclic Loading Conditions", Journal of Polymer Composites, Mar. 06th, 2014, DOI: 10.1002/pc.22955. I was responsible for the concept formation and the data collection and analysis as well as the manuscript composition. Dr. J. D. Wolodko and Dr. M. Lipsett were the supervisory authors and were involved with manuscript revision.

Chapter 3 is a modified version of a paper that was published as Ahmed Fotouh, J. D. Wolodko, M. Lipsett, "Isotherm Moisture Absorption Kinetics in Natural-Fiber-Reinforced Polymer under Immersion Conditions", Journal of Material Composites, May 15th, 2014, DOI: 10.1177/0021998314533366. I was responsible for the concept formation and the data collection and analysis as well as the manuscript composition. Dr. J. D. Wolodko and Dr. M. Lipsett were the supervisory authors and were involved with manuscript revision.

Chapter 4 is a modified version of a paper that was published as Ahmed Fotouh, J. D. Wolodko, M. Lipsett, "Characterization and Modeling of Strain Rate Hardening in Natural-Fiber-Reinforced Viscoplastic Polymer", Journal of Polymer Composites, Feb. 06th, 2014, DOI: 10.1002/pc.22894. I was responsible for the concept formation and the data collection and analysis as well as the manuscript composition. Dr. J. D. Wolodko and Dr. M. Lipsett were the supervisory authors and were involved with manuscript revision.

Chapter 5 is a modified version of a paper that was published as Ahmed Fotouh, J. D. Wolodko, M. Lipsett, "Uniaxial Tensile Behaviour Modeling of Natural-Fiber-

Reinforced Viscoplastic Polymer Using Normalize Stress-Strain Curves", Journal of Material Composites , Aug. 21st, 2014, DOI: 10.1177/0021998314547427. I was responsible for the concept formation and the data collection and analysis as well as the manuscript composition. Dr. J. D. Wolodko and Dr. M. Lipsett were the supervisory authors and were involved with manuscript revision.

Chapter 6 is a modified version of a paper that was published as Ahmed Fotouh, J. D. Wolodko, M. Lipsett, "Fatigue of Natural Fiber Thermoplastic Composites", Journal of Composites Part B: Engineering, Vol. 62, pp. 175-192, Jun. 20th, 2014. I was responsible for the concept formation and the data collection and analysis as well as the manuscript composition. Dr. J. D. Wolodko and Dr. M. Lipsett were the supervisory authors and were involved with manuscript revision.

ACKNOWLEDGEMENTS

First, I want to thank God for providing me with the strength and the knowledge light that I needed to finish this work.

I would like to express my deepest gratitude and sincere appreciation to my supervisors, Dr. John Wolodko and Dr. Michael Lipsett, for their guidance and continuous support throughout all stages of this research. Thanks are also due to Dr. Kirill Alameskin, Ron Rau and Lisa Sopkow at AITF for the help that they provided during this work.

I would like to express my great thanks to my father, Mohamed and my mother, Nagat, for their continuous support and unconditional love. Great thanks to my wonderful wife, Mona; I want to thank her for her encouragement and support all the way through this study, and I devote this work for her.

CONTENTS

LIST OF TABLES

LIST OF FIGURES

CHAPTER 1: INTRODUCTION

1.1 RESEARCH MOTIVATION

The demand for Natural Fibre Reinforced Polymers (NFRPs) has increased rapidly in the last few years in applications such as interior parts for automobiles, packaging, and construction industries [1, 2]. This growing demand is based on the fact that natural fibres have many advantages over synthetic fibres [1, 3, 4] :

1. Low density with reasonable mechanical properties;
2. Environmental benefits (sustainable, lower inherent energy to produce);
3. Lower cost;
4. Health benefits (less harmful to workers), and less wear to manufacturing equipment than glass fibres.

While natural fibre composites offer a number of benefits, full utilization in industrial applications is still limited due to a lack of an established supply chain, standardization, and available test data for a variety of composite formulations.

1.2 RESEARCH OBJECTIVE AND APPROACH

This study focuses on experimentally characterizing the tensile monotonic and fatigue behaviour of biocomposite materials. Additionally, as natural fibres are hydrophilic in nature, the sorption and diffusion mechanisms were experimentally investigated and modeled to provide a better understanding of the monotonic and cyclic behaviour of NFRPs under wet conditions. In addition, this study also models the monotonic and cyclic loading behaviour of these NFRPs. The proposed models capture the failure of short NFRPs under monotonic and cyclic loading using the minimum number of destructive tests to calculate the models' parameters. Therefore, this research aims to develop mechanical behaviour models that form an engineering tool in which new products of NFRPs can be designed for reliable service. To achieve this goal, three elements are integrated in this research to study and model the mechanical behaviour of

NFRPs: 1) hydrophilic nature and absorption mechanism; 2) monotonic behaviour and strain rate effect; and 3) cyclic behaviour. (see Figure 1.1). The following approach was proposed to develop the research based models:

1. Review the literature to better understand the monotonic and cyclic behaviour of NFRPs and the methods that might be suited to model this behaviour.

2. Perform isotherm sorption tests to understand the kinetics of water sorption for natural fibre reinforced polymers;

3. Perform monotonic and cyclic tests to investigate the mechanical behaviour of the tested composites;

4. Develop constitutive models to simulate the monotonic and cyclic behaviour of NFRPs. This includes the following steps:
    - Develop an exponential model to represent the monotonic behaviour of unreinforced polymer matrix and NFRPs, based on the monotonic tests analysis;
    - Introduce the effect of fibre volume fraction in the monotonic exponential model;
    - Investigate and introduce the effect of strain rate in the model;
    - Use mechanistic models to simulate the relation between developed monotonic and cyclic models' parameters and fibre volume fractions. Additionally, other mechanistic models will be used to simulate some of the mechanisms of NFRPs behaviour under cyclic loading;
    - Combine the provided mechanistic models with an analytical solution in order to predict NFRPs monotonic cyclic behaviour;
    - Introduce the effect of fatigue stress ratio (R) in the developed fatigue model. Furthermore, the effect of approximated strain rate,

corresponding to the fatigue load ramping, will also be taken into consideration;

- Introduce the effect of moisture degradation to the developed monotonic and cyclic models by adding a moisture effect parameter via other sets of experiments.

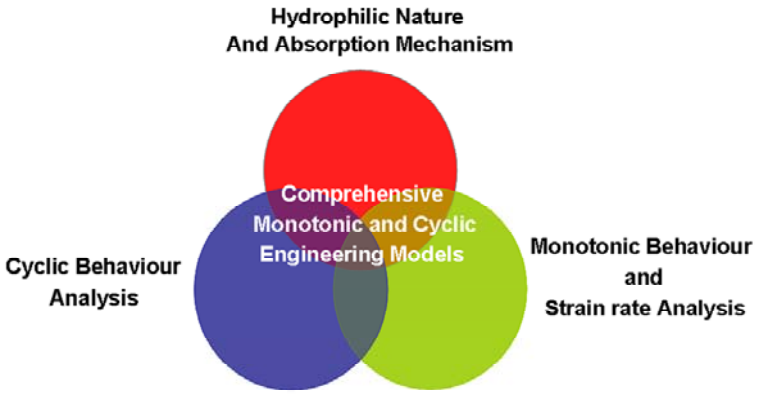

Fig. 1.1 Schematic Diagram represents the three elements forming this research to develop comprehensive monotonic and cyclic models.

1.3 THESIS ORGANIZATION

In addition to the introduction and conclusions chapters, six other chapters are included in this study. Chapter 2, A Review of Aspects Affecting Performance and Modeling of Short-Natural-Fiber-Reinforced Polymers Under Monotonic and Cyclic Loading, discusses 4 main aspects related to NFRPs: 1) effect of the hydrophilic nature of natural fibers on the mechanical behaviour of NFRPs; 2) effect of manufacturing and processing parameters on the mechanical behaviour of short NFRPs; 3) monotonic behaviour of short NFRP and its modeling; 4) cyclic behaviour of short NFRP and its modeling. From Chapter 2, it was found that statistical and empirical modeling techniques are highly suited to model the complex mechanical behaviour of NFRPs; therefore, semi-analytical modeling techniques were developed in this study to incorporate different mechanistic models into analytical techniques to best model both monotonic and cyclic

behaviour of NFRPs. Chapter 3, Isotherm Moisture Absorption Kinetics in Natural-Fiber-Reinforced Polymer under Immersion Conditions, investigates the kinetics of moisture sorption of NFRPs under immersion conditions to provide a better the understanding of water and moisture sorption behaviour of NFRPs; additionally, the matrix stiffness and its contraction effect are investigated, and the NFRPs diffusivity is evaluated and modeled to characterize the ability of liquid molecules to diffuse into these composite at different hemp fiber volume fractions. Chapter 4, Characterization and Modeling of Strain Rate Hardening in Natural-Fiber-Reinforced Viscoplastic Polymer, investigates and models the effect of strain rate ($\dot{\varepsilon}$) on the mechanical properties of short NFRPs at different fiber volume fractions (v_f). Chapter 5, Uniaxial Tensile Behaviour Modeling of Natural-Fiber-Reinforced Viscoplastic Polymer Based on Normalized Stress-Strain Curves, develops a semi-analytical monotonic model for short NFRP based on a better understanding of monotonic behaviour mechanism and the effect of $\dot{\varepsilon}$ on the mechanical properties of the tested composites. Chapter 6, Fatigue of Natural Fiber Thermoplastic Composites, investigates the fatigue behavior of NFRPs using fatigue-life (S-N) curves at different fiber volume fractions, and develops a fatigue life model that is capable of predicting the fatigue behaviour of short NFRPs at different fiber fractions and fatigue stress ratios under dry and wet conditions.

CHAPTER 2: A REVIEW OF ASPECTS AFFECTING PERFORMANCE AND MODELING OF SHORT-NATURAL-FIBER-REINFORCED POLYMERS UNDER MONOTONIC AND CYCLIC LOADING CONDITIONS*

ABSTRACT

The use of short natural fibers as reinforcing fibers was hampered by uncertainties associated with the performance of these developed short-fiber-reinforced composites. Much of this uncertainty comes from an unclear understanding of different aspects controlling the properties and the behaviour of natural fibers and their developed composites. This study provides a benchmark review that highlights several factors affecting the performance of Short-Natural-Fiber-Reinforced Polymers (SNFRPs). Additionally, the study also reviews the research related to the short term (monotonic) and the long-term (cyclic) behaviour as well as the potential monotonic and life prediction models and techniques suited for SNFRPs.

---

* This is a modified version of a paper that was published as Ahmed Fotouh, J. D. Wolodko, M. Lipsett, "A Review of Aspects Affecting Performance and Modeling of Short-Natural-Fiber-Reinforced Polymers under Monotonic and Cyclic Loading Conditions", Journal of Polymer Composites, Mar. 06th, 2014, DOI: 10.1002/pc.22955.

KEYWORDS

Reinforced Polymers, Short Natural Fibers, Manufacturing and processing effects, Mechanical behavior, Modeling and life prediction.

2.1 INTRODUCTION

The demand for the use of natural-fiber-reinforced polymers (thermoset and thermoplastic) has been increasing rapidly [1]. Applications of these composites include variety of interior parts for automobiles, packaging, and components used in the aerospace and construction industries [1, 2]. Compared to synthetic fibers (e.g. glass fibers, one of the most important synthetic fibers), natural fibers provide many features:

1. They feature a low density and acceptable mechanical properties (see Table 2.1); hence, there will be lower fuel consumption if the natural fiber composite is used for parts in the aerospace and automobile industries.
2. They are an economical and sustainable source of fibers, rendering the composite product toward being an ecological and, most likely, a biodegradable material, depending on the matrix [1, 3].
3. They are easier to manufacture with lower production energy use; for example, the energy needed to produce 1 Kg of flax-fiber mats is about 9.55MJ/Kg, which is 83% less than the energy needed to produce 1 Kg of glass-fiber mats [1].
4. They offer less abrasive wear to the processing machine parts [4].
5. They avoid many of the health and ecological problems caused by synthetic fibers, such as the hazard of small particles emitted during manufacturing, skin irritation, renewability and recyclability [1, 4, 5].

Natural fibers can be divided into two main categories [6, 7]: 1) longitudinal fibers (outer/bast fibers); and radial fibers (inner/radial fibers). While the radial fibers are considered compressive load-bearing cells, the outer fibers, which are

longer and have a vertical orientation, are much more capable of withstanding the longitudinal loads (tensile) in their axial direction, [6]. The outer fibers are more commonly used to produce reinforced polymers with a higher longitudinal strength, but this longitudinal strength is reduced by increasing the percentage of the radial fibers in the reinforcing fiber mix [7].

The different types of natural fibers used in natural-fiber-reinforced composites applications can be divided into four main categories [1, 5, 8]:

1. Bast Fibers (e.g. Hemp, Flax, Kenaf…etc.);
2. Cereal straws (e.g. wheat, Triticale,….etc.);
3. Leaf fibers (e.g. Abaca, Sisal …..etc.)
4. Wood.

Most of the natural fibers used in reinforcing polymers are short randomly oriented fibers. These short natural fibers are commonly used over the long natural fibers for the following reasons: 1) most natural fibers are processed from agricultural crops or waste, which are chopped into smaller sizes; and 2) it is much easier to introduce short fibers to an inexpensive technique such as injection molding.

With regard to the mechanical behaviour (monotonic and cyclic) of Short-Natural-Fiber-Reinforced Polymers (SNFRPs), there are few studies investigating these topics, especially the cyclic behaviour. That could be attributed to the level of complexity that is associated with SNFRPs. The lack of studies investigating the monotonic and cyclic behaviour of SNFRPs, and the factors affecting these behaviors, is one of the factors hindering the broader application of these newly developed materials. The current study presents a benchmark review of the aspect affecting the mechanical behaviour of SNFRPs as well as the possible modeling techniques that are suited to model and simulate both monotonic and cyclic behaviours of SNFRPs.

Table 2.1 Mechanical properties of main natural and synthetic fibers [1, 8]:

Fiber	Density (g/cm^3)	Elongation (%)	Tensile strength (MPa)	Elastic Modulus (GPa)
Cotton	1.5-1.6	7.0-8.0	400	5.5-12.6
Jute	1.3	1.5-1.8	393-773	26.5
Flax	1.5	2.7-3.2	500-1,500	27.6
Hemp	147	2.0-4.0	690	70.0
Kenaf	1.45	1.6	930	53.0
Ramie	1.5	3.6-3.8	400-938	61.4-128.0
Sisal	1.5	2.0-2.5	511-635	9.4-22.0
Coir	1.2	30.0	593	4.0-60.0
Softwood Kraft (wood)	1.5	4.4	1,000	40.0
E-glass	2.5	0.5	2,000-3,500	70.0
S-glass	2.5	2.8	4,570	86.0
Aramid	1.4	3.3-3.7	3,000-3,150	63.0-67.0
Carbon (standard)	1.4	1.4-1.8	4,000	230-240

2.2 EFFECT OF THE HYDROPHILIC NATURE OF NATURAL FIBERS

Normally, the moisture sorption in composites is divided into three main mechanisms [2, 9-11]: (I) micro-gaps in polymer chains; (II) interfacial fiber-matrix gaps by capillary action; (III) micro-voids in the polymeric matrix. By using short natural fibers to reinforce polymers, another sorption mechanism was added as a result of the hydrophilic nature of these fibers that absorb moisture [2, 8, 12-18]. It might be difficult to evaluate the exact contribution of each sorption

mechanism in the overall sorption process; however, the overall integrated effect of all sorption mechanisms can be estimated as a diffusion process [2, 9-11, 13, 15, 19-24].

2.2.1 Construction and Hydrophilic Nature of Natural Fibers

Generally, four main elements make natural fiber a hydrophilic material [2, 8, 12-18]. These elements are [8, 12, 16-18]: 1) cellulose; 2) hemicellulose (pentosan); 3) pectin; and 4) lignin. The effect of each element on natural fiber properties varies depending on the percentage of that element in the natural fiber; this in turn depends on the type of natural fiber and cultivating techniques [12, 16]. In general, natural fiber can be considered as an amorphous structure of hemicellulose and lignin that is reinforced by micro cellulose fibers [8, 16, 18]. Table 2.2 shows the percentages of the main constitutive elements of some of the natural fibers that commonly used. From Table 2.2, the highest percentage is for cellulose, which is the main element that is responsible for strengthening the natural fibers [8, 16, 18].

Table 2.2 Percentage of main components forming some commonly used natural fibers [8, 25, 26]:

Fiber	Cellulose	Hemicellulose	Lignin	Pectin
Fiber flax	71%	18.6%-20.6%	2.2%	2.3
Seed flax	43–47	24–26	21–23	-
Hemp Bast	75%-78.3%	4%-5.4%	2%-2.9%	2.5%-4%
Jute	45%-71.5%	12%-26%	13.6%-21%	0.2%
Kenaf	31%–57%	21.5%–23%	15%–19%	-
Ramie	68.6%–91%	5%–16.7%	0.6%–0.7%	1.9%
Sisal	73.1%	13.3%	11%	0.9%

On the molecular scale, cellulose is a semicrystalline polysaccharide [8, 12, 27] containing a large number of hydroxyl groups (OH), which gives the natural fiber its hydrophilic property [8, 18, 28]. On the other hand, hemicellulose has an open structure of fully amorphous polysaccharide, and has a lower molecular weight

than cellulose [8, 12, 29]. This open structure of hemicellulose contains many hydroxyl (OH) and acetyl (C_2H_3O) groups, which renders the hemicellulose partially soluble in water and makes it capable of absorbing moisture from the environment [8, 29]. Therefore, hemicellulose is the main element in natural fibers that is responsible for biodegradation, thermal degradation and moisture sorption [16]. Lignin, on the molecular scale, is mainly formed by an organic polymer compound of phenylpropane units (C_9H_{11}), which have an amorphous structure [8, 27]. Lignin is a thermally stable element that has a limited effect on natural fiber water sorption; however, lignin is degradable by Ultraviolet (UV) [8, 12, 16, 29]. The fourth main element forming natural fibers is pectin, which is a polysaccharide that holds fibers together, and is soluble in water [8, 12, 16, 30].

2.2.2 Effect of the Hydrophilic Nature of Natural Fibers on the Composite Strength

As a result of the hydrophilic nature of natural fibers, Short-Natural-Fiber-Reinforced Polymers (SNFRPs) absorb moisture from the air or from being in contact with water or moisture [2, 12-15]. As shown in Figure 2.1, while almost no moisture is absorbed by unreinforced polyethylene matrices with different crystallinity [31-33], the amount of moisture absorbed by their natural-fiber-reinforced composites varies depending on the natural fiber volume fraction and the crystallinity/density of the matrix; the higher the natural fiber volume fraction and the lower the matrix crystallinity/density, the higher the absorbed moisture will be with time [34]. Therefore, moisture sorption in SNFRP (with untreated fibers) mainly depends on [2, 15, 18, 29, 34, 35]: 1) the type of natural fibers; 2) the amount of fiber volume fraction; 3) the emersion condition temperature and time, and 4) the matrix crystallinity level.

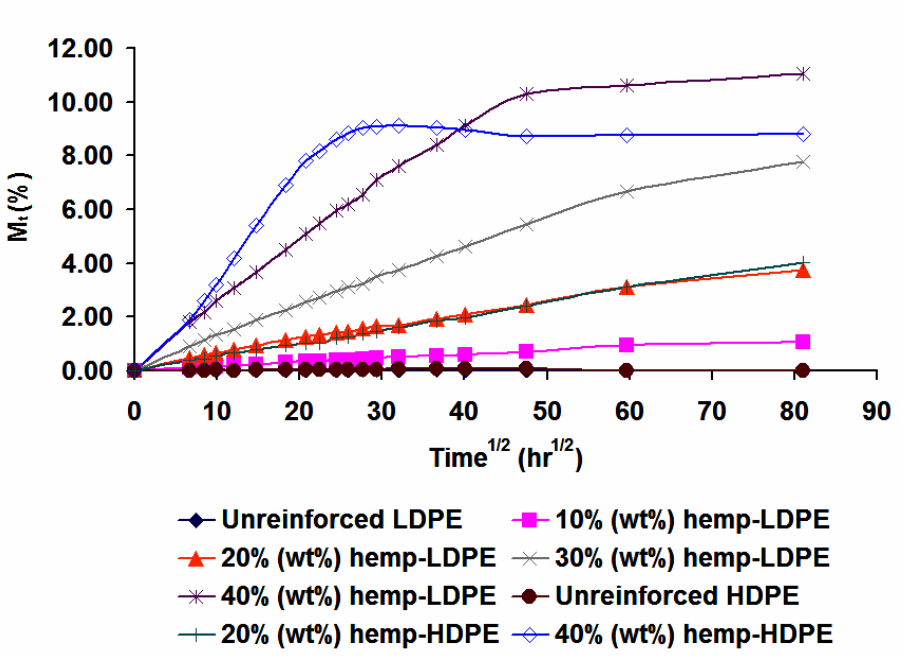

Fig. 2.1 Typical absorbed moisture percentages of short-hemp-bast-fiber-reinforced High Density Polyethylene (HDPE) and Low Density Polyethylene (LDPE) at different hemp fiber weight percentages [34].

Moisture absorption reduces the overall strength of the natural-fiber-reinforced composites, as it reduces the natural fiber strength [2, 12, 15]. Additionally, water or moisture absorption causes natural fibers to swell [2], reducing the interfacial strength between the natural fibers and the polymer matrix; as a result, fibers are easily separated from the matrix [2], as shown in Figure 2.2. This figure shows the fracture surface of a tensile-tensile fatigue test specimen of 20% hemp-reinforced HDPE that was immersed in water for 35 days; the image reveals that most of the hemp fibers were separated from the matrix; this can be attributed to the weakening effect of moisture absorption on the fiber-matrix interfacial strength [36, 37]. This weakening effect of moisture absorption reduces the overall strength of natural-fiber-reinforced composites [37], as shown in Figure 2.3. As moisture absorption reduces the monotonic strength of SNFRPs, it reduces

Fig. 2.2 Scanning Electron Microscope (SEM) image of a tension-tension fatigue fracture surface of short-hemp-bast fiber-reinforced HDPE (20% hemp-reinforced HDPE) immersed in water for 35 days; the fatigue test was performed at maximum fatigue stress of 19 MPa with frequency f=3.0 Hz and fatigue stress ratio R=0.1 [36].

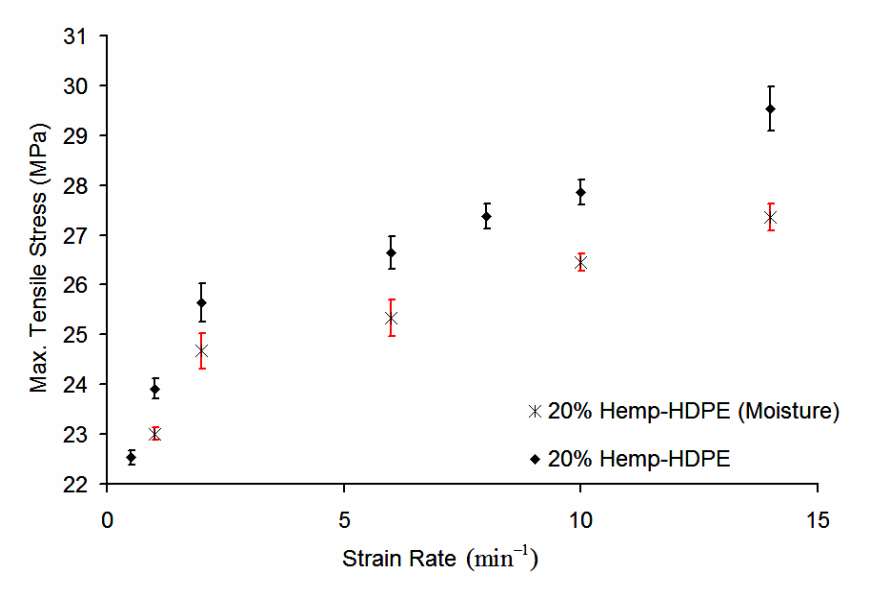

Fig. 2.3 Typical plot of the effect of strain rate on maximum tensile stress of hemp-fiber-reinforced HDPE (20% hemp with 80% HDPE) at different strain rate values after being immersed in water for 35 days [37].

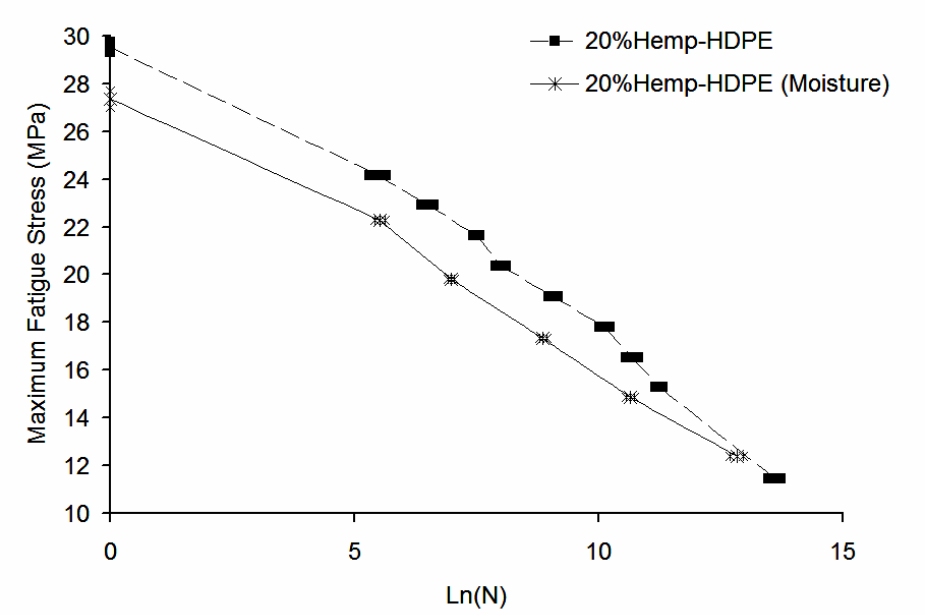

Fig. 2.4 Typical S-N curves for short hemp-fiber-reinforced HDPE (20% hemp with 80% HDPE) shows the effect of moisture absorption on SNFRP fatigue strength after immersing in water for 35 days; the test was performed under tension-tension loading conditions at ratio (R) = 0.1 and fatigue frequency (f)=3.0 Hz. [36, 38].

their fatigue strength [38], as indicated by the fatigue-life (S-N) curves shown in Figure 2.4. The S-N curves in Figure 2.4 represent the relationships between the maximum applied fatigue stress and the natural logarithm of the corresponding life cycles (N) for 20% hemp-reinforced HDPE before and after immersing in water for 35 days. At a very high applied maximum fatigue stress, N is equal to one (i.e. ln(N) is equal to zero); and by decreasing the amount of applied maximum fatigue stress, N is increased. Figure 2.4 shows degradation in the fatigue strength after immersing the specimens in water; this can be attributed to the weakening effect of the absorbed moisture [38], which was discussed previously.

2.2.3 Effect of Natural Fiber Chemical Treatment and Coupling

In natural-fiber-reinforced composites, the hydrophilic (polar) nature of natural fibers is different from the hydrophobic (non-polar) nature of typical polymer matrix materials such as polyethylene. Therefore, another factor affecting the application of SNFRPs is their weak fiber/matrix interfacial strength [7, 39]. There are two main methods of enhancing the bonding between natural fibers and the polymer matrix. The first is to use one of the fiber chemical treatments to increase the strength of the fibers as well as to clean and roughen the surface to place single fibers in direct contact with the matrix and to create a mechanical bond [8, 40]. Alkali treatment is considered one of the most important treatments used to increase the strength of natural fibers [41-43]. This treatment increases the fiber strength by removing the non-cellulose contents, which are about 23%-31% of hemp fiber [41-43]. When Alkali treatment is used, single fibers are exposed to a direct contact with the matrix, creating superior interfacial properties with matrix and increasing the strength of the composite material. Furthermore, alkaline treatment of natural fibers reduces the differences in inner-fiber orientations, giving fibers the capability to produce more elongation [43]. There are a number of other fiber chemical treatments, including Silane treatment, which creates much stronger connection between fiber and matrix than alkaline treatment with a higher thermal stability [8, 44-46], and Acetylation treatment, which increases the composite bio-resistance, thus increasing the temperature of bio-degradation, but produces less strength than Silane treatment [47, 48] Benzoylation, Permanganate and Isocyanate treatments are also used to improve the fiber strength and its adhesion with the matrix [8].

The second method of increasing the interfacial strength is to use a polymer coupling agent (Co-polymer), as it improves the chemical bonding between the natural fiber and the polymer matrix [8]. The use of a coupling agent increases the overall strength of SNFRPs [43]; as, by increasing the interfacial strength between the fibers and the matrix, it transfers a greater load to the fibers, which increases

their overall strength [7]. The preferable coupling agent is chosen according to: 1) the type of the matrix; and 2) the overall effect of the coupling agent on the strength of the SNFRP [7].

2.3 EFFECT OF MANUFACTURING AND PROCESSING PARAMETERS

2.3.1 Effect of the Length, Diameter and Volume Fraction Fibers

The average length (L_f) and diameter (d_f) of short fibers interact to affect the mechanical properties. In general, there is a certain critical fiber length (L_c) that represents the optimum effective length of short fibers; if L_f is shorter than L_c, failure tends to occur at the fiber/matrix interface; otherwise, if L_f is longer than L_c, failure tends to occur in the fiber itself [49]. There is a correlation by which the L_c can be determined, as follows [49]:

$$L_c = \sigma_{fu}\left(\frac{d_f}{2\tau}\right) \quad \text{..... 2.1}$$

where σ_{fu} is the ultimate tensile strength of the fibers, and τ is the fiber/matrix interfacial shear strength or the matrix shear strength, whichever is smallest.

The amount of fiber volume fraction affects the over all strength and stiffness of the reinforced composites [38, 50-52]. The strength of a reinforced polymer can be calculated using the following rule of mixture [42, 49, 53-55]. Equation 2.2 represents one of the forms of the rule of mixture assuming a constant interfacial strength, and neglecting the effect of the fiber length [53]:

$$\sigma_{cu} = \sigma_{fu} v_f + \sigma_{mu}(1-v_f) \quad \text{..... 2.2}$$

where σ_{cu} is the ultimate tensile strength, v_f is the fiber volume fraction, , and σ_{mu} is the matrix ultimate tensile strength.

Based on equation 2.2, the effect of the fiber strength increases when the fiber volume fraction (V_f) is increased, which means that the strength of the reinforced composites increases as well; this holds true up to a certain fiber volume fraction (around 40% for natural fibers [7, 42]), after which the composites starts to lose its integrity and its ability to sustain a load [7, 42]. However, when the fiber volume fraction is increased, the modulus of elasticity continues to increase [7]. On the other hand, when the fiber content is increased, the elongation and the impact strength of the reinforced composites decrease [7].

A formula similar to equation 2.2 can be reformulated to evaluate the stiffness as follows [53]:

$$E_c = E_f v_f + E_m (1 - V_f) \quad \textbf{2.3}$$

where E_c is the strength of the composite, E_f is the strength of the fibers and E_m is the strength of the polymer or the matrix.

2.3.2 Effects of Processing Parameters

The composite processing temperature can greatly affect the mechanical properties of the reinforcing natural fibers. It should be kept around 150^{o}C for a long processing time; however, it can be raised up to around 200^{o}C for a short processing time [39]. At high temperatures (higher than 150^{o}C) over long processing times, there is a possibility of degradation in the lignocelluloses of the natural fibers or a poor adhesion between the fibers and the matrix [1, 39].

In general, processing speed also can affect the mechanical properties of an short-fiber-reinforced polymers. In the case of injection moulding, the injection speed

affects the orientation of the short fibers, which affects the mechanical properties [56]. At high injection speeds, the fibers do not distribute well, and matrix rich regions appear, which reduces the strength of the specimen [56]. At low injection speeds, by contrast, the orientation of the fibers at the outer skin of the produced part is parallel to the direction of the injection flow, and the orientation at the center of the part is normal to the direction of injection or randomly distributed [6, 49, 56], which reduces the strength of the produced part [56]. Therefore, the strength of reinforced composites is higher in the molding direction than in the direction normal to the molding direction for thin specimens (i.e. with thicknesses around 2.5mm) [57]. There is a certain maximum injection speed at which the fibers are well distributed randomly across the section, and the structure is nearly homogeneous; in this case, the strength of the produced part is at the maximum [56].

For thermoplastics with a semicrystalline structure, it is possible that different types of spherulitic structures occur throughout the thickness of produced fiber-reinforced polymers. The cross section morphology changes throughout the thickness according to the cooling rate; the areas near the surfaces with high cooling rates have a fine spherulitic structure, while the core zone with a low cooling rate have a coarser spherulitic structure, which can be identified through its contents of more voids and even holes in some extreme conditions [6]. The coarse spherulitic structure has a lower strength, a lower elongation and a lower fracture toughness than other spherulitic structures with a fine structure [6].

There are some other features that appear as a result of processing parameters; these include voids, matrix-rich zones, fiber-rich zones and bent fibers. These features may affect the mechanical behaviour, depending on how extreme they are [6].

2.4 MONOTONIC BEHAVIOUR

2.4.1 Effect of the Amount and Type of Short Fibers

Adding natural or synthetic fibers to polymers typically increases their monotonic strength and stiffness [41, 58-62], as shown in Figures 2.5 and 2.6, respectively. However, unlike the behavior of long-fiber-reinforced polymers, which are fiber dominated, the mechanical behaviour of SNFRPs is mainly driven by the matrix material, specially the matrix/fiber interfacial strength [38, 50, 62]. To illustrate, the curves in Figures 2.5 and 2.6 are almost parallel in each other, which implies that the slope of the curves (i.e. the sensitivity of curves) is matrix-dominated.

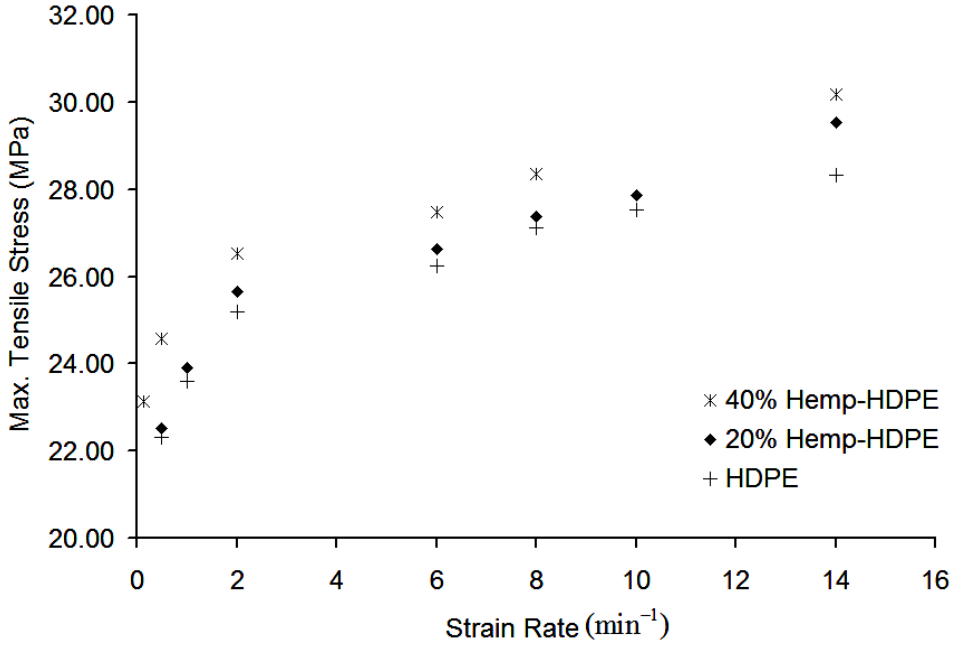

Fig. 2.5 The effect of strain rate on maximum tensile stress of unreinforced HDPE, 20% and 40% hemp-reinforced HDPE [38, 50].

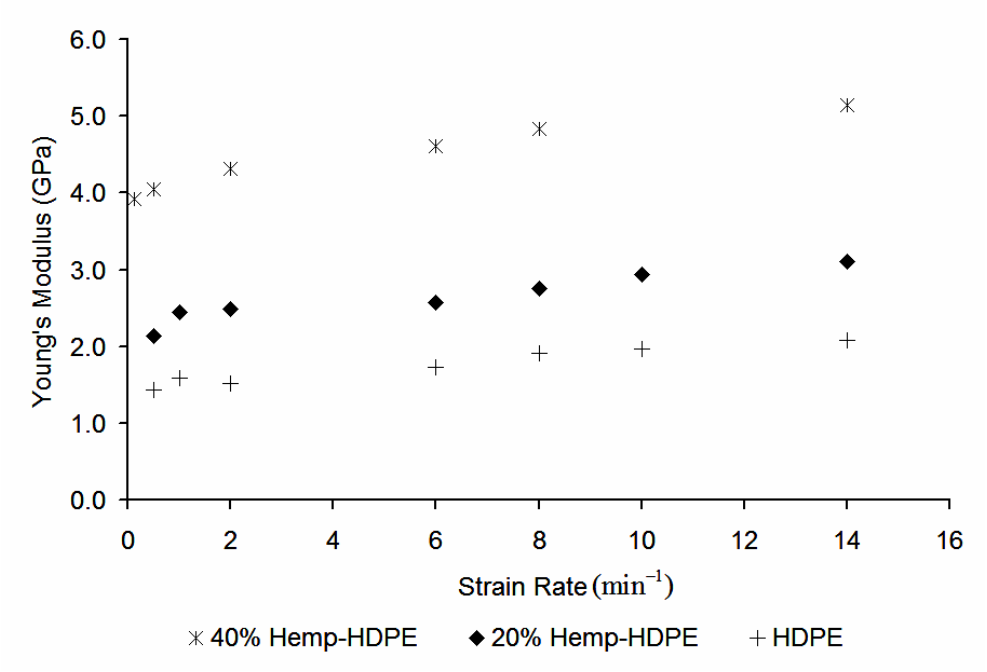

Fig. 2.6 The effect of strain rate on Young' modulus of HDPE unreinforced HDPE, 20% and 40% hemp-reinforced HDPE [50].

2.4.2 Monotonic Behaviour Modeling

The rule of mixture is used extensively to evaluate the strength and the stiffness of short fiber reinforced polymers. The following equation is one of the forms representing the rule of mixture [42, 49, 54, 55]:

$$\sigma_{cu}=\sigma_{fu}v_f\eta_o\eta_l+\sigma_{mu}(1-v_f) \quad \text{..... 2.4}$$

$$\left.\begin{aligned}\eta_l&=\frac{L_f}{2L_c} \qquad \text{for} \quad L_f \le L_c\\ \eta_l&=1-\frac{L_c}{2L_f} \qquad \text{for} \quad L_f > L_c\end{aligned}\right\} \quad \text{..... 2.5}$$

where σ_{cu} is the ultimate tensile strength, v_f is the fiber volume fraction, η_l is the fiber length efficiency factor, η_o is the orientation factor (equal to 1 if fibers are

aligned), L_c is the fiber critical length represented in equation 2.1, and σ_{mu} is the matrix ultimate tensile strength.

In some cases, a term related to the fiber/matrix interfacial shear strength (τ_{fm}) is added to equation 2.4 to represent the effect of the interfacial shear strength as follows [6]:

$$\sigma_{cu}=\sigma_{fu} v_f \eta_o \eta_l+\sigma_{mu}(1-v_f)+\tau_{fm}\alpha\ v_f \quad \textbf{2.6}$$

where α is a factor which is a function of L_c .

The stiffness can be also modeled using the rule of mixture similer to the one represented in equation 2.4, as follows [42, 55]:

$$E_{cu}=E_{fu} v_f \eta_o \eta_l+E_{mu}(1-v_f) \quad \textbf{2.7}$$

where E_c is the strength of the composite, E_f is the strength of the fibers and E_m is the strength of the polymer or the matrix.

Other models were developed to consider the viscoplastic characteristic of the matrix and how the monotonic behaviour gets affected by the loading strain rate ($\dot{\varepsilon}$). The model in equation 2.8 is a nonlinear one-dimensional interpretation for Norton-Hoff rheology model for viscoplastic material [38, 50, 63-67]. In this model, both unreinforced HDPE and hemp reinforced HDPE are assumed to be nonlinear viscoplastic materials.

$$\sigma_{cu}=k_\sigma\left(\frac{\partial u}{\partial x}\right)^{m_\sigma}=k_\sigma(\dot{\varepsilon})^{m_\sigma} \quad \textbf{2.8}$$

where, k_σ is a material constant, $(\partial u/\partial x)$ is the velocity gradient normal to the cross section plane, and m_σ is behaviour index (or strain rate sensitivity) [66]. The material

parameters, K_σ and m_σ, are considered functions of natural fiber volume fraction, and they can represented as follows [38, 50]:

$$k_\sigma = \frac{1}{a_k + b_k\ (v_f)^{c_k}} \quad \text{..... 2.9}$$

where a_k, b_k and c_k are matrix properties; and

$$m_\sigma = \frac{1}{a_m + b_m\ (v_f)^{c_m}} \quad \text{..... 2.10}$$

where a_m, b_m and c_m are matrix properties

2.5 FATIGUE BEHAVIOUR

As noted previously, adding short or long fibers to a matrix improves the tensile and compressive strength of this matrix; additionally, adding short fibers to a polymeric matrix improves its fatigue strength [41, 58-62].

It is wrong to consider a certain or a global relationship that can represent both the failures of long or short reinforced polymers and the failure of metallic material, especially when it comes to a complicated mechanical behaviour such as fatigue [68]. This is due to the complex geometry of the reinforced composites and their complex damage progression; this complexity increases when one accounts for the stress concentration coming from the short fibers and the fiber/matrix interface [69]. For SNFRPs, the complexity of stress distribution is expected to increase due to the inconsistent fibers geometry and distribution within the stressed section [38].

In short-fiber-reinforced polymers, fatigue damage occurs because of damage accumulation and stiffness degradation through the stressed section; in addition, the damage is multi-directional [68, 70]. This kind of damage is different from the

localized single macro-crack propagation type that occurs in metals [68, 70-72]. Short-fiber-reinforced polymers damage accumulation includes [70, 71, 73, 74]: 1) debonding that takes place because of microvoids initiation and propagation around the ends and the surface of fibers; 2) fiber failure that might or might not occur depending on the type of fibers used; and 3) matrix cracking that takes place in the matrix itself. All of the previous damage accumulation mechanisms might function independently or interactively [59]. Figure 2.7 shows the fracture surface of 20% hemp-reinforced HDPE under tensile- tensile fatigue loading; the image shows a distinguished matrix-fiber interfacial separation (IS) as well as matrix failure (MF) and fiber failure (FF) [36]. Therefore, as a result of these many damage accumulation mechanisms taking place during the fatigue loading, it can be concluded that the fatigue fracture of short-fiber-reinforced polymers has some sort of a statistical nature. Statistical functions are thus among the most common functions used to represent the fatigue behaviour of fiber-reinforced polymers; additionally, empirical forms conducted from experimental data are widely used to simulate fatigue behaviour [36, 59].

Behaviour under compression fatigue loading is another difference between composites and metals. The compressive strength of a composite, unlike that of metals, is lower than its tensile strength, and it depends on the reinforcement materials [59, 68]; this rule is the same under fatigue loading [68]. Furthermore, there is a possibility of failure during compressive fatigue loading, which is not likely to happen in metals [59, 68]. This can be attributed to the fact that under compressive loading, whether the fibers are long or short, the fibers do not have much effect on the behaviour of composites, as the significant factors controlling the compressive behaviour in composites are: 1) matrix modulus and strength; 2) fiber/matrix interfacial strength; and 3) fibers misalignments [75]. Therefore, in some compressive applications of composite materials, the ratio between fatigue strength and ultimate tensile strength may not exceed 0.3 [68]. Additionally, there is always a risk of buckling when entering the compression zone, and more precautions are needed in order to stop the occurrences of buckling [59]. The

longitudinal natural fibers used to reinforce polymers are more suited to longitudinal tensile loading [6, 7, 53]. Therefore, it might be advisable to use SNFRPs under tensile loading conditions for both monotonic and cyclic loading [38, 50, 76].

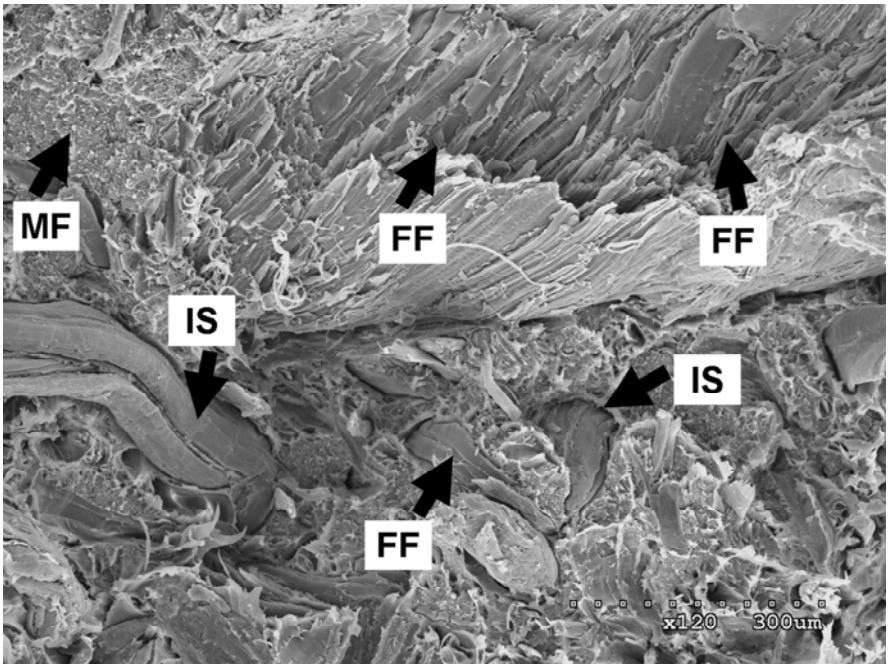

Fig. 2.7 Scanning Electron Microscope (SEM) image of a tension-tension fatigue fracture surface of short-hemp-bast-reinforced HDPE (20% hemp-reinforced HDPE); the fatigue test was performed at maximum fatigue stress of 19.8 MPa with frequency f=3.0 Hz and fatigue stress ratio R=0.1. The image shows different types of failure mechanisms: matrix-fiber interfacial separation (IS); matrix failure (MF); and fiber failure (FF) [36].

Similar to monotonic behaviour of SNFRP, the fatigue tests on SNFRPs showed that the fatigue sensitivity (i.e. the slope and the shape of the S-N curve) is controlled by the matrix material, regardless of the type of fibers used, assuming a good fiber/matrix adhesion [38, 62], as shown in Figure 2.8. The curves in Figure 2.8 illustrate the relationships between the maximum applied fatigue stress and the natural logarithm of the corresponding life cycles (N) for unreinforced HDPE

as well as 20% and 40% hemp-reinforced HDPE. Generally, the fatigue strength increases by increasing the fiber percentages, and this creates a set of parallel S-N curves (i.e. matrix dominated behaviour). However, it should be mentioned that the S-N curve of the unreinforced HDPE shows a ductile-brittle behaviour causing the curve to be shifted after N= 10,000 cycles [38]; this can be attributed to the appearance of crazing, which increases the fracture toughness of the specimens [62]. The matrix-dominated behaviour recorded in Figure 2.4 can be attributed to the fact that short fibers used in reinforcing are very short (i.e. less than millimeters), with a length/diameter ratio ranging around 10; therefore, neither the type of short fibers nor the percentage amount used has much effect on the sensitivity of reinforced composites behaviour [62]. However, fatigue sensitivity is sometimes affected by the used fiber type, which can be explained by the amount of debonded fibers that is varied from type to another during failure [62].

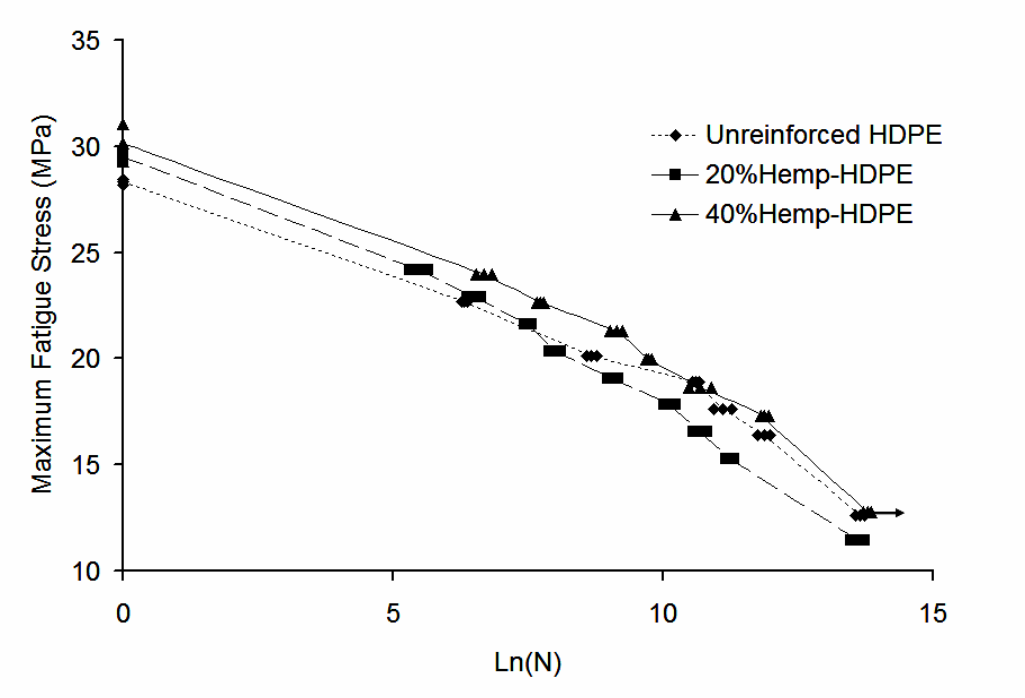

Fig. 2.8 S-N curves for unreinforced HDPE, 20% and 40% hemp-reinforced HDPE at stress ratio R=0.1 and fatigue frequency f=3 Hz [38].

2.5.1 Time-Dependent Effect

For fatigue loading of thermoplastic polymeric-based composites, viscoelasticity and loading rate effects should be considered or controlled during experiments [57, 59, 62, 71].

During the fatigue test, the effect of viscoelasticity is reflected in an increase in temperature (autogenous temperature) [71]. To reduce or to control the autogenous temperature effect, the fatigue test should be done within a frequency at which there is a limited raise in the specimen temperature during the test [59, 62]. For a ductile matrix, the limit of recommended frequency is around 2 or 3 Hz; however, for a brittle matrix, the limit of recommended frequency can be raised to reach between 5 and 10 Hz [57, 62].

Fatigue tests at different load amplitude under constant frequencies will lead to different loading rates [59, 62]. To eliminate the effect of different loading rates, there are two solutions:

1. Each fatigue test (i.e. each test point on the fatigue life curve) is conducted at a different frequency, depending on the maximum fatigue stress level at each test [62] (i.e. the higher is the applied fatigue stress, the lower is the frequency used in the fatigue test);
2. The fatigue life curve conducted at a constant frequency might be normalized by the fatigue strength of one fatigue life cycle; this procedure is highly effective after eradicating the effect of autogenous temperature [59].

2.5.2 Fatigue Modeling and Life Prediction

The complex nature of fatigue behaviour makes it difficult to reach an analytical model to simulate this fatigue behaviour (see section 2.4). Therefore, the fatigue models are usually built on empirical forms conducted from

experimental data. There are two main methodologies used to analyze and predict the fatigue behaviour (they are used for metals and composites as well) [3]:

1. The first methodology, fracture mechanics, predicts fatigue damage using empirical equations of crack growth, which is generally assumed to be under linear elastic mechanics;
2. The second methodology is based on the use of stress-life (S-N) curves and fatigue damage accumulation (such as residual strength and stiffness degradation); sometime this methodology is referred to as the safe life technique.

2.5.2.1 Representation of stress/strain-fatigue life curves

As noted previously, fatigue failure in short-fiber-reinforced composites has a complex nature as a result of damage accumulation and stiffness degradation, and it is a multi-directional damage [68, 70]. Therefore, the modeling technique using fatigue life curves is one of the most suited techniques to studying the fatigue behaviour of SNFRP under cyclic loading.

Stress based:

S-N curves are considered to be the most popular method of characterizing the fatigue behaviour of materials [60]. The power law is commonly used to describe the S-N curves to predict the fatigue strength for certain numbers of cycles [57]:

$$\sigma_{max}=\sigma'_f N^r \quad \text{..... 2.11}$$

where σ_{max} is the maximum cyclic stress, σ'_f is the fatigue strength coefficient, N is the number of cycles to failure under σ_{max}, and r is the fatigue strength exponent.

There are some other simple laws that were conducted to represent the relationship between σ_{max} and N based on data regression from S-N curves; one of these laws is as follows [59]:

$$\sigma_{max}=\sigma_{ut}\text{-BlogN} \quad \textbf{2.12}$$

where, σ_{ut} is the monotonic ultimate tensile strength, and B is a constant.

Equation 2.12 can be adjusted to deal with a normalized fatigue stress as follows [59, 77]:

$$\sigma_{max}/\sigma_{ut}=1-\text{ b logN} \quad \textbf{2.13}$$

To get a better representation of the S-N curve, instead of fitting the S-N curve in a liner equation as in equation 2.12, a polynomial equation can be used as follows [59]:

$$\sigma_{max}=\sigma_{ut}+\text{b logN}+\text{c(logN)}^2 \quad \textbf{2.14}$$

Which means that N can be represented as a polynomial function of σ_{max} [59]:

$$\text{LogN=a+b }\sigma_{max}+\text{c}(\sigma_{max})^2 \quad \textbf{2.15}$$

Strain based:

One of the most important relationships that were developed for strain controlled fatigue tests is the Manson-Coffin relation.

As illustrated in Figure 2.9, the total fatigue strain ($\Delta\varepsilon$) is equal to the summation of both elastic ($\Delta\varepsilon_e$) and plastic ($\Delta\varepsilon_p$) strains [78]:

$$\Delta\varepsilon=\Delta\varepsilon_e+\Delta\varepsilon_p \quad \text{..... 2.16}$$

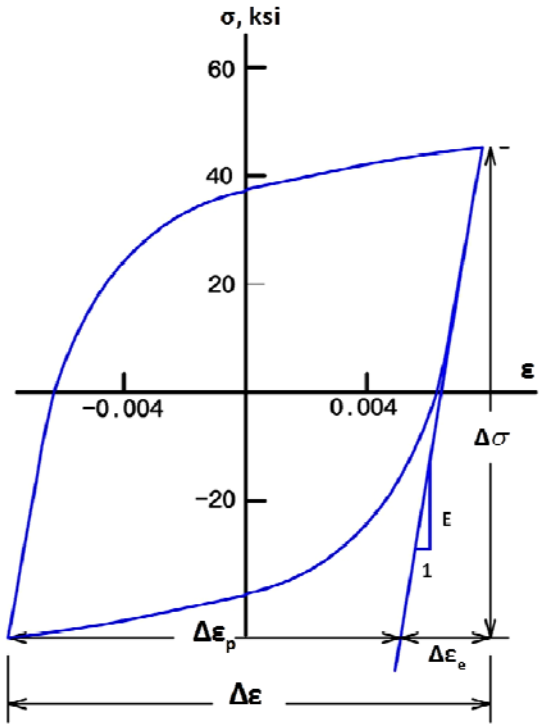

Fig. 2.9 Fully reversed (R=-1) steady state (40% - 50% of N_f) stress-strain loop [78].

The Manson-Coffin relation can be represented as follows [78, 79]:

$$\frac{\Delta\varepsilon}{2}=\frac{\sigma'_f}{E}(2N)^b+\varepsilon'_f(2N)^c \quad \text{..... 2.17}$$

where $\Delta\varepsilon/2$ is strain amplitude (ε_a), $\frac{\sigma'_f}{E}$ and ε'_f are one-reverse intercepts of elastic and plastic curves respectively with total strain amplitude axis (see Figure 2.10), N is the number of cycles to failure under $\Delta\varepsilon$, and b and c are the slope of elastic and plastic curves respectively, as shown in Figure 2.10.

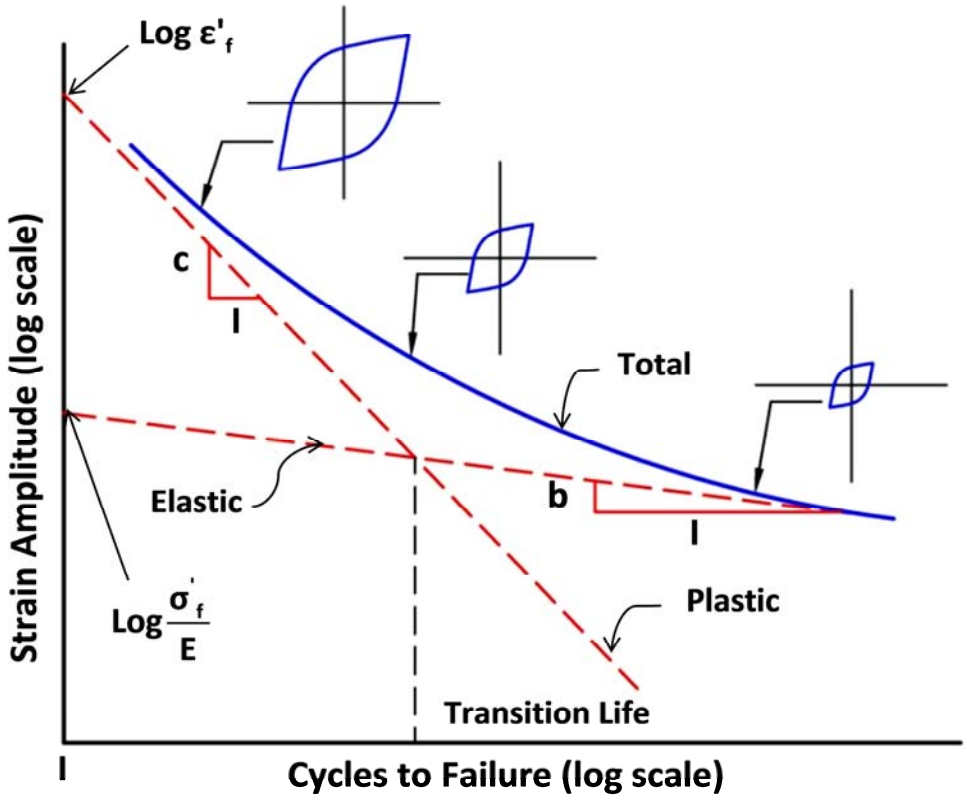

Fig. 2.10 Schematic diagram of fatigue test representing the total strain amplitude, plastic and elastic strain [79, 80].

The parameters b and c can be approximately calculated as a function of the cyclic strain hardening exponent (n'), as follows [80]:

$$b = n'c \quad \text{..... 2.18}$$

$$c = \frac{-1}{1+5n'} \quad \text{..... 2.19}$$

Fatigue modeling using the strain control test is a good approach, especially if the fatigue amplitude is hitting the plastic zone with a small gap between σ_{max} and yield strength σ_y and large gap between ε_{max} (i.e. the strain produced by σ_{max})

and ε_y (i.e. the strain produced by σ_y). However, for compliant materials such as polyethylene, the cyclic fatigue loops with tensile stress limits under strain control will shift such that compressive stress limits emerge throughout the fatigue cycles as a result of the fatigue creep or fatigue accumulative strain.

2.5.2.2 Damage accumulation and strength/stiffness degradation

Damage accumulation is considered to be one of the failure measurements of fatigue. In the following sections, some of the rules and the parameters used to asses the fatigue damage accumulation will be discussed.

Miner's rule:

One of the most basic damage accumulation rules is Miner's rule, which assumes linear damage accumulation as follows [81-83]:

$$\sum_{i=1}^{n} \frac{n_i}{N_i} = 1 \quad \text{..... 2.20}$$

Miner's rule assumes that a failure will occur when the sum of the number of cycles (n_i), at certain loading conditions, divided by the number of cycles to fail (N_i), under the same loading conditions, is equal to one [81-83]. There are many non-linear forms that have been developed from Miner's rule, such as [59]:

$$\Delta = \sum_{i=1}^{n} \left[A_i \left(\frac{n_i}{N_i} \right) + B_i \left(\frac{n_i}{N_i} \right)^2 \right] \quad \text{..... 2.21}$$

where, Δ is the damage scale, and A_i and B_i are constant. At failure, B_i is negative and Δ is equal to unity for failure.

Residual strength:

Based on the damage accumulation phenomenon, one of the theories of fatigue failure is that failure occurs when the residual strength of specimens is reduced to the value of the applied stress [82]. Therefore, it was important to formulate some equations to predict failure using residual strength; in these equations, failure is assumed to occur when the residual strength is equal to the applied stress. One of the most frequently used formulas is as follows [82]:

$$\sigma_r = \sigma_a \left[1+(N-1)f\right]^s \quad \text{..... 2.22}$$

where, σ_r is the residual strength, σ_a the stress range, and N is the number of cycles to failure, while f and s are functions of the stress ratio (R).

Stiffness degradation:

Stiffness degradation was also introduced as a measure for damage accumulation. Stiffness degradation can be represented by one of three parameters [61, 84-86]: 1) fatigue modulus, F(n); 2) secant modulus, S(n); and 3) elastic modulus, E(n). Figure 2.11 shows a schematic diagram illustrating the three stiffness degradation parameters. Stiffness degradation models are designed to model fatigue failure using measurements of these macro-scale properties (i.e. fatigue modulus, secant modulus, and elastic modulus) [87, 88].

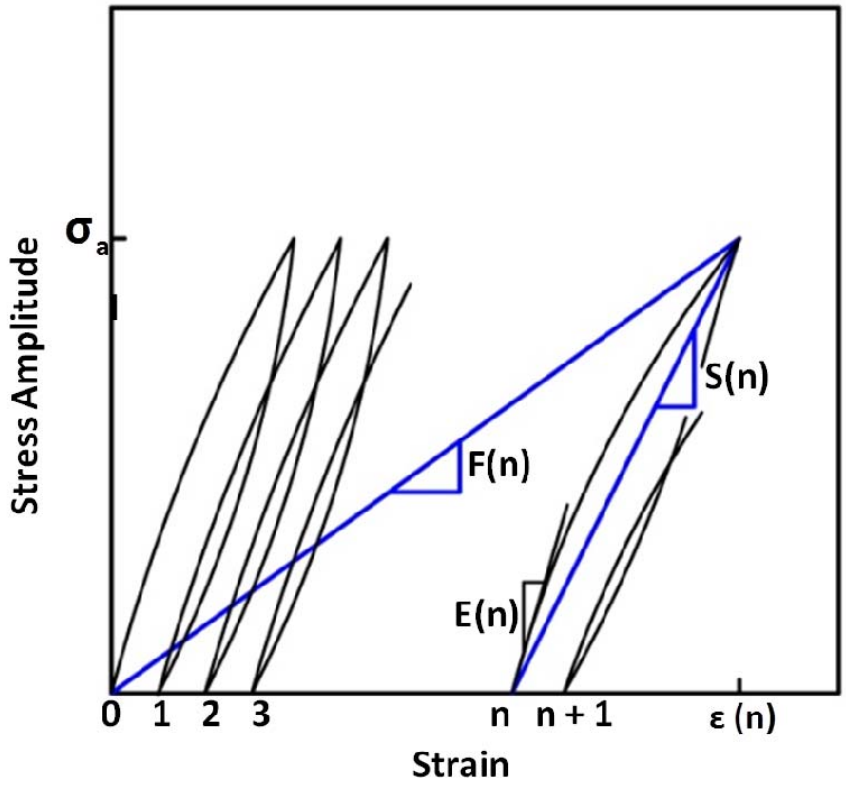

Fig. 2.11 Schematic diagram of stiffness degradation parameters [61, 84].

In the case of fiber-dominated composites, the stress-strain relationship is almost constant, which makes it easy to measure E(n) [61, 89]. On the other hand, for the matrix- dominated composite or SFRP, the stress-strain relationship is nonlinear [61, 89], which makes it more difficult to measure or calculate E(n). Furthermore, the behaviour of a matrix-dominated composite is controlled by the matrix material, which sometimes has a constant value of S(n) through the fatigue cycles, as shown in Figure 2.11. Therefore, it is advisable to avoid the use of either E(n) or S(n) to represent the stiffness degradation in matrix-dominated composites. However, while E(n) and S(n) do not give a real indication of stiffness degradation, the Fatigue modulus (F(n)) can be an alternative solution, representing two damage phenomena occurring during the fatigue test [79]:

1. Stiffness Degradation: causes an incremental relative movement between the top and the lower points in the fatigue hysteresis loops.

2. Fatigue Creep: appears through an incremental shift of the hysteresis loops due to the accumulative strain that is added after each fatigue cycle as a result of using a compliant matrix material, as shown in Figure 2.11.

Damage factor:

The damage accumulation can be evaluated by using a damage factor (D), which can be a function of the stiffness (E) as follows [83, 90]:

$$D=1-\frac{E(n)}{E} \quad \text{..... 2.23}$$

where, $E(n)$ is the elastic modulus of damaged specimen, which is a function of n (number of fatigue cycles). E is the undamaged elastic modulus of the specimen.

Additionally, D can also be defined as a function of the number of fatigue cycles [83, 90]:

$$D=1-\left[1-\frac{n}{N}\right]^{\frac{1}{p+\beta+1}} \quad \text{..... 2.24}$$

where, n is the number of cycles for damage D, N is the number of cycles to failure, and p and β are material constants.

2.5.2.3 Constant life diagrams

For the most part, life diagrams are constructed from fatigue test data in order to be used as a design tool. Life diagrams come in different forms, but all of them are formulated between two axes: 1) fatigue stress amplitude; and 2) mean stress [59]. All such diagrams aim to assign failure/safe design boards [59]. It is important to clarify that there is no an actual physical fatigue limit, especially for

polymeric composite materials; however, 10^6 and 10^7 cyclic lives have been used widely as a fatigue limit for a long time for several applications [91].

2.5.2.4 Micromechanical modeling

The mechanical properties of any material are highly affected by its microstructure. Micromechanical models were proposed to simulate the mutual effect among the constituent elements forming the composites. However, there are some serious obstacles facing microscale modeling of SFRPs; the main obstacle is the fact that it is extremely difficult to quantify the distributions and orientations of actual fibers. In order to compensate for this deficiency in microstructure controllability, some assumptions should be made:

1. The constituent elements have a random distribution, regardless of the meaning or causes of this distribution [92].
2. The random distribution of the constituent elements will form some sort of homogeneity or regularity allover a certain volume of the material; this assumption will give satisfactory results as long as there is no concern about failure in the microscale (i.e. localized failure such as microcracks) [92].

For SNFRPs, the nature of natural fibers makes it extremely difficult to assign certain values for fiber geometrical features (e.g. diameter, length and orientation), which even adds more obstacles toward including natural fibers into a micro mechanical model.

2.5.2.5 Energy method modeling

The energy method has been used as one of the methods of predicting the damage accrued during cyclic loading. Many approaches have been proposed to evaluate fatigue damage using the energy method [59, 68, 70, 71, 93]. Some of these approaches are developed based on elastic and plastic strains, and they require

some parameters to be calculated using fully reversed strain-controlled fatigue tests [59, 68, 93]. Other energy methods work to evaluate the energy based on the failure modes that occur during fatigue loading; however, it is not totally accurate, in the case of SFRPs, to identify a particular failure mode (i.e. matrix cracking, interfacial cracking or fibers failure) as being responsible for failure at any time during a fatigue test [59, 68, 70, 71]. Sometime it is difficult to estimate the amount of energy released near the beginning or the end of the fatigue test, because the energy method is mainly a linear method [73, 84]. Additionally, when using the energy method, it is difficult to differentiate accurately between energy causing the fatigue failure and energy lost due to radiation, conduction and convection [84, 86, 94].

2.5.2.6 Statistical and empirical modeling

When it comes to SNFRPs, there is no consistent geometry that can be assigned to the fibers inside the matrix. Additionally, the level of randomization of natural fibers inside the matrix is not consistent, and it is highly dependent on many factors such as the percentage of natural fibers in the composite and the manufacturing process of the SNFRP constitutive materials. Therefore, the statistical and empirical models are highly suited to model SNFRP and SFRP mechanical behaviours, especially cyclic behaviours [38, 50, 59].

Mechanistic models can be used instead of using empirical models [38, 50], as the mechanistic models capture the mechanism by which the experimental data of the tested variables respond [95]. Recently, the mechanistic models were used successfully along with semi-analytical approaches to reach comprehensive mathematical expressions that accurately simulate the fatigue behaviour of SNFRPs under different loading conditions[38]. Equation 2.25 presents one of the fatigue models that was developed using mechanistic models, it calculates the maximum applied fatigue stress (σ_{max}) under certain number of cycles to failure

(N); the model takes into consideration the fatigue stress ratio (R) and fatigue frequency (f) [38].

$$\sigma_{max} = \left(\frac{2k_\sigma \left(4\frac{k_\varepsilon}{k_\sigma} f(1\text{-}R) \right)^{\frac{m_\sigma}{(m_\sigma - m_\varepsilon + 1)}} \left(\eta \ln(N)\text{-}1 \right)}{\eta \ln(N)\ (1+R)\text{-}2} \right)^{\frac{m_\sigma - m_\varepsilon + 1}{1 - m_\varepsilon}} \quad \text{..... 2.25}$$

where k_ε, k_σ, m_ε and m_σ are parameters measured from monotonic test, and they are functions in fiber volume fraction (v_f) [38].

2.6 CONCLUSIONS

The current study reviewed the aspects affecting the mechanical behaviour of Short-Natural-Fiber-Reinforced Polymers (SNFRPs). On the other hand, the study also reviewed the monotonic and cyclic behaviour of these composites along with the various possible modeling techniques that are suited for modeling and simulating both monotonic and cyclic behaviours of SNFRPs.

There are many factors and aspects that might affect the behaviour of SNFRPs. These factors include the hydrophilic nature of natural fibers; the difference between hydrophilic natural fibers and hydrophobic polymeric matrixes; and the different parameters that characterize manufacturing and process of natural fibers and their SNFRPs. As usually the natural fibers used in SNFRPs are more suited to support tensile longitudinal loading, it is recommended to use the products of SNFRPs in tensile loading applications.

Different models and modeling techniques were reviewed from perspective of modeling both monotonic cyclic behaviours. Rules of mixture as well as rheology models integrated with mechanistic models were among the models that are used

to model the monotonic behaviour. On the other hand, there was a wide variety of models and techniques that are used to model the fatigue life under cyclic loading. It is concluded that statistical and empirical models as well as models that were developed using mechanistic modeling approach are more suited to model the mechanical behaviour of SNFRPs; this is due to the high statistical nature associated with the mechanical behaviour of SNFRPs, as there is a large number of factors that act independently and/or interactively to define the mechanical behaviour of these SNFRPs.

More studies should be conducted focusing on the analysis and modeling of both monotonic and cyclic behaviours of SNFRPs. The models thus developed from these studies will be the basis for an engineering design tool, which will help the products of SNFRPs to evolve from being more eco-friendly products to being reliably engineered and designed products.

CHAPTER 3 ISOTHERM MOISTURE ABSORPTION KINETICS IN NATURAL-FIBER-REINFORCED POLYMER UNDER IMMERSION CONDITIONS[†]

ABSTRACT

In Natural-Fiber-Reinforced Polymer (NFRP), absorption of water or moisture is a significant issue in maintaining strength and stiffness. To enhance the understanding of water and moisture sorption behaviour, the kinetics of moisture sorption in NFRPs are investigated under immersion conditions. Samples of hemp-bast-fiber-reinforced polyethylene are prepared using an injection moulding technique at different hemp fiber volume fractions (v_f). The samples are then immersed in water for 274 days. Moisture content and uptake rate are analyzed at different fiber volume factions and matrix crystallinity percentages. A simplified 2-D contraction model is developed to investigate the contraction effect on the moisture uptake; it shows that a matrix with high crystallinity has more stiffness contraction on the reinforcing natural fibers, which limits the maximum amount of the absorbed moisture. The Fickian diffusion is found to be the dominant absorption behaviour, shifting toward pseudo-Fickian or anomalous diffusion depending on the natural fiber volume fraction and the crystallinity percentages of the matrix. The NFRPs diffusivity is evaluated and modeled to characterize the ability of liquid molecules to diffuse into these composite at different hemp fiber volume fractions. Both the crystallinity

---

[†] This chapter is a modified version of a paper that was published as Ahmed Fotouh, J. D. Wolodko, M. Lipsett, "Isotherm Moisture Absorption Kinetics in Natural-Fiber-Reinforced Polymer under Immersion Conditions", Journal of Material Composites, May 15th, 2014, DOI: 10.1177/0021998314533366.

percentage of the matrix material and the volume fraction of the reinforcing fibers were found to interactively affect the sorption kinetics of the tested NFRPs.

KEYWORDS

Natural-Fiber-Reinforced Polymer (NFRP), Moisture diffusion behaviours, Matrix crystallinity, Fiber volume fraction, Matrix/fiber contraction.

3.1 INTRODUCTION

Natural fibers are generally hydrophilic materials [1-5], comprising mainly cellulose, hemicellulose (pentosan), pectin, and lignin [1, 6-9]. Each component affects the overall properties of natural fibers according to their respective mass fractions, which vary according to fiber types as well as growing and harvesting processes [1, 6]. On the microscale, natural fibers are cellulose microfibrils reinforcing an amorphous matrix structure of hemicellulose and lignin [6, 10]. Cellulose is a semicrystalline polysaccharide [1, 7, 11]. The cellulose is responsible for strengthening natural fibers [7, 9]; and the high percentage of hydroxyl groups (OH) in the cellulose gives the fiber its hydrophilic propriety [7, 9, 12]. Hemicellulose is a fully amorphous polysaccharide that has a lower molecular weight than that of cellulose [1, 7]. Because hemicellulose has an open structure containing many hydroxyl (OH) and acetyl (C_2H_3O) groups, hemicellulose is partially soluble in water; and it absorbs moisture from air [7, 13]. For this reason, hemicellulose is the main contributor to biodegradation, thermal degradation, and moisture sorption in natural fibers [6, 10]. By contrast, lignin has an amorphous structure, which is mainly formed by a natural polymer formed by phenylpropane units (C_9H_{11}) [7, 11]. Lignin has a small effect on moisture sorption and is thermally stable, but it is prone to degradation by ultraviolet light [1, 6, 7, 13]. Pectin is a polysaccharide that is soluble in water; and it is also responsible for holding fibers together [1, 6, 7, 14].

Natural-Fiber-Reinforced Polymer (NFRP) contains natural fibers, which are hydrophilic, that are embedded in a polymer matrix, which is usually hydrophobic. This difference in the nature of the materials causes some challenges for expanding the production of NFRPs, and the main challenge is moisture that is absorbed by natural fibers. Moisture sorption in NFRP depends on the type of natural fibers, the amount of fiber volume fraction, and the surrounding condition temperature [3, 5, 9, 13, 15]. Additionally, there is another uninvestigated factor that could affect the moisture absorption; this factor is the level of crystallinity in the polymeric matrix. In a NFRP, natural fibers gain moisture from the air or from contact with water or other liquids [1-5]. Moisture sorption causes fibers to swell [3], weakening fiber strength and causing fibers to separate from the matrix, thereby reducing the overall strength of the NFRP [1, 3, 5].

The objective of the present work is to provide a better understanding of moisture sorption in natural-fiber-reinforced polymers, by investigating moisture sorption kinetics at different hemp bast fiber volume fractions. Furthermore, the effect of matrix crystallinity is also investigated by testing natural-fiber-reinforced composites at two different crystallinity percentages of polyethylene matrixes; High Density Polyethylene (HDPE); and Low Density Polyethylene (LDPE). LDPE as a polymer has a high number of short methylene (CH_2^{2-}) side chains, which prevent an LDPE polymer from crystallizing to the same degree as in an HDPE polymer; on the other side, an HDPE polymer contains a smaller number of longer CH_2 side chains, giving HDPE a relatively high crystallinity percentage [16, 17].

3.2 EXPERIMENTS AND METHODOLOGY

3.2.1 Material Selection for Experiments

Hemp bast fibers (USO14) were used as the natural reinforcing fibers in the experiments, as they are well suited for longitudinal (tensile) loading [18, 19].

This can be attributed to the high percentage of cellulose found in the hemp bast fibers, as shown in Table 3.1; the variation in the percentages of hemp fiber constituents can be attributed to: the accuracy of the testing methods, the maturity level of the hemp plant, and the type of hemp crop as well as the harvest time in the season.

The high cellulose percentage provides hemp bast fiber with good mechanical properties, making it a good candidate to replace synthetic fibers, such as glass fibers, in some applications [20]. Table 3.2 shows the mechanical properties of typical hemp bast fibers.

Table 3.1 Percentage of main components forming hemp bast fiber at maturity [21, 22]:

Fiber	Cellulose	Hemicellulose	Lignin	Pectin
Hemp Bast	75%-78.3%	4%-5.4%	2%-2.9%	2.5%-4%

Table 3.2 Mechanical properties of hemp bast fiber [3, 7, 20, 23-25]:

	Tensile strength (MPa)	Elongation (%)	Young's modulus (GPa)	Density (g/cm^3)
Hemp Bast	550-900	1.6-4	60-70	1.48

Fig. 3.1 Decorticated hemp bast fibers (black line is 5.0 mm)

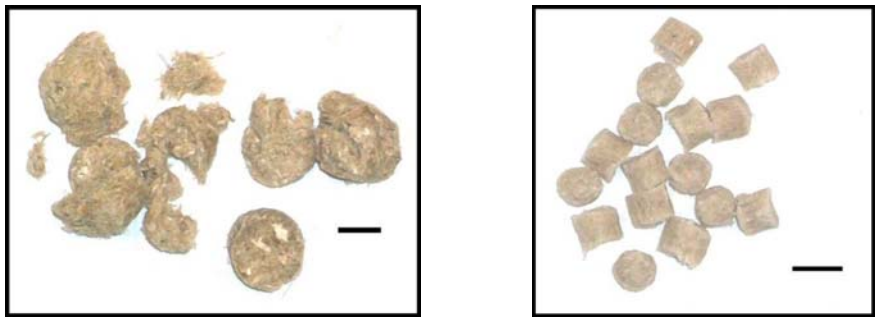

(a) **(b)**

Fig. 3.2 Pellets of (a) hemp bast fibers and (b) 20 wt% hemp-fiber-reinforced HDPE (black line is 5.0 mm)

In the current experiments, hemp bast fibers with a length of 5 mm were isolated using a short fiber decortication system at Alberta Innovates Technology Futures (AITF), in Edmonton, Alberta. A photograph of the decorticated fibers is shown in Figure 3.1. Hemp fibers were subsequently pelletized, as shown in Figure 3.2-a, in order to feed the fibers in the extruder system for compounding. These pellets were dried at 100^{o} C for 12 hours.

Hemp pellets and polyethylene pellets were compounded (mixed) and continuously extrude. An example of the compounded pellets is shown in Figure 3.2-b. Figure 3.3 shows the main components of the NFRP pellets production line: (1) Control Unit (2) HDPE Pellets Feeder (3) Natural Fiber Pellets Feeder (4) Batch Mixture Extruder (5) Cooling Water Bath (6) Pelletizer.

Hemp fibers and Low Density Polyethylene (LDPE) were mixed at various hemp weight percentages: 10 wt%, 20 wt%, 30 wt% and 40 wt%. This corresponds to 6.3%, 13.3%, 20.6% and 29.1% of fiber volume fractions (v_f), respectively, based on measured density of the component. Separate compounded material was also prepared with hemp fibers mixed and High Density Polyethylene (HDPE) at 20 wt% and 40% hemp fibers (corresponding to 13.5% and 30.1% of fiber volume fractions, respectively). Table 3.3 shows the mechanical and physical properties of the matrix materials used in this study.

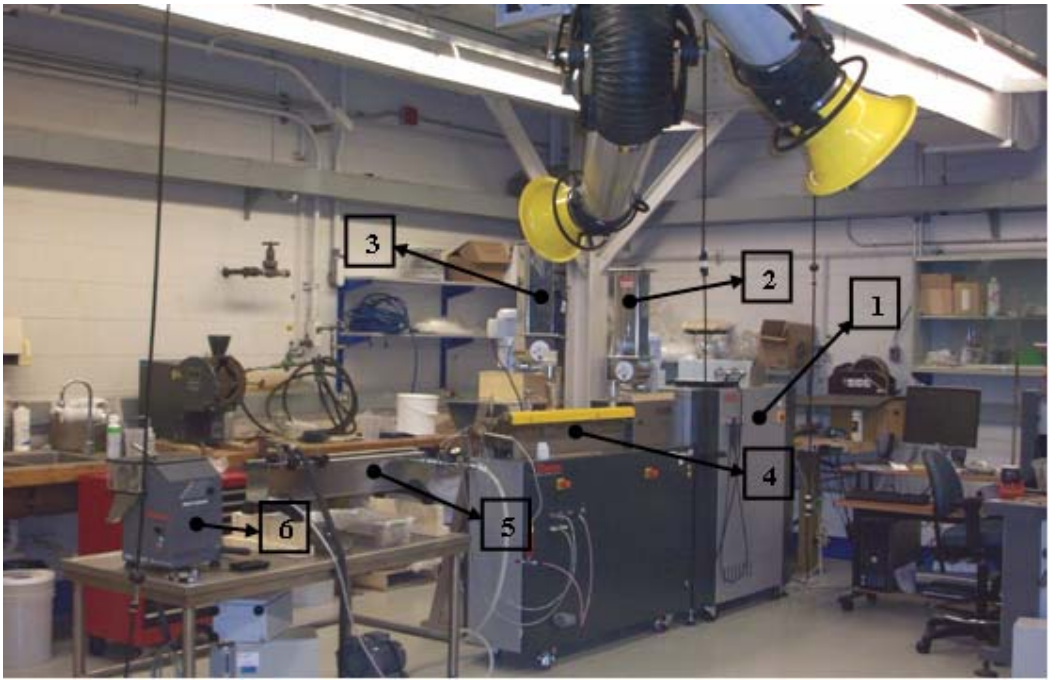

Fig. 3.3 NFRP pellet production line: (1) Control Unit (2) HDPE Pellets Feeder (3) Natural Fiber Pellets Feeder (4) Batch Mixture Extruder (5) Cooling Water Bath (6) Pelletizer.

Table 3.3 Mechanical and physical properties of HDPE and LDPE:

Property	HDPE	LDPE	Test Method
Density	0.943 g/cm^3	0.911 g/cm^3	ASTM D1505
Crystallinity [16, 26]	70-90%	40-50%	- Density; - X-Ray; - Calorimetry.
Melt mass flow rate (MFR) (190^{o}C/2.16Kg)	7.5 g/10min	12 g/10min	ASTM D1238
Hardness (Shore D)	67	47	ASTM D2240
Tensile Strength at yield(50mm/min)	24 MPa (at yield)	9 MPa (at break)	ASTM D638
Stiffness (Young's modulus) (50mm/min)	1.8 GPa	0.1 GPa	ASTM D638
Elongation at yield (50mm/min)	9%	129%	ASTM D638

3.2.2 Test Specimens and Procedures

Test specimens were manufactured using an injection moulding process using a Battenfield 100 injection moulding machine. Table 3.4 shows the different injection pressures used to produce the test specimens. The injection pressure was found to increase with increase volume fraction of fibers (v_f) as a result of changing flow characteristics of polymer/fiber blends. All test measurements were taken based on the average readings from 5 test specimens. The moisture sorption amount (M_t), is evaluated by calculating the change in the sample mass with respect to its original mass according to the following formula:

$$M_t = \left(\frac{W_t - W_o}{W_o}\right) 100\ \% \quad \textbf{3.1}$$

where W_t is specimen mass at time t and W_o is the initial dry mass of the specimen before it is immersed in water.

The specimens were immersed in water for 274 days to allow for moisture sorption under immersion conditions. As shown in Figure 3.4, sample mass measurements were taken at different time intervals to allow for moisture to be absorbed between readings. All tests were performed in a controlled environment, at a temperature of 23 ± 2^o C and relative humidity of 50 ± 5%.

Table 3.4 Injection pressure used to produce testing samples:

Material	Injection pressure psi. (MPa.)
Unreinforced LDPE	700 (4.83)
Unreinforced HDPE	800 (5.52)
10% (wt%) hemp-LDPE	800 (5.52)
20% (wt%) hemp-LDPE	800 (5.52)
30% (wt%) hemp-LDPE	900 (6.21)
40% (wt%) hemp-LDPE	1000 (6.89)
20% (wt%) hemp-HDPE	800 (5.52)
40% (wt%) hemp-HDPE	1300 (8.96)

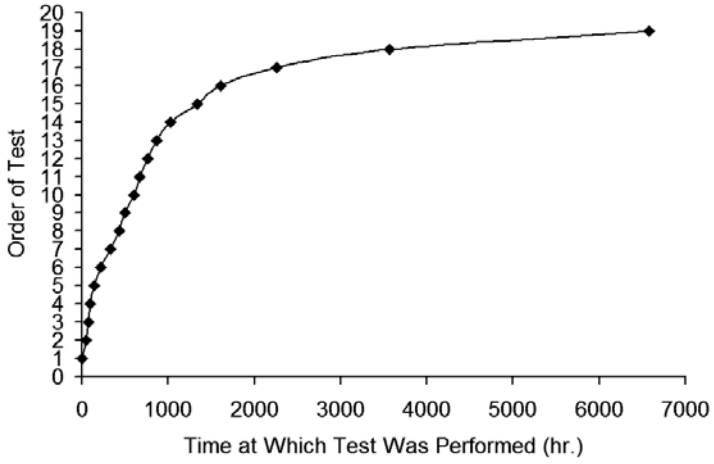

Fig. 3.4 Mass measurement intervals

3.3 RESULTS AND ANALYSIS OF MOISTURE SORPTION BEHAVIOR

Figure 3.1 show the moisture absorption behaviour of the tested NFRPs and their matrixes. No absorbed moisture was detected for unreinforced LDPE or unreinforced HDPE, which indicates that the reinforcing hemp fibers were responsible for the moisture sorption in the tested hemp-fiber-reinforced polymers. The maximum moisture uptake rate was recorded for 40% hemp-

HDPE; those of the 40% hemp-LDPE and 30% hemp-LDPE followed. The fraction of hemp fibers in 20% hemp-LDPE and 20% hemp-HDPE was not sufficiently large to demonstrate the sorption behaviour of 40% hemp composites; in fact, the sorption behavior was similar for both 20% hemp-LDPE and 20% hemp-HDPE composite samples, as shown in Figure 3.1.

The theoretical amount of moisture that can be absorbed by reinforcing natural fibers can be evaluated by calculating the absorbed moisture as a percentage of the reinforcing natural fibers weight as follows:

$$M_{tf} = \frac{M_t}{W_f} 100\ \% \quad \text{..... 3.2}$$

where M_{tf} is moisture sorption as a percentage of natural fiber contents at time t, M_t is the moisture sorption at time t, and W_f is the fiber mass percentage in the specimen.

At room temperature, hemp bast fibers can absorb moisture in quantities of up to 67%-70% of the weight of dried fibers after immersing in water for 3 days [27]. From equation 3.2, the theoretical amount of absorbed moisture by hemp fibers in a polyethylene matrix declines to a value of 28% after being in water for 274 days, as shown in Figure 3.6. This reduction in the total absorbed moisture by the fibers can be attributed to the reduced exposure of fibers to water transport due to isolation of fibers in the matrix. This lack of complete interconnectivity between fibers as well as constraining the fiber swelling by the surrounding matrix will alternately reduce the total amount of moisture absorption.

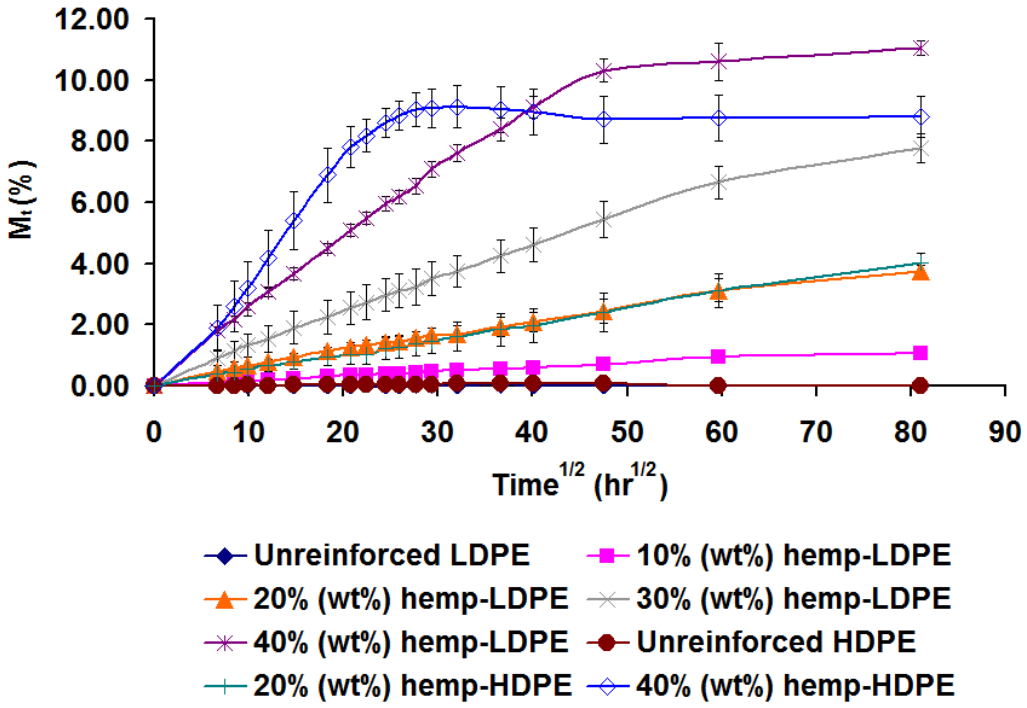

Fig. 3.5 Moisture sorption (M_t) of tested matrixes and composites at different hemp fiber weight percentages; errors bars are equal to ± the standard deviation (S.D.) calculated from experiments.

The leaching effect for 40% hemp-HDP and its fast absorption rate can be seen by the dip in the curve in Figure 3.6. The moisture sorption rate increases as the fiber volume fraction (v_f) is increased, as shown in Figure 3.6; the same behaviour was noticed in Figure 3.1. For 40% hemp-HDPE, Figure 3.6 shows that the moisture sorption reaches a maximum and then decreases by about 2.96 %. This drop in the weight percentage is near the value of the soluble pectin percentage shown in Table 3.1. Additionally, there was a clear discoloration in the soaking water containing 40% hemp-HDPE samples, which is another indication that the drop in the sorption curve in Figures 3.1 and 3.6 was due to the leaching out of the soluble substances that are contained in the hemp fibers. Furthermore, the high sorption rate of 40% hemp-HDPE allows more hemp fibers to be involved in the

leaching process in a smaller period of time compared to the one for other composites, and that leads to this noticeable leaching effect for 40% hemp-HDPE.

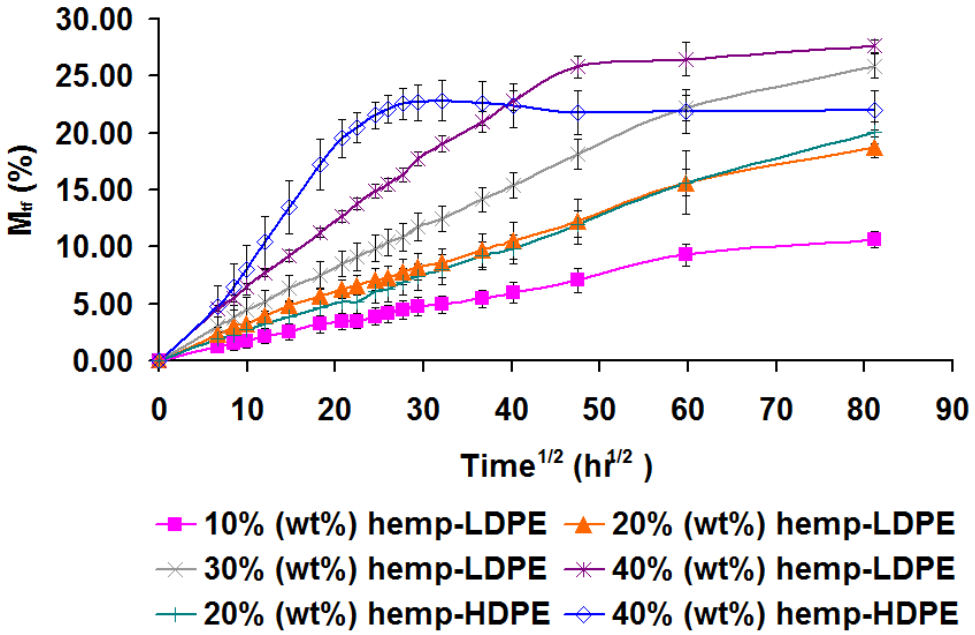

Fig. 3.6 Moisture sorption as a percentage of fiber weight (M_{tf}) of tested composites at different hemp fiber weight percentages; errors bars are equal to ± the standard deviation (S.D.) calculated from experiments.

Figures 3.7 and 3.8 show the maximum moisture absorbed as a percentage of the weights of tested composite samples (M_{tmax}) and a percentage of the reinforcing natural fibers' weights (M_{tfmax}), respectively, at different hemp-fiber weight percentages. Figure 3.7 shows that, even though the volume fraction of hemp fibers in 40% hemp-HDPE is slightly higher than that of 40% hemp-LDPE, the M_{tmax} absorbed by 40% hemp-LDPE (11.06%) is higher than that absorbed by 40% hemp-HDPE (8.80%). Figure 3.8 shows that the M_{tfmax} for both 40% hemp-LDPE (27.66%) and 30% hemp-LDPE (25.87%) are much higher than that of 40% hemp-HDPE (22.00%); however, the volume fraction of the hemp fiber (v_f)

in 40% hemp-HDPE is higher than that of those in 40% hemp-LDPE and 30% hemp-LDPE.

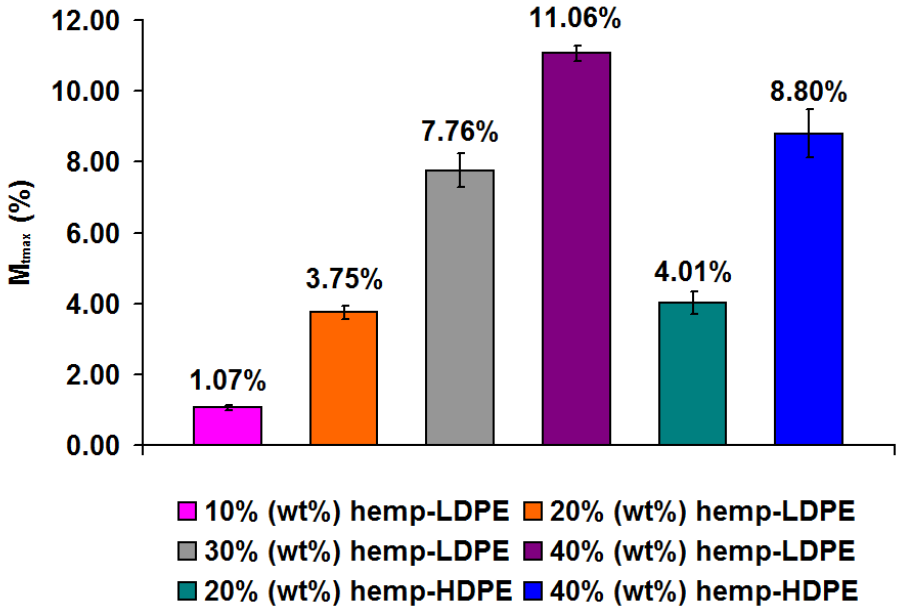

Fig. 3.7 Maximum moisture absorbed (M_{tmax}) of tested composites at different hemp fiber weight percentages; errors bars are equal to ± the standard deviation (S.D.) calculated from experiments.

These differences in the sorption levels for both M_{tmax} and M_{tfmax} shown in Figures 3.7 and 3.8, respectively, could be explained within the context of the matrix stiffness and the matrix-fiber contraction forces, as both of these factors are expected to control the swelling level of the reinforcing natural fibers; hence, they will affect the maximum amount of the absorbed moisture (i.e. M_{tmax} and M_{tfmax}). Moreover, Figure 3.8 shows that fibers within the same matrix absorbed similar amount of moisture. However, the connectivity between fibers is reduced by decreasing fiber volume fraction (v_f); therefore, within the same matrix, the values of M_{tfmax} absorbed by fibers was found to increase with increasing the value v_f, as shown in Figure 3.8.

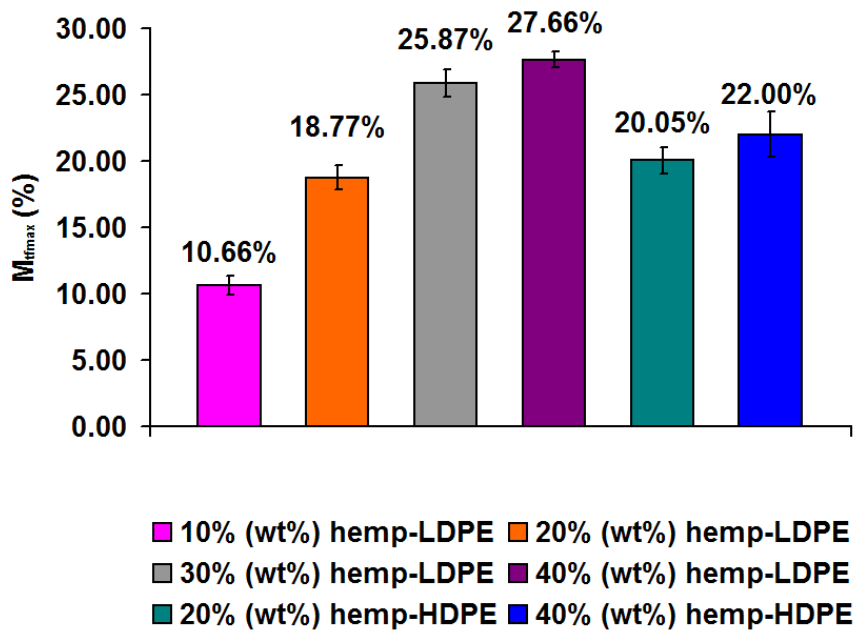

Fig. 3.8 Maximum moisture sorption as a percentage of fiber weight (M_{tfmax}) of tested composites at different hemp fiber weight percentages; errors bars are equal to ± the standard deviation (S.D.) calculated from experiments.

3.4 CONSTRAINTS OF MATRIX CRYSTALLINITY

The matrix stiffness as well as the matrix-fiber contraction can provide a possible explanation to the variation in the maximum amount of the absorbed moisture between LDPE and HDPE matrices. The higher crystallinity level in the polymer, the higher is the polymer stiffness, and the more is the resistance to swelling [28]. The stiffness factor affects the maximum amount of absorbed moisture by applying constraints on the swelling of natural fibers within the matrix. To illustrate, the more stiffness the matrix has, the more constrained the swelling of natural fibers will be; this limits the value of M_{tmax} and the M_{tfmax}, as the scenario involving the 40% hemp-HDPE composite (with the higher crystallinity and stiffness) demonstrated, as shown in Figures 3.7 and 3.8.

Another factor that affects the levels of M_{tmax} and M_{tfmax} is the contraction forces applied on the natural fibers by the matrix. To investigate the effect of this contraction factor, a simplified two dimensional (2-D) contraction mode has been developed.

3.4.1 2-D Matrix-Fiber Contraction Model

The 2-D contraction model developed in this study simulates the natural fiber and the surrounding matrix by taking the form of two cylinders, a solid fiber cylinder inside a matrix cylinder. After contraction, a contact pressure (P_c) is developed on the interface between the fiber and the matrix, as shown in Figure 3.9.

The constitutive equations of the principal stresses for a cylinder under internal and external pressure, shown in Figure 3.10, are represented as in equations 3.3 and 3.4 [29].

$$\sigma_r = \frac{r_i^2 p_i - r_o^2 p_o}{r_o^2 - r_i^2} - \frac{r_i^2 r_o^2 (p_i - p_o)}{r^2 (r_o^2 - r_i^2)} \quad \text{.....3.3}$$

where σ_r is the radial principal stress at any radius r, r_i is the internal radius, r_o is the outer radius, p_i is the internal applied pressure, and p_o is the outer applied pressure.

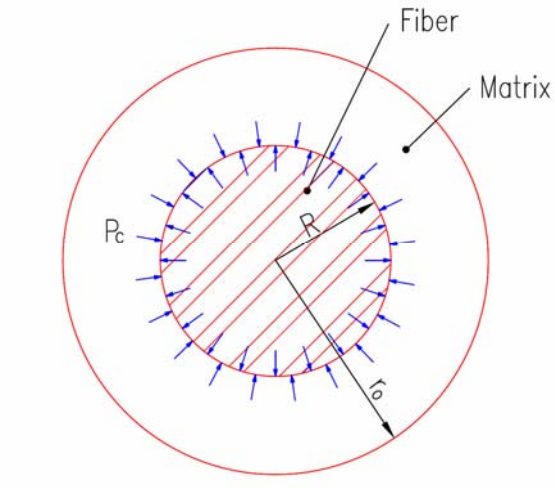

Fig. 3.9 Contact pressure generated as a result of contraction on the outer surface of the fiber and the inner surface of the matrix.

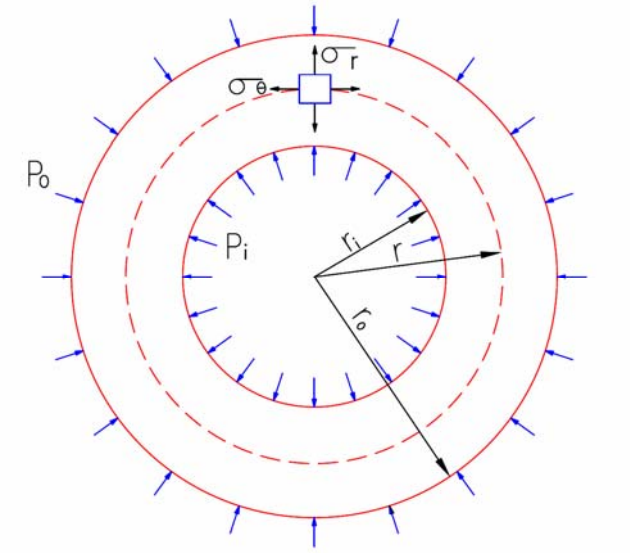

Fig. 3.10 Schematic Diagram of a cylinder under internal and external pressure.

$$\sigma_\theta = \frac{r_i^2 p_i - r_o^2 p_o}{r_o^2 - r_i^2} + \frac{r_i^2 r_o^2 (p_i - p_o)}{r^2 (r_o^2 - r_i^2)} \quad \text{..... 3.4}$$

where σ_θ is the hoop principal stress at any radius r.

Based on equations 3.3 and 3.4 at p_o is equal to zero, the equations of stresses, generated at the surface of the fiber as a result of the P_c, are represented using equations 3.5 and 3.6.

$$\sigma_{rf} = -P_c \quad \textbf{3.5}$$

where σ_{rf} is the radial principal stress at the surface of a fiber with radius R, and P_c is the interfacial pressure due to the contraction.

$$\sigma_{\theta f} = -P_c \quad \textbf{3.6}$$

where $\sigma_{\theta f}$ is the hoop principal stress at the surface of a fiber with radius R.

Using equations 3.3 and 3.4, the principal interfacial stresses of the matrix are represented in equations 3.7 and 3.8.

$$\sigma_{rm} = -P_c \quad \textbf{3.7}$$

where σ_{rm} is the radial principal stress at the inner radius R of the matrix.

$$\sigma_{\theta m} = \frac{P_c\left(R^2 + r_o^2\right)}{r_o^2 - R^2} \quad \textbf{3.8}$$

where $\sigma_{\theta m}$ is the hoop principal stress at the inner radius R of the matrix, and r_o is the outer radius of the modeled matrix cylinder.

The total interfacial contraction-displacement (Δ) can be calculated as a result of the interaction between the fiber contraction displacement (δ_f) and the matrix contraction displacement (δ_m), which are shown in Figure 3.11. The mathematical expression of Δ is represented by equation 3.9.

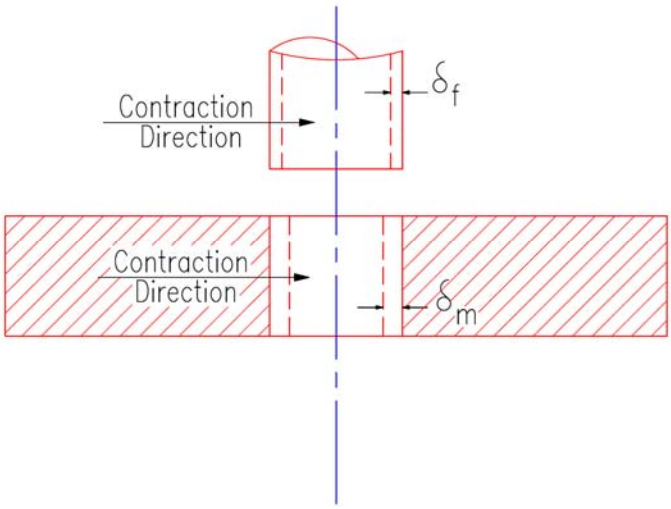

Fig. 3.11 The displacements of unrestrained fiber and matrix due to contraction.

$$\Delta=2(\delta_m-\delta_f) \quad \textbf{3.9}$$

The generalized constitutive equation of stress-strain relationship is represented in equation 3.10 [30].

$$\varepsilon_{ij}=\frac{1+\nu}{E}\sigma_{ij}-\frac{\nu}{E}\sigma_{\alpha\alpha}\delta_{ij} \quad \textbf{3.10}$$

where ε_{ij} is the strain for the i and j coordinates, σ_{ij} is the corresponding stress for the i and j coordinates, E is the stiffness coefficient (Young's Modulus),ν is the Poisson's ratio, $\sigma_{\alpha\alpha}$ is the summation of normal stresses, and δ_{ij} is the Kronecker's delta.

Using equations 3.5, 3.6 and 3.10, the constitutive equation of δ_f can be represented as in equation 3.11.

$$\delta_f=\frac{RP_c}{E_f}(\nu_f-1) \quad \textbf{3.11}$$

where E_f is the stiffness coefficient of the fiber, and ν_f is the Poisson's ratio of the fiber.

Based on equations 3.7, 3.8 and 3.10, equation 3.12 can be developed as the constitutive equation of δ_m.

$$\delta_m = \frac{RP_c}{E_m}\left(\frac{R^2+r_o^2}{r_o^2-R^2}+\nu_m\right) \quad \textbf{3.12}$$

where E_m is the matrix stiffness coefficient, and ν_m is the Poisson's ratio of the matrix.

Δ can be expressed as in equation 3.13 by using equations 3.9, 3.11 and 3.12.

$$\Delta = \frac{2RP_c}{E_m E_f}\left(E_f\left(\frac{R^2+r_o^2}{r_o^2-R^2}+\nu_m\right)+E_m\left(1-\nu_f\right)\right) \quad \textbf{3.13}$$

Δ can be approximately calculated in terms of thermal displacement as in equation 3.14.

$$\Delta = 2T_\Delta\left(\gamma_m\ \left(r_o-R\right)-\gamma_f R\right) \quad \textbf{3.14}$$

where T_Δ is the temperature difference causing the contraction, γ_m is the matrix thermal expansion, and γ_f is the fiber thermal expansion.

By using equations 3.13 and 3.14, an expression was derived to calculate the value of P_c; this expression is demonstrated in equation 3.15.

$$P_c = \frac{T_\Delta E_m E_f\left(\gamma_m\ \left(r_o-R\right)-\gamma_f R\right)}{R\left(E_f\left(\frac{R^2+r_o^2}{r_o^2-R^2}+\nu_m\right)+E_m\left(1-\nu_f\right)\right)} \quad \textbf{3.15}$$

In equation 3.15, the value of P_c is affected by two matrix parameters, the thermal expansion coefficient and the stiffness. Generally, due to the higher crystallinity of HDPE, its thermal contraction coefficient is lower than the thermal contraction coefficient of LDPE; however, the stiffness of HDPE is higher than the stiffness of LDPE. The values in Table 3.5 were selected for the parameters in equation 3.15 to assess which matrix, the HDPE or the LDPE, causes more contraction pressure (P_c) on the fibers. The Poisson's ratio of hemp fibers (ν_f) is very difficult to measure [31]; therefore the value of P_c will be calculated at three values of ν_f, 0.0, 0.25, 0.35, as shown in Table 3.6.

Table 3.5 Selected values for parameters in equation 3.15:

The parameter	The value
T_Δ	20 ^oC
γ_m	150 μ strain/ ^oC (HDPE), 200 μ strain/ ^oC (LDPE) [32]
γ_f	20 μ strain/ ^oC [33]
R	1 unit.
r_o	2 units
ν_m	0.47 (HDPE), 0.49 (LDPE) [34]
E_m	From Table 3.3: 1.8GPa (HDPE), 0.1 GPa (LDPE)
E_f	From Table 3.2: 65 GPa.

The changes in the value of ν_f did not significantly affect the values of P_c, as shown in Table 3.6. The calculated values of P_c demonstrate more contractions in the case of the HDPE matrix, and this is another explanation for limiting the values of M_{tmax} and M_{tfmax} for HDPE natural-fiber-reinforced composites more than those for LDPE composites. To illustrate, by increasing the contraction pressure of HDPE matrix, the swelling of hemp fibers is limited due to the generation of more constraining surrounding pressure, and that leads to limiting the values of M_{tmax} and M_{tfmax} for HDPE natural-fiber-reinforced composites, as shown in Figures 3.7 and 3.8.

Table 3.6 Estimated values P_c ad different values of ν_f:

The value of ν_f	The estimated values of P_c For HDPE matrix (MPa)	The estimated values of P_c for LDPE matrix (MPa)
0.00	2.162	0.166805
0.25	2.192	0.166825
0.35	2.172	0.166847

3.5 ANALYSIS AND MODELING OF ISOTHERM SORPTION KINETICS IN NFRP

3.5.1 Effect of Matrix Crystallinity on the Absorption Behaviour of NFRP

Figure 3.12 shows that at the beginning of the experiments, the sorption capacity ($L_s=M_t/M_{tmax}$) increases with the increase of the natural fiber volume fraction (V_f), with the highest capacity seen in the 40% hemp-HDPE sample. For 10%, 20% and 30% hemp-LDPE, sorption capacities are similar; however, the sorption capacity for 30% hemp-LDPE is slightly higher because of the fiber volume fraction is higher than those of the 10% and 20% hemp-LDPE samples. 20% hemp-HDPE has the lower sorption capacity (L_s). This can be attributed to: the constraints generated by the HDPE matrix; as well as the limited amount of fibres in the matrix.

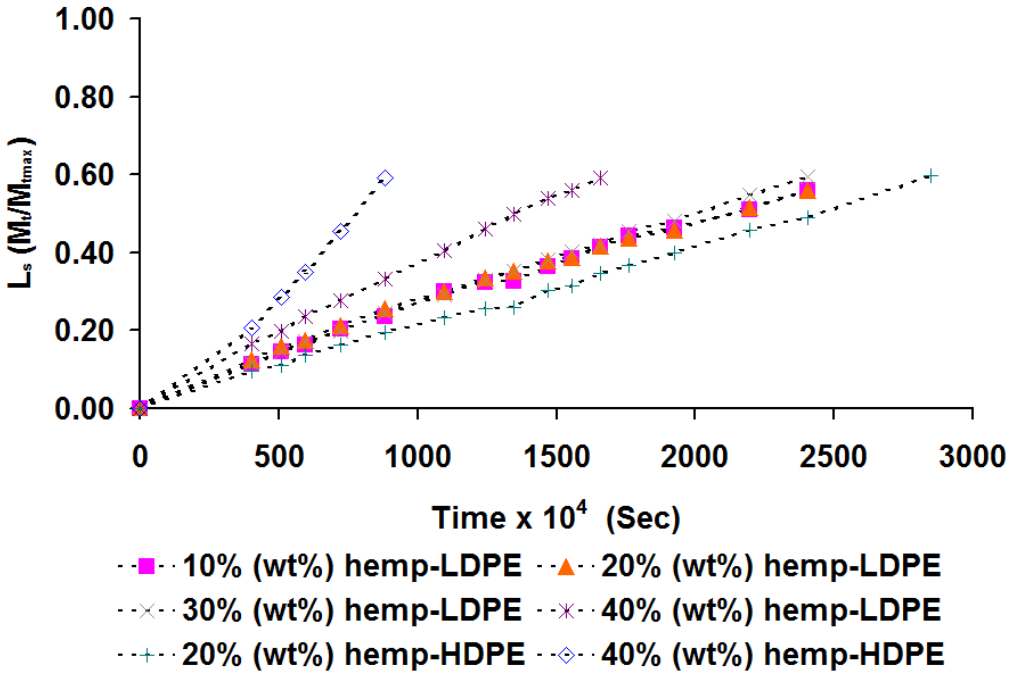

Fig. 3.12 Sorption curves of short term sorption for the tested NFRPs.

One possible explanation for the significant increase in the short term absorption of 40% hemp-HDPE is the formation of the shrinkage micro-voids as a result of the high crystallinity level in HDPE. To illustrate, when a linear polymer such as polyethylene cools down, the polymer chains are aligned in plates known by crystalline lamellae [35]. As a result, spherical semicrystalline regions (semicrystalline structure) of the crystalline lamellae (with low specific volume) within amorphous structure (with high specific volume) are formed in the polymer [35, 36]; therefore, polymers with a semicrystalline structure tend to have smaller specific volumes (relatively higher densities) than do polymers with an amorphous structure [35, 37], and this difference in the specific volumes is decreased by decreasing the level of crystallinity [37]. As a result of this difference in specific volume between the crystalline lamellae and the amorphous structure, negative pressure micro voids are formed during the crystallization shrinkage within the semicrystalline polymers at the interface between the crystalline lamellae and the amorphous structure [36, 38-44]. The negative

pressure formed in this shrinkage voids could reach values between -5 and -20 MPa [39].

As the HDPE has a high crystallinity level than the crystallinity level in the LDPE, it is reasonable to assume that shrinkage micro voids are more likely to be formed in HDPE (higher crystallinity) than in LDPE (lower crystallinity) [43]. Therefore, it is logical to assume that the relatively high adsorption of the 40% hemp-HDPE, as shown previously in Figure 3.12, is a result of increasing the negative pressure effect generated from the relatively high number of micro voids in the HDPE matrix. There is another factor that increased the effect of the shrinkage vacuumed micro voids in the 40% hemp-HDPE; this factor is the decompaction of the reinforcing fibers after the release of the applied moulding pressure [45]. As the matrix-fibers mix is moulded under a relatively high pressures (see Table 3.4), the fibers store some elastic energy due to their compaction [45]. After removing the moulding stress, the released forces from fibers decompaction causes the shrinkage micro voids to grow into larger voids; additionally, the released compaction forces can produce new cavitation micro voids [45]. On the other hand, even though the NFRPs of both 20% hemp-HDPE and 40% hemp-HDPE shared the same HDPE matrix, the sorption rate was far higher for 40% hemp-HDPE, as shown in Figure 3.12. This can be attributed to two factors: 1) increasing the fiber volume fraction from 13.5% for 20% hemp-HDPE to 30.10% for 40% hemp HDPE; 2) increasing the moulding pressure of 40% hemp-HDPE, which also increased the decompaction of the fibers, especially with the relatively high volume fraction (30.10%). Therefore, the 20% hemp-HDPE composites did not demonstrate sorption behaviour similar to the sorption behaviour of 40% hemp-HDPE. in the end, it should be mentioned that hypothesis of the effect of the shrinkage micro-voids on the absorption rate needs to be investigated further using specialized characterization techniques, such as Scanning Electron Microscope (SEM) [46, 47]. This is outside the scope of the current study.

3.5.2 Modeling of Isotherm Absorption Kinetics in NFRP

Generally, there are three possible factors causing moisture sorption in synthetic Fiber-Reinforced Polymers (FRP) [3, 48-50]:

1) polymer chains micro-gaps;
2) interfacial gaps between fibers and matrix through capillary action;
3) matrix micro-voids.

Each factor forms an individual sorption mechanism. For hydrophilic natural-fiber-reinforced polymers, the moisture absorbed by natural fibers is an additional sorption mechanism. As it is difficult to determine how much each sorption mechanism contributes to the overall sorption process, the overall integrated effect of all previous mechanisms can be evaluated as a diffusion process [3, 48-50].

To estimate the short-term diffusion process kinetics (i.e., up to $M_t/M_{tmax}=0.6$ [51]), the sorption curves in Figure 3.12 can be simulated using an empirical power law equation [3, 51, 52]. The sorption curve power law equation can represent either linear or non-linear diffusion processes, using the following expression [3, 51-54]:

$$L_s = k_s t^{n_s} \quad \text{..... 3.16}$$

where $Ls=M_t/ M_{tmax}$ is the sorption level (also known by sorption capacity) at a given temperature, t is sorption time, k_s is material parameter at a given temperature, and n_s is the sorption index at a given temperature. When $n_s=0$, $k_s=L_s$.

Diffusion process can be described using equation 3.16 based on the value of the sorption index (n_s) [3, 51-53, 55]. In case I (classical/Fickian diffusion) for $n_s=0.5$, the amount of diffusion flux of moisture mass is proportional to the moisture concentration gradient in sorption direction. In case II (non-Fickian diffusion) for

n_s=1.0, the diffusion occurs at a constant rate. In case III (anomalous diffusion) for $0.5<n_s<1.0$, the diffusion is nonlinear with time. There are also two subcases: pseudo-Fickian for $n_s< 0.5$, and supercase II for $n_s>1.0$.

The values of k_s and n_s in equation 3.16 found using the data shown in Figure 3.12 are presented in Table 3.7.

Table 3.7 k_s and n_s for hemp-fiber-reinforced polyethylene:

	10% (wt%) hemp-LDPE	**20% (wt%) hemp-LDPE**	**30% (wt%) hemp-LDPE**	**40% (wt%) hemp-LDPE**	**20% (wt%) hemp-HDPE**	**40% (wt%) hemp-HDPE**
k_s (S^{-ns}) x 10^{-4}	7.10	10.9	5.40	6.76	2.48	0.69
n_s	0.428	0.401	0.450	0.457	0.488	0.667

As Table 3.7 reveals, most n_s values are in the region of a value of n_s=0.5, which is the value for Fickian diffusion. The values of n_s for hemp-fiber-reinforced LDPE range between 0.40 and 0.457. Since the values of n_s for LDPE natural-fiber-reinforced composites are all less than 0.5, the behaviour appears to shift toward pseudo-Fickian diffusion. The value of n_s for 20% hemp-HDPE is 0.488, which is nearly 100% Fickian diffusion; for 40% hemp-HDPE, the value of n_s is 0.67, indicating a swing toward anomalous diffusion. The physical causes of pseudo-Fickian diffusion are not exactly known. However, elastic stresses, caused by natural fiber swelling, might be one of the causes [3, 54], because these elastic stresses affect the free surface, which in turn affects the diffusion coefficient of the medium [56]. The value of n_s for 20% hemp-LDPE is lower than the value of n_s for 10% hemp-LDPE. This can be attributed to the greater effect of the swelling stress in 20% hemp-LDPE due to the higher value of the hemp fiber volume fraction for 20% hemp-LDPE. With more fibers to swell in 20% hemp-LDPE, the resultant residual stress increases, which affects the developed residual stresses. However, by increasing the fiber volume factions in 30% and 40% hemp-LDPE, the diffusion behaviour changes to provide a more Fickian diffusion. As the fiber

volume fraction increases in 30% and 40% hemp-LDPE, the fiber randomization level is increased, thereby increasing the level of homogeneity in the diffusion process and making it much closer to Fickian diffusion.

For 20% hemp-HDPE, the value of n_s jumps to 0.488 from 0.40 for 20% hemp-LDPE, prompting the diffusion behaviour to provide almost 100% Fickian diffusion. This can be attributed to the use of HDPE as a matrix; to illustrate, as HDPE is stiffer and causes more contraction on the fibers than LDPE, the effect of fiber swelling is reduced, which makes the diffusion behaviour in 20% hemp-HDPE is almost 100% Fickian. By increasing hemp fiber volume fraction in 40% hemp-HDPE, the diffusion behaviour shifts toward anomalous diffusion. As a result of the high fiber volume percentage in 40% hemp-HDPE and its high absorption rate caused by the effect of vacuumed micro voids, which is enforced by the decompaction forces, the diffusion behaviour of 40% hemp-HDPE shifts toward anomalous diffusion.

3.5.3 Diffusivity Evaluation and Modeling

As illustrated in Figure 3.1, there was no significant moisture absorbed by the unreinforced LDPE or HDPE, and hence the diffusion coefficients for both LDPE and HDPE are relatively very low (varied between 1.3 to 10 $x10^{-8}$ mm^2/sec for LDPE and HDPE [57]); therefore, the diffusion coefficient can be considered a direct measure of the diffusivity of hemp-fiber-reinforced polyethylene. A simplified form of the solution for Fick's second law equation can be used to estimate the diffusion coefficient (D), for short term sorption time (i.e. up to $L_s \leq 0.6$) [51, 58], as follows [2, 3, 5, 51, 58, 59]:

$$L_s = \frac{4}{\sqrt{\pi}}\left(\frac{D\,t}{h_o^{\,2}}\right)^{0.5} \quad \text{..... 3.17}$$

where, L_s is sorption level (M_t/M_{tmax}), h_o is the specimen initial thickness (mm), t is sorption time (sec.), and D_o is the diffusion coefficient (mm^2/sec.).

For Fickian diffusion with a linear relation between L_s and $t^{0.5}$, D is assumed to be constant with time (t) as well as with the initial thickness (h_o); therefore, the following partial differential equation can be developed from equation 3.17:

$$\frac{\partial L_s}{\partial \sqrt{t}} = \frac{4}{\sqrt{\pi}} \left(\frac{D}{h_o^2} \right)^{0.5} \quad \text{..... 3.18}$$

where, $\left(\frac{\partial L_s}{\partial \sqrt{t}} \right)$ is the slope of the linear relation between L_s and $\sqrt{t}$.

From equation 3.18, the diffusion coefficient (D) can be found:

$$D = \left(\frac{\sqrt{\pi} h_o}{4} \right)^2 \left(\frac{\partial L_s}{\partial \sqrt{t}} \right)^2 \quad \text{..... 3.19}$$

Fick's second law (as well as its simplified solution in equation 3.17) were mainly developed for short term Fickian diffusion [51, 58], in which there is a linear relationship between L_s and $\sqrt{t}$. To verify the fact that Fickian diffusion is the dominant diffusion behaviour in short-term sorption, the relations between L_s and $\sqrt{t}$ have been plotted as shown in Figure 3.13.

The plot of experimental data points in Figure 3.13 shows good linearity between L_s and $\sqrt{t}$ for all samples of the tested NFRPs. The coefficient of determination (R^2) was used to assure the linearity of L_s-$\sqrt{t}$ relations plotted in Figure 3.13 [60].

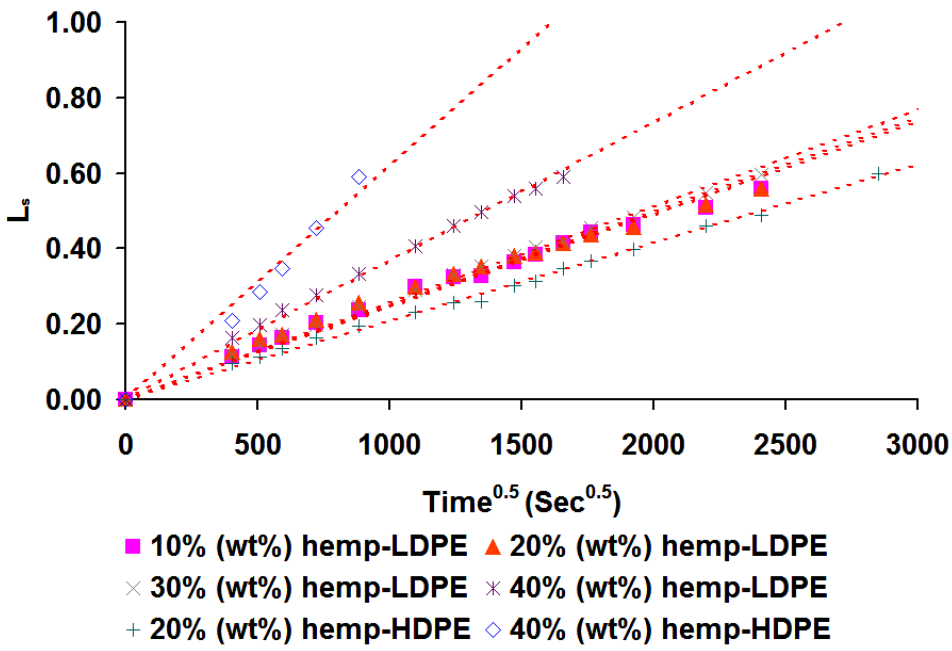

Fig. 3.13 linear relationships of the experimental points of L_s and its corresponding $t^{0.5}$ for short term sorption.

Table 3.8 shows very high values for R^2 which provides a very high confidence in the linearity of L_s-$\sqrt{t}$ relations. Therefore, the hypothesis that Fickian diffusion is the key diffusion behaviour in short-term sorption can be assumed to be valid. Equation 3.5 is thus applicable in calculating the diffusion coefficient for hemp-polyethylene composites. Diffusion coefficient values (D) calculated using equation 3.5 are represented in Table 3.9.

Table 3.9 shows a general trend: D increases as the fiber volume fraction increases. The 40% hemp-HDPE has the highest diffusivity. This may be due to the 40% hemp-HDPE: 1) having the highest hemp fiber volume fraction of samples tested; and 2) using HDPE as a matrix, as the voids in the HDPE matrix and the relatively high decompaction forces promote the sorption rate of the large amount of hemp fibers in 40% hemp-HDPE. These factors all made the hemp fibers in 40% hemp-HDPE act like a sponge to absorb a significant amount of moisture in a short time. This also explains why the diffusion behaviour tends to shift from Fickian diffusion toward anomalous diffusion for 40% hemp-HDPE.

The value of D_o for 20% hemp-HDPE is 30% lower than that of 20% hemp-LDPE. This is probably because the moisture sorption capacity (L_s) at this early sorption stage is lower for 20% hemp-HDPE than for 20% hemp-LDPE, given that the HDPE matrix has a higher stiffness and a higher contraction on the fibers than the LDPE matrix. Therefore, the diffusivity of 20% hemp-HDPE was less than that of 20% hemp-LDPE, especially when the decompaction forces were suppressed because of the low amount of hemp in 20% hemp-HDPE, which also limited the tendency of the cavitation voids in the HDPE matrix to increase the diffusivity.

Table 3.8 The Goodness of the liner fit for data pints in Figure 3.13:

	10% (wt%) hemp-LDPE	**20% (wt%) hemp-LDPE**	**30% (wt%) hemp-LDPE**	**40% (wt%) hemp-LDPE**	**20% (wt%) hemp-HDPE**	**40% (wt%) hemp-HDPE**
Goodness of the liner fit for L_s-$\sqrt{t}$ relation (R^2)	0.9847	0.9718	0.9938	0.9962	0.9966	0.9753

Table 3.9 Values of $\left(\frac{\partial L_s}{\partial \sqrt{t}}\right)$ and D for hemp-fiber-reinforced polyethylene:

	10% (wt%) hemp-LDPE	**20% (wt%) hemp-LDPE**	**30% (wt%) hemp-LDPE**	**40% (wt%) hemp-LDPE**	**20% (wt%) hemp-HDPE**	**40% (wt%) hemp-HDPE**
$\left(\frac{\partial L_s}{\partial \sqrt{t}}\right)$ ($sec^{-0.5}$) x 10^{-4}	2.4546	2.4924	2.5588	3.6753	2.0779	6.2038
D (mm^2/sec) x 10^{-8}	21.294	21.955	23.141	47.741	15.260	136.025

3.6 CONCLUSIONS

The moisture sorption behaviour of hemp-fiber-reinforced HDPE and LDPE was investigated under immersion conditions in water. Increasing the hemp volume fraction increased the moisture take-up rate. Increasing the crystallinity in addition to the fiber volume faction increased the moisture sorption rate for the tested NFRPs. A simplified 2-D contraction model was developed. The model showed that the matrix with a higher crystallinity (higher stiffness) created a relatively high contraction in the reinforcing fibers, which can explain why the maximum amount of moisture absorbed by the tested NFRPs was increased by decreasing the crystallinity percentage of the matrix material for the same hemp fiber weight percentage. Therefore, it can be concluded that the moisture absorption of NFRPs depends mainly on two factors: 1) the natural fiber volume fraction; 2) the matrix crystallinity level.

The dominant moisture diffusion behaviour for hemp-fiber-reinforced polyethylene was found to be Fickian diffusion, in which the flux of the diffused moisture mass is proportional to the moisture concentration gradient in the diffusion direction. The diffusion behaviour shifts toward pseudo-Fickian by decreasing the hemp fiber for LDPE as a matrix, and it shifts towards anomalous diffusion by increasing the hemp fibers using HDPE as a matrix. The diffusivity is estimated based on the calculated diffusion coefficient using Fick's second law. Diffusivity increased when the hemp volume fractions were increased. In addition, in 40% hemp, diffusivity was significantly increased by using the HDPE as a matrix; this can be attributed to: 1) the slightly larger amount of hemp fibers included in 40% hemp-HDPE; and 2) possible effect of the negative pressure voids, which was elevated as a result of the increase in decompaction forces.

CHAPTER 4: CHARACTERIZATION AND MODELING OF STRAIN RATE HARDENING IN NATURAL-FIBER-REINFORCED POLYMER[‡]

ABSTRACT:

The effect of strain rate ($\dot{\varepsilon}$) on the mechanical properties of short-hemp-fiber-reinforced High Density Polyethylene (HDPE) is characterized and modeled at different values of $\dot{\varepsilon}$ and hemp fiber volume fraction (v_f) under dry and wet conditions. Based on the experiments, a generalized comprehensive power law model is developed to predict the behaviour of the mechanical properties as functions of v_f, $\dot{\varepsilon}$ and moisture absorption. It is demonstrated that the developed model successes to accurately simulate the effects of v_f, $\dot{\varepsilon}$ and moisture absorption on the mechanical properties of the natural-fiber-reinforced composites as well as the unreinforced polymer.

KEYWORDS:

Natural Fibers; Viscoplastic Polymer; Strain Rate Hardening; Modeling; Moisture Effect.

[‡] This chapter is a modified version of a paper that was published as Ahmed Fotouh, J. D. Wolodko, M. Lipsett, "Characterization and Modeling of Strain Rate Hardening in Natural-Fiber-Reinforced Viscoplastic Polymer", Journal of Polymer Composites, Feb. 06th, 2014, DOI: 10.1002/pc.22894.

4.1 INTRODUCTION

The importance of using natural fibers as reinforcing fibers in composites has increased considerably in the last decade [1, 2]. This is a result of natural fibers having many favorable properties compared to synthetic fibers [1, 3-5]. This increasing demand for natural fibers as reinforcing fibers is a motivation for studies not only to characterize and investigate the properties of natural-fiber-reinforced polymers, but also to model these properties.

The behaviour of short-fiber-reinforced polymer material is dominated by the material properties of the matrix [6-8]. Therefore, if the properties of the matrix polymer are affected by the strain rate ($\dot{\varepsilon}$), the properties of the developed short-natural-fiber-reinforced polymer will be consequently affected by $\dot{\varepsilon}$. The present study investigates the effect of $\dot{\varepsilon}$ on the mechanical properties, maximum tensile stress (σ_{ut}) and its corresponding strain (ε_{ut}) along with Young's modulus (E), of short-hemp-fiber-reinforced High Density Polyethylene (HDPE). Samples are tested at different hemp fiber volume fractions (v_f). Tests are performed at different $\dot{\varepsilon}$ using monotonic uniaxial tensile stress. Some of the specimens are immersed in water for 35 days to assess and model the effect of wet-service conditions.

4.2 MATERIALS AND TESTING PROCEDURES

Short, hemp-bast fibers and HDPE were mixed at two fiber weight percentages: 20% and 40%. Based on the measured densities of the hemp-bast fiber and HDPE (1.475 g/cm^3 and 0.924 g/cm^3, respectively), the corresponding fiber volume fractions (v_f) were determined to be 13.5% and 30.1% for 20% and 40% weight fractions, respectively..

Test specimens were produced using an injection molding process according to ASTM D638 Type 1 configurations with 50 mm gage length. The overall

dimensions of the tensile test specimen are shown in Figure 4.1. Tensile tests were performed at different engineering strain rates of 0.13, 0.50, 1.00, 2.00, 6.00, 8.00, 10.00 and 14.00 min^{-1}, corresponding to elongation speeds of 6.50, 25, 50,100,300,400,500 and 700 mm/min, respectively. Monotonic uniaxial tensile tests were performed using an Instron 8501 universal testing machine with an extensometer mounted to the test specimens to monitor changes in the strain during the test.

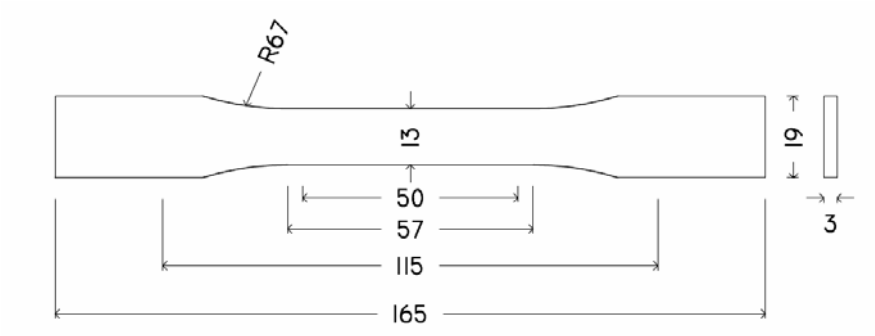

Fig. 4.1 Schematic diagram showing the overall dimensions of D638 Type 1 configuration with 50 mm gage length.

20% hemp-HDPE was selected to test the effect of moisture absorption on the behaviour of the mechanical properties. Tensile test specimens were immersed in water for 35 days prior to mechanical testing. While there was no water absorbed by the unreinforced HDPE, the specimens of 20% hemp-HDPE absorbed approximately 2.4% of its dry weight.

Each monotonic tensile test was repeated three times for homogeneous unreinforced HDPE. On the other hand, each monotonic tensile test was repeated five times for 20% and 40% hemp, because the samples were expected to have more variability due to the level of the heterogeneity of the material. Failure criteria were assigned depending on the failure mode. For tested unreinforced HDPE, the failure mode was ductile, and necking was considered to be the failure point at which the maximum engineering tensile stress (σ_{ut}) was measured. The

strain values corresponding to the measured values of σ_{ut} were considered to be the maximum tensile strains (ε_{ut}). For 20% and 40% hemp–HDPE, the failure criterion was a brittle fracture on the macro scale; the maximum tensile stress before failure was assumed to be σ_{ut}, and its corresponding engineering tensile strain was assumed to be ε_{ut}. For both of the elastic and the brittle failure modes, Young's Modulus (E) was defined as the tangent elastic modulus of the engineering stress-strain curve.

4.3 EFFECT OF STRAIN RATE AND FIBER VOLUME FRACTION

The results of σ_{ut} from the monotonic tensile tests for the unreinforced HDPE as well as the short-hemp-reinforced composites are shown in Figure 4.2. The bars indicate the range of test results for each condition. Figure 4.2 shows consistent general behaviour at which the increase of strain rate ($\dot{\varepsilon}$) increases the resulting σ_{ut}. This phenomenon is known as strain rate hardening, in which the strength of the material is increased by increasing the strain rate ($\dot{\varepsilon}$) or forming speed [9]. On the other hand, there is a slight increase in the value of σ_{ut} when the hemp fiber weight percentage is increased. Additionally, Figure 4.2 demonstrates that σ_{ut}-$\dot{\varepsilon}$ relationships for the unreinforced HDPE and the developed composites are parallel.

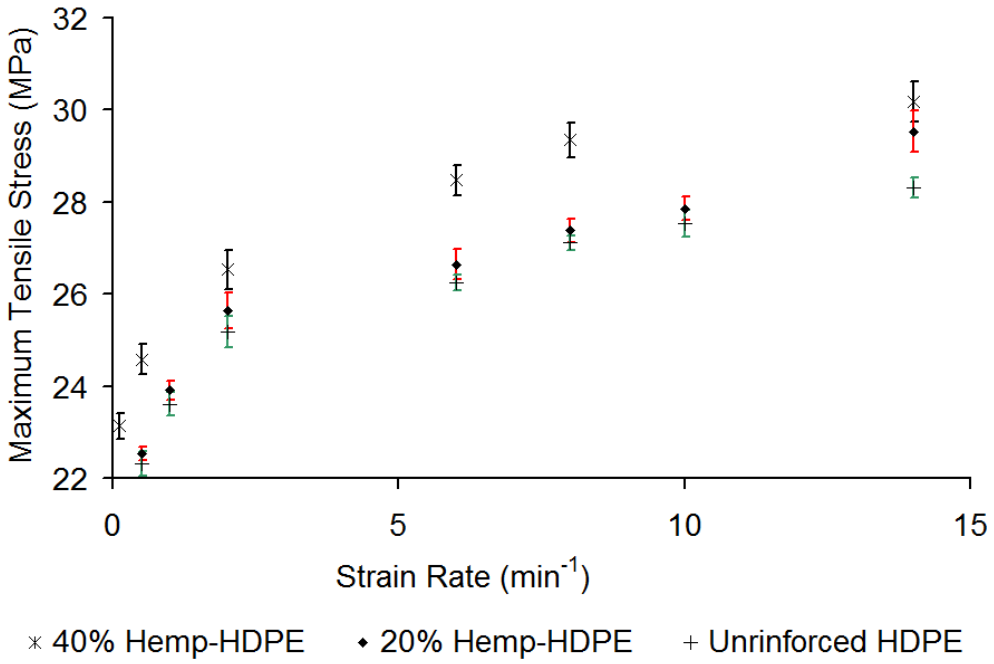

Fig. 4.2 The effect of strain rate on the maximum tensile stress (σ_{ut}) of unreinforced HDPE, 20% hemp-HDPE and 40% hemp-HDPE.

As a result of strain rate hardening, the values of tangent Young's modulus (E) of the unreinforced HDPE and the reinforced composites increase as $\dot{\varepsilon}$ increases, as shown in Figure 4.3. A significant increase in E was recorded as a result of increasing the hemp fiber weight percentage. Similar to σ_{ut}-$\dot{\varepsilon}$ relationship, Figure 4.3 shows that E-$\dot{\varepsilon}$ relationships for unreinforced HDPE and the tested short hemp-HDPE composites behave in a parallel fashion.

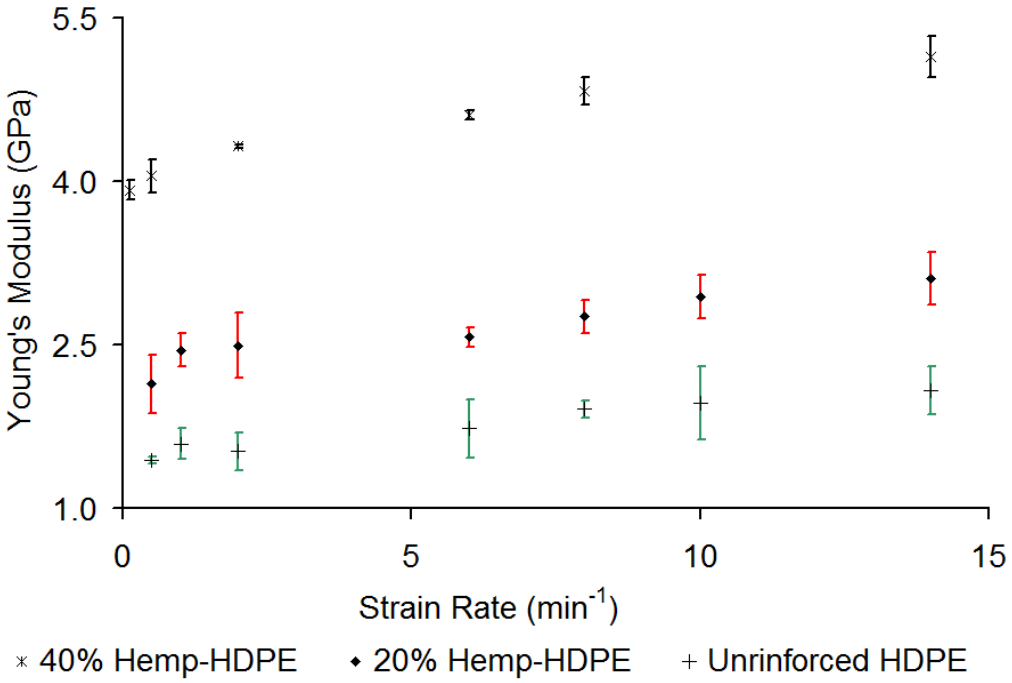

Fig. 4.3 The effect of strain rate on the Young's modulus (E) of unreinforced HDPE, 20% hemp-HDPE and 40% hemp-HDPE.

In contrast to the effect of $\dot{\varepsilon}$ on both σ_{ut} and E, the increasing of strain rate $\dot{\varepsilon}$ reduces the value of the maximum tensile strain (ε_{ut}), as shown in Figure 4.4. This reduction in the elongation is expected as a result of the increase in E and σ_{ut} (i.e. as a result of strain rate hardening). Figure 4.4 shows that, for unreinforced HDPE and HDPE-composite samples, the maximum tensile strain (ε_{ut}) decreases when $\dot{\varepsilon}$ is increased. This effect can be attributed to the increase that occurs in both σ_{ut} and E as a result of increasing $\dot{\varepsilon}$; additionally, there is a parallel trend in the curves in Figure 4.4 in a manner similar to the σ_{ut}-$\dot{\varepsilon}$ and E-$\dot{\varepsilon}$ relationships.

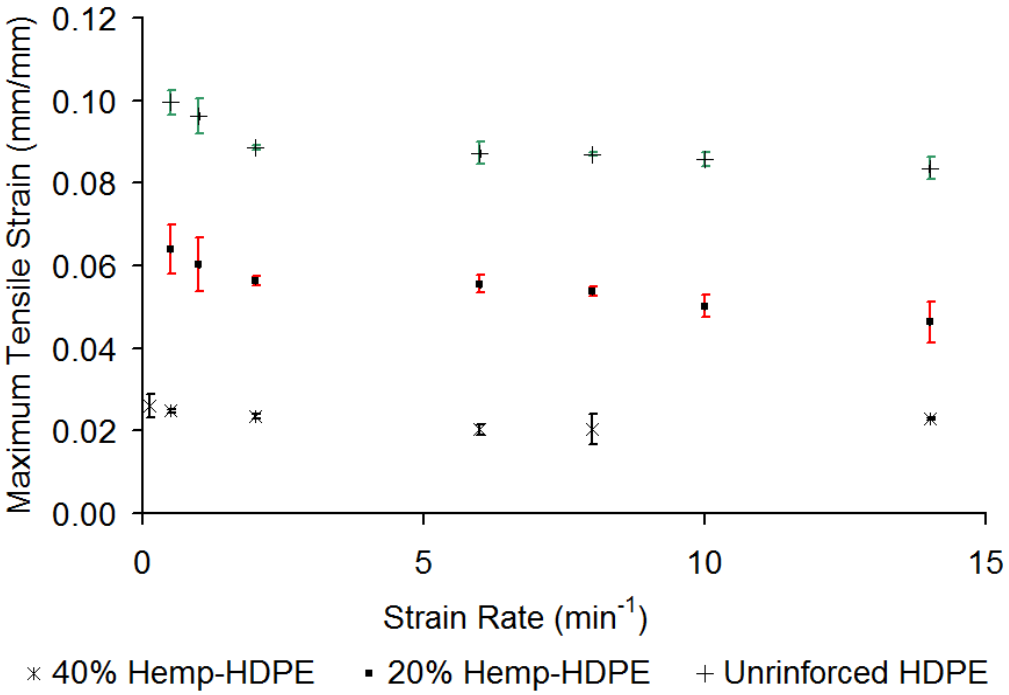

Fig. 4.4 The effect of strain rate on maximum tensile strain (ε_{ut}) of unreinforced HDPE, 20% hemp-HDPE and 40% hemp-HDPE.

4.4 EFFECT OF MOISTURE ABSORPTION

Figure 4.3 shows the effect of moisture absorption on σ_{ut} for 20% hemp-HDPE at different values of $\dot{\varepsilon}$. Hemp-bast fibers are natural fibers that have a hydrophilic nature [2, 10-13]. Moisture absorption causes natural fibers to swell [2], which increases the interfacial stress between the fiber and the matrix and can cause fibers to separate from the matrix; as well, absorbed moisture weakens natural fibers [2, 10, 13]. Therefore, after moisture was absorbed, σ_{ut} values of 20% hemp-HDPE dropped even below the σ_{ut} values of the unreinforced HDPE, as shown in Figure 4.3.

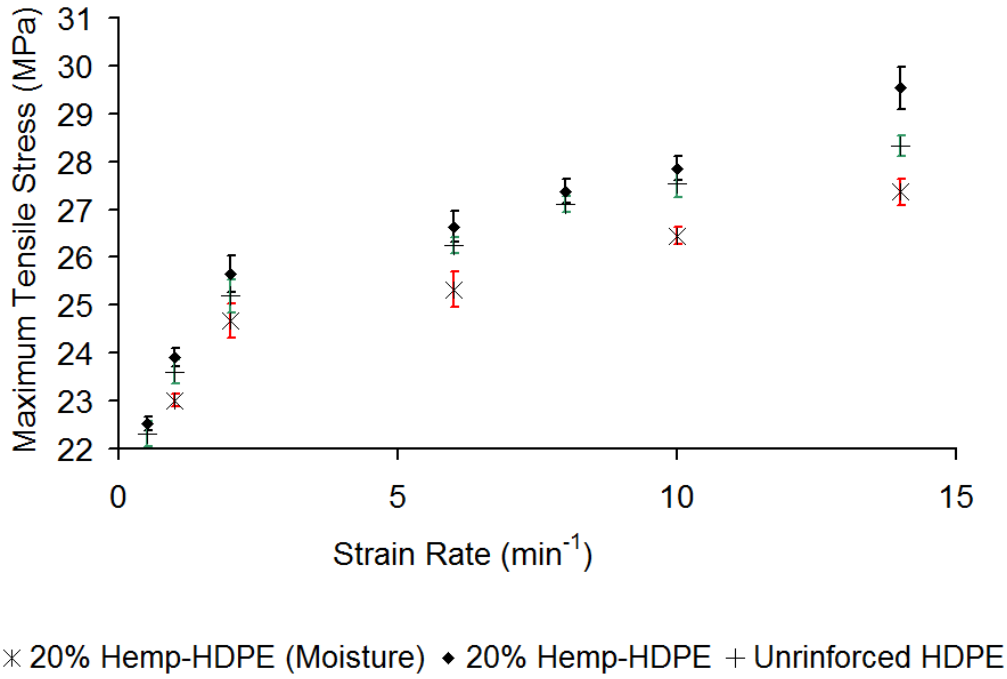

Fig. 4.5 The effect of strain rate on the maximum tensile stress (σ_{ut}) of unreinforced HDPE, 20% hemp-HDPE with and without moisture.

Figure 4.6 shows the effect of moisture absorption on the ε_{ut} of 20% hemp-HDPE at different values of $\dot{\varepsilon}$. The ε_{ut} values of 20% hemp-HDPE after 35 days in water were higher than the original ε_{ut} values of 20% hemp-HDPE, likely as a result of the weakened interfacial fibre/matrix bonding due to swelling as well as the degradation of fiber strength due to moisture absorption. On the other hand, Figure 4.7 shows that E did not change for 20% hemp-HDPE after immersing in water for 35 days.

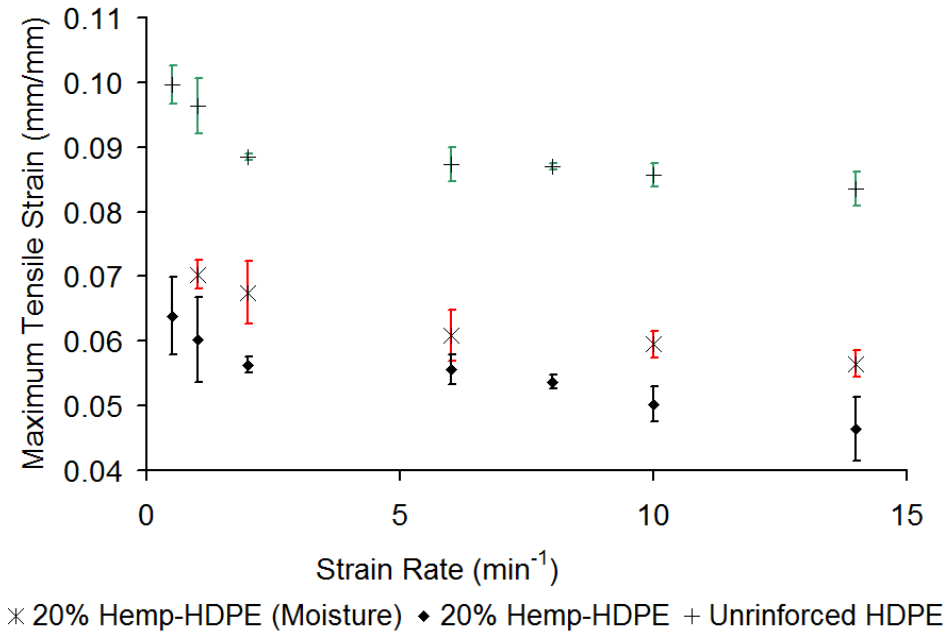

Fig. 4.6 The effect of strain rate on maximum tensile strain (ε_{ut}) of unreinforced HDPE, 20%hemp-HDPE with and without moisture.

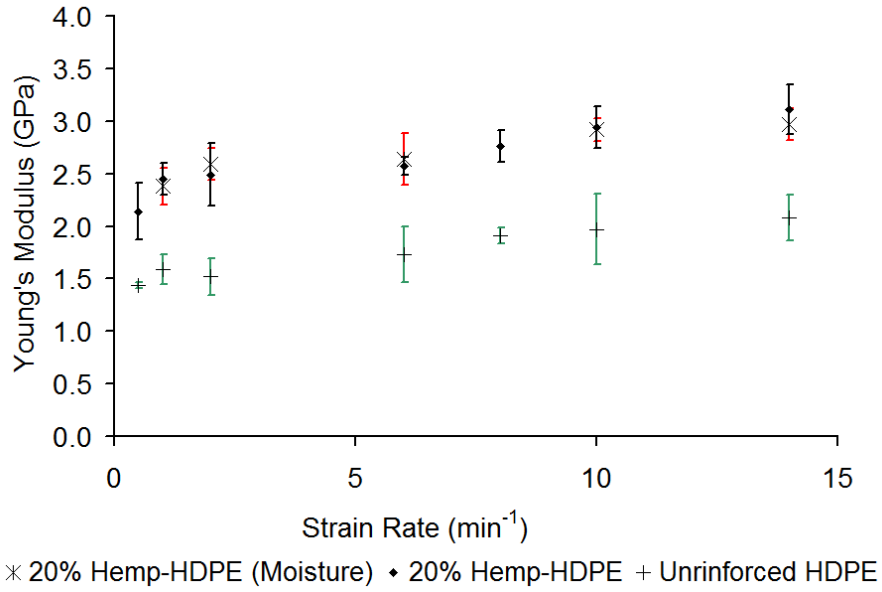

Fig. 4.7 The effect of strain rate on the Young's modulus (E) of unreinforced HDPE, 20% hemp-HDPE with and without moisture.

4.5 MODELING OF STRAIN RATE HARDENING

4.5.1 Model Development

4.5.1.1 Effect of strain rate on maximum tensile stress

For both unreinforced and reinforced HDPE, Figures 4.2 and 4.3 show that σ_{ut}-$\dot{\varepsilon}$ relationships, without and with moisture effect, form a set of convex parallel curves. Therefore, one single equation can be used to represent all curves in both Figures 4.2 and 4.3. To simulate this type of behaviour, the non-linear one-dimensional interpretation of Norton-Hoff rheology model for viscoplastic material can be applied [14-18], as the matrix of HDPE has a viscoplastic properties [19]. The viscoplastic rheology model of Norton-Hoff can be represented as follows:

$$\sigma_{ut} = k_{\sigma}(\dot{\varepsilon})^{m_{\sigma}} \quad \text{.....} \quad \textbf{4.1}$$

where σ_{ut} is the maximum tensile stress (MPa) at strain rate $\dot{\varepsilon}$ (min^{-1}) and constant temperature, k_{σ} is a material constant ($MPa.min^{m_{\sigma}}$), and m_{σ} is a behaviour index for σ_{ut} (dimensionless). k_{σ} and m_{σ} can be considered to be functions of hemp fiber volume fraction (v_f).

The Harris mechanistic model, part of yield models [20, 21], can be applied to represent the relationships amongst the calculated k_{σ} and m_{σ} values and v_f [7, 8]. However, even though the Harris model is highly suited mechanistic model to simulate the effect of v_f on both monotonic and cyclic behaviour of short-natural-fiber-reinforced composites [7, 8], a more simplified model can be proposed for monotonic applications to reduce the number of parameters required for the Harris model; hence, a simplified linear model can be proposed to simulate the effect of v_f on the monotonic behaviour of natural-fiber-reinforced polymer. In this proposed linearized model, k_{σ} and m_{σ} can be represented as follows:

$$k_\sigma = k_{\sigma o}(1 + a_{k_\sigma} v_f) \quad \text{..... 4.2}$$

where $k_{\sigma o}$ is k_σ for the matrix polymer ($MPa.\min^{m_\sigma}$), v_f is the hemp fiber volume fraction, and a_{k_σ} is a dimensionless matrix-dependent parameter; and

$$m_\sigma = m_{\sigma o}(1 + a_{m_\sigma} v_f) \quad \text{..... 4.3}$$

where $m_{\sigma o}$ is m_σ for the matrix polymer (dimensionless), and a_{m_σ} is a dimensionless matrix-dependent parameter.

The estimated solutions of parameters in the linearized model system are presented in Tables 4.1 and 4.2.

Table 4.1 Values of the parameters $k_{\sigma o}$ and a_{k_σ} from equation 4.2:

Parameter	Estimated Value
$k_{\sigma o}$	23.6 ($MPa.\min^{m_\sigma}$)
a_{k_σ}	0.287 (dimensionless)

Table 4.2 Values of the parameters $m_{\sigma o}$ and a_{m_σ} from equation 4.3:

Parameter	Estimated Value
$m_{\sigma o}$	0.066 (dimensionless)
a_{m_σ}	0.822 (dimensionless)

The effect of moisture absorption can be introduced as a coefficient that is expected to be a function of matrix crystallinity, natural fiber volume fraction, and moisture absorption rate. Because hemp fibers are the main cause of moisture absorption, the moisture coefficient will be assumed to affect v_f terms in equations

4.2 and 4.3; hence, these equations can be rewritten as shown in equations 4.4 and 4.5, respectively:

$$k_\sigma = k_{\sigma o}(1 + a_{k_\sigma} w_{k_\sigma} v_f) \quad \text{..... 4.4}$$

where w_{k_σ} is a moisture absorption coefficient (dimensionless). For 20% hemp-HDPE immersed in water for 35 days $w_{k_\sigma} \approx$ -0.114. For dry conditions (no moisture), w_{k_σ} is assumed to be 1.00 for this analysis.

$$m_\sigma = m_{\sigma o}(1 + a_{m_\sigma} w_{m_\sigma} v_f) \quad \text{..... 4.5}$$

where w_{m_σ} is a moisture absorption coefficient (dimensionless). For 20% hemp-HDPE immersed in water for 35 days, $w_{m_\sigma} \approx$ -1.881. For dry conditions, w_{m_σ} is assumed to be 1.00.

4.5.1.2 Effect of strain rate on Young's modulus

Figures 4.3 and 4.7 reveal that E-$\dot{\varepsilon}$ relationships form a set of convex curves for both unreinforced and reinforced HDPE, without and with the effect of moisture, respectively. For convex curves, a power mechanistic model, similar to the one used in equation 4.1, can be used to simulate E-$\dot{\varepsilon}$ relationship [21] as follows:

$$E = k_E(\dot{\varepsilon})^{m_E} \quad \text{..... 4.6}$$

where E is Young's modulus (GPa) at strain rate $\dot{\varepsilon}$ (min^{-1}) and constant temperature, k_E is a material constant ($GPa.min^{m_E}$), and m_E is the dimensionless power law index for E.

Because all of the E-$\dot{\varepsilon}$ curves in Figures 4.3 and 4.7 can be assumed to be parallel to each other, equation 4.6 can be used to represent this family of curves. As well, k_E and m_E in equation 4.6 can be assumed to be functions of the hemp fiber volume fraction (v_f) as well as the moisture absorption effect. Using a linear model, k_E and m_E can be represented as follows:

$$k_E = k_{Eo}(1 + a_{k_E} w_{k_E} v_f) \quad \textbf{4.7}$$

where k_{Eo} is k_E for the matrix polymer, a_{k_E} is a dimensionless matrix-dependent parameter, and w_{k_E} is a dimensionless moisture absorption coefficient; and

$$m_E = m_{Eo}(1 + a_{m_E} w_{m_E} v_f) \quad \textbf{4.8}$$

where m_{Eo} is m_E for the matrix polymer, a_{m_E} is a dimensionless matrix-dependent parameter, and w_{m_E} is a dimensionless moisture absorption coefficient. The estimated values of the parameters in equations 4.7 and 4.8 are in Tables 4.3 and 4.4, respectively.

Table 4.3 Values for parameters k_{Eo} and a_{k_E} in equation 4.7:

Parameter	Estimated Value
k_{Eo}	1.36 ($GPa.\min^{m_E}$)
a_{k_E}	6.82 (dimensionless)
w_{k_E} (w_{k_E} assumed to be 1.00 in dry testing conditions)	≈ 1.00, because the change in E behaviour was insignificant after the specimens were immersed in water

Table 4.4 Values for parameters m_{Eo} and a_{m_E} in equation 4.8:

Parameter	Estimated Value
m_{Eo}	0.112 (dimensionless)
a_{m_E}	-1.53 (dimensionless)
w_{m_E} (w_{m_E} is assumed to be 1.00 in dry testing conditions)	≈ 1.00, because the change in E behaviour was insignificant after the specimens were immersed in water

4.5.1.3 Effect of strain rate on maximum tensile strain

Similar to the relationships discussed previously, the ε_{ut} - $\dot{\varepsilon}$ relationship can be represented using the same power law expression:

$$\varepsilon_{ut} = k_{\varepsilon}(\dot{\varepsilon})^{m_{\varepsilon}} \quad \text{.....} \quad \textbf{4.9}$$

where ε_{ut} is the strain corresponding to σ_{ut} at strain rate $\dot{\varepsilon}$ (min^{-1}) and under a constant temperature, and, as previously defined, k_{ε} is a material constant ($min^{m_{\varepsilon}}$), and m_{ε} is a dimensionless power law index.

Like the previous relationships found for σ_{ut}-$\dot{\varepsilon}$ and E-$\dot{\varepsilon}$; equation 4.9 can be used to represent the family of curves in either Figure 4.4 or Figure 4.6. The corresponding linearized model yields the following expressions for k_{ε} and m_{ε}:

$$k_{\varepsilon} = k_{\varepsilon o}(1 + a_{k_{\varepsilon}} w_{k_{\varepsilon}} v_f) \quad \text{.....} \quad \textbf{4.10}$$

and

$$m_{\varepsilon} = m_{\varepsilon o}(1 + a_{m_{\varepsilon}} w_{m_{\varepsilon}} v_f) \quad \text{.....} \quad \textbf{4.11}$$

For 20% hemp-HDPE immersed in water for 35 days, the estimated values for moisture absorption coefficients in equations 4.10 and 4.11 are as follows: $\omega_{k_\varepsilon} \approx 0.616$; $\omega_{m_\varepsilon} \approx 1.384$; $w_{k_\varepsilon} \approx 0.739$; $w_{m_\varepsilon} \approx -9.338$, respectively. For dry conditions, all of the moisture absorption coefficients in equations are assumed to take the value of 1.00. Tables 4.5 and 4.6 represent the estimated values for the rest of the parameters in equations 4.10 and 4.11.

Table 4.5 Values for parameters $k_{\varepsilon o}$ and a_{k_ε} in equation 4.10:

Parameter	Estimated Value
$k_{\varepsilon o}$	0.094 (min^{m_ε})
a_{k_ε}	-2.50 (dimensionless)

Table 4.6 Values for parameters $m_{\varepsilon o}$ and a_{m_ε} in equation 4.11:

Parameter	Estimated Value
$m_{\varepsilon o}$	-0.060 (dimensionless)
a_{m_ε}	-0.278 (dimensionless)

4.5.2 Generalized Comprehensive Model

As illustrated in equations 4.1, 4.6 and 4.9, the form of the power law can be used to represent the effect of the strain rate hardening on the tested composites. Therefore, a general comprehensive power law model can be introduced to integrate all of the developed models in one general model; this general model can simulate the relationship between $\dot{\varepsilon}$ and the mechanical properties of a viscoplastic matrix reinforced by short natural fibers; the general power law model can be represented as follows:

$$\Psi = k_\Psi (\dot{\varepsilon})^{m_\Psi} \quad \text{..... 4.12}$$

where $\dot{\varepsilon}$ is the strain rate (min^{-1}), Ψ is an arbitrary variable representing the mechanical properties (i.e. σ_{ut}, ε_{ut} and E), k_Ψ is a composite parameter that is a function of the matrix and the short natural fiber volume fraction (v_f), and m_Ψ is the power law index that is defined as a function of the matrix polymer and v_f. The dimensions of Ψ, k_Ψ and m_Ψ, for different mechanical properties, are illustrated in Table 4.7. The parameters and the variables in Table 4.7 were defined in the previous section.

Using the simplified linearized form, the parameters k_Ψ and m_Ψ in equation 4.12 can be represented as a function of the matrix polymer, v_f , and the moisture absorption effect, as follows:

$$\Lambda\Big|_{\substack{\Lambda=k_\sigma,\, m_\sigma,\, k_E,\, m_E,\\ k_\varepsilon,\, m_\varepsilon}} = \Lambda_o \left(1 + a_\Lambda w_\Lambda v_f\right) \quad \textbf{4.13}$$

where Λ is a variable that represents k_σ, m_σ, k_E, m_E, k_ε or m_ε, Λ_o is the value of variable Λ for the used matrix, a_Λ is a matrix-dependent parameter, and w_Λ is a moisture absorption coefficient. The variables and parameters represented by Λ, a_Λ and w_Λ are tabulated in Table 4.8, and they were defined in the previous section.

Table 4.7 Variables and parameters represented by Ψ, k_Ψ and m_Ψ:

Variable Ψ	Parameter k_Ψ	Power Law Index m_Ψ
σ_{ut} (MPa)	k_σ ($MPa.\min^{m_\sigma}$)	m_σ (dimensionless)
E (GPa)	k_E ($GPa.\min^{m_E}$)	m_E (dimensionless)
ε_{ut} (dimensionless (mm/mm))	k_ε ($\min^{m_\varepsilon}$)	m_ε (dimensionless)

Table 4.8 Variables and parameters represented by Λ, Λ_o, a_Λ and w_Λ:

Variable Λ	Parameter Λ_o	Parameter a_Λ	Parameter w_Λ
k_σ $(MPa.\min^{m_\sigma})$	$k_{\sigma o}$ $(MPa.\min^{m_\sigma})$	a_{k_σ} (dimensionless)	w_{k_σ} (dimensionless)
m_σ (dimensionless)	$m_{\sigma o}$ (dimensionless)	a_{m_σ} (dimensionless)	w_{m_σ} (dimensionless)
k_E $(GPa.\min^{m_E})$	k_{Eo} $(GPa.\min^{m_E})$	a_{k_E} (dimensionless)	w_{k_E} (dimensionless)
m_E (dimensionless)	m_{Eo} (dimensionless)	a_{m_E} (dimensionless)	w_{m_E} (dimensionless)
k_ε $(\min^{m_\varepsilon})$	$k_{\varepsilon o}$ $(\min^{m_\varepsilon})$	a_{k_ε} (dimensionless)	w_{k_ε} (dimensionless)
m_ε (dimensionless)	$m_{\varepsilon o}$ (dimensionless)	a_{m_ε} (dimensionless)	w_{m_ε} (dimensionless)

4.5.3 Model Comparison with Experiments

Figures 4.8 and 4.9 represent the values of σ_{ut} from experiments and from the developed power law model. There is a good match between σ_{ut} measured from experiments and σ_{ut} calculated from the model for unreinforced HDPE and 40% hemp-HDPE, shown in Figure 4.8, and 20% hemp-HDPE with and without moisture, shown in Figure 4.9.

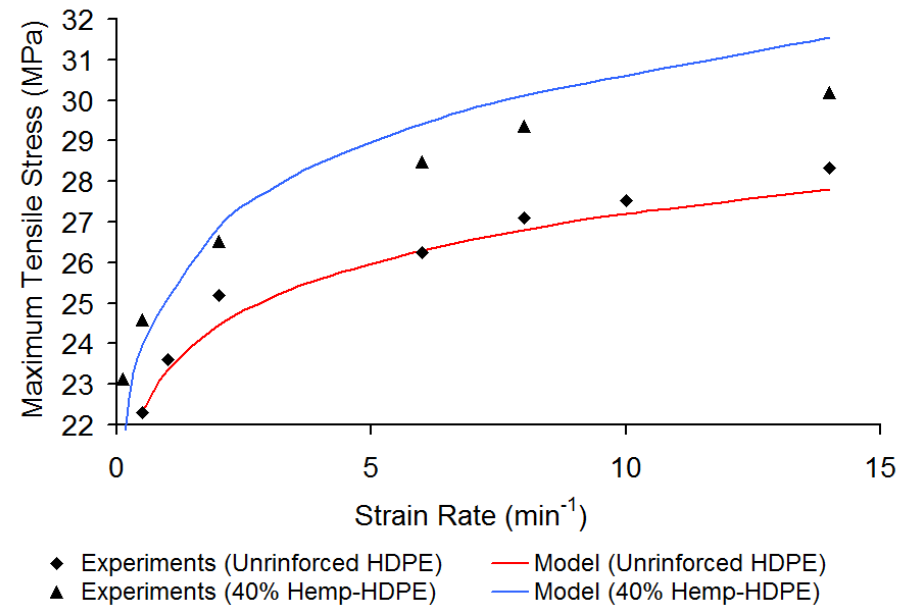

Fig. 4.8 σ_{ut} from experiments and calculated from the power law for unreinforced HDPE and 40% hemp-HDPE.

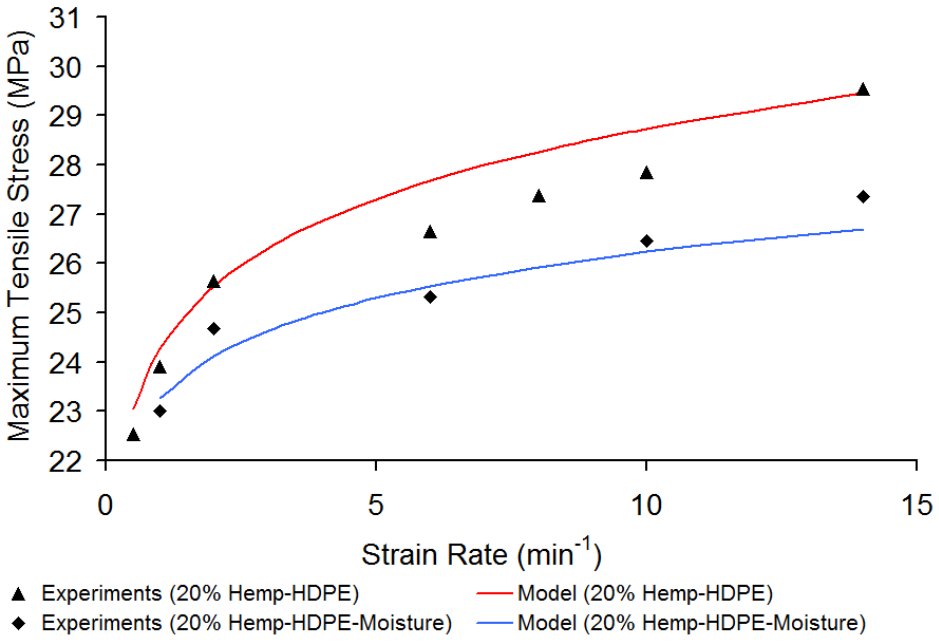

Fig. 4.9 σ_{ut} from experiments and calculated from the power law for 20% hemp-HDPE with and without moisture.

For Yong's modulus (E) modeling shown in Figure 4.10, there is a very close match between the values of E measured from experiments and the values calculated from the power law model for unreinforced HDPE and 40% hemp-HDPE. As it was discussed previously, there was no significant change in the values of E after absorbing moisture; therefore, the values of E were calculated from the model did not changed after absorption. As a result, one simulation curve represented the behaviour of E for 20% hemp-HDPE before and after the moisture absorption, as shown in Figure 4.11; this is due to the assumption that the moisture coefficient did not change in the model either before or after the absorbed moisture (i.e. it remained equal to one).

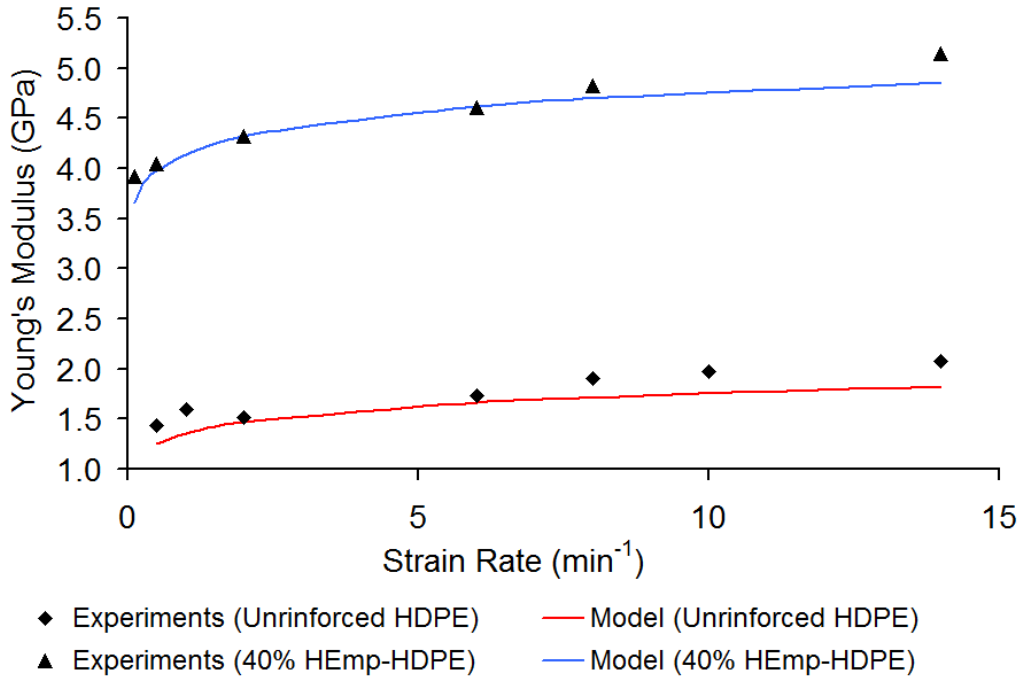

Fig. 4.10 E from experiments and calculated from the power law for unreinforced HDPE and 40% hemp-HDPE.

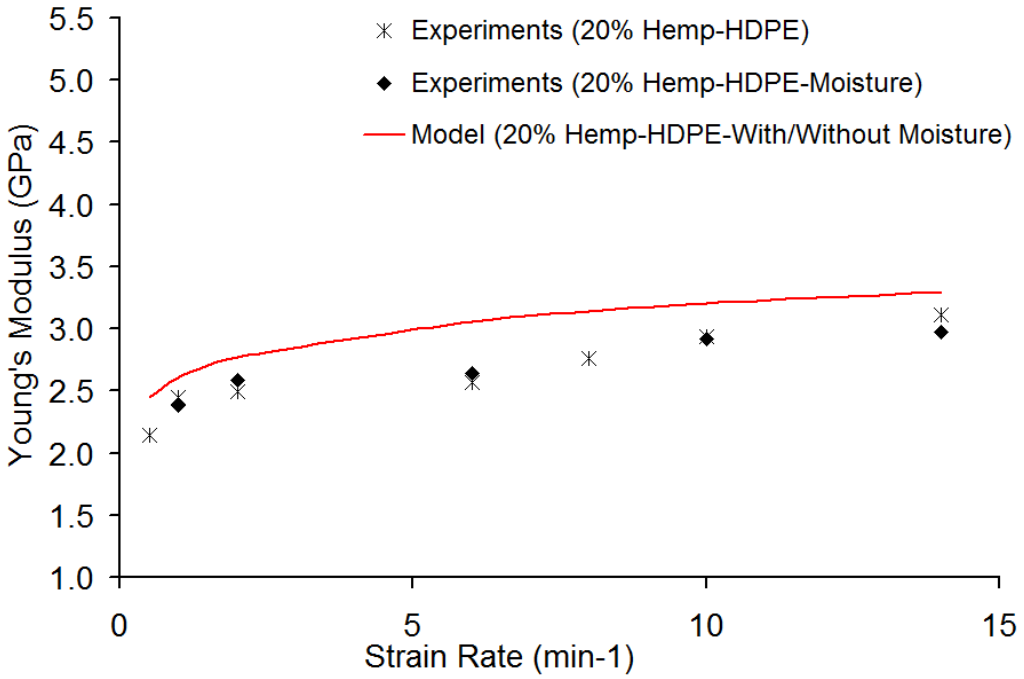

Fig. 4.11 E from experiments and calculated from the power law for 20% hemp-HDPE with and without moisture.

Figures 4.12 and 4.13 show a very good match between the values of ε_{ut} measured from experiments and the values calculated from the developed model for unreinforced HDPE and 40% hemp-HDPE as well as 20% hemp-HDPE with and without moisture, respectively,

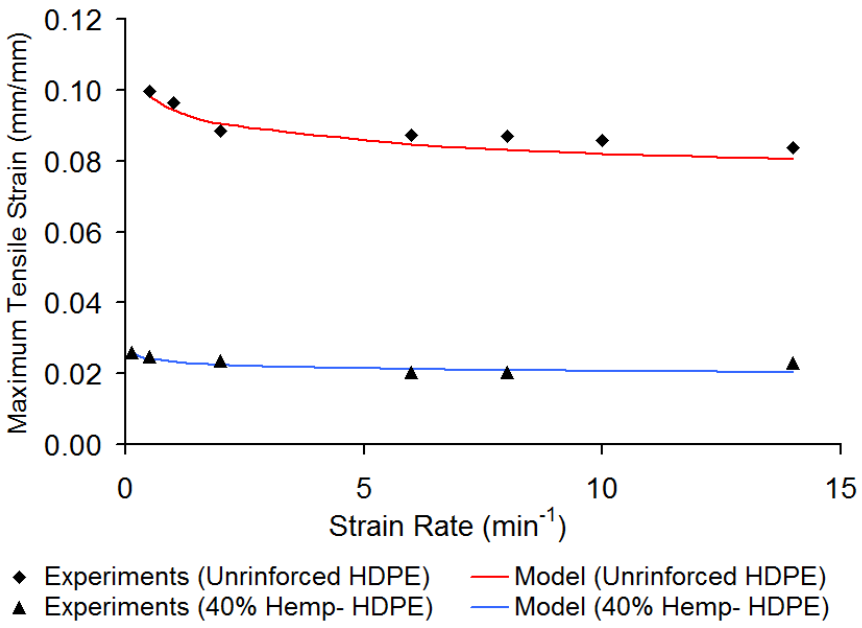

Fig. 4.12 ε_{ut} from experiments and calculated from the power law for unreinforced HDPE and 40% hemp-HDPE.

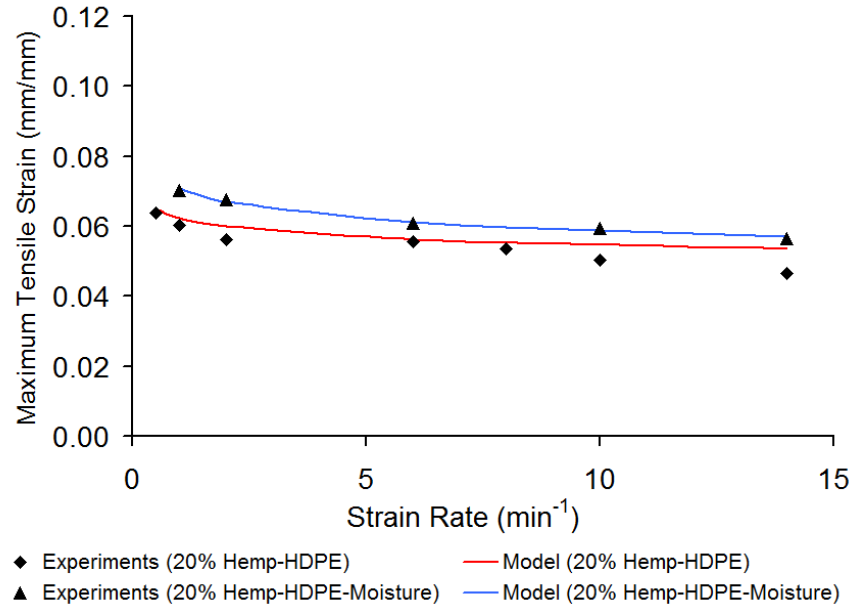

Fig. 4.13 ε_{ut} from experiments and calculated from the power law for 20% hemp-HDPE with and without moisture.

There are some limited deviations between the simulated date from the developed power law model and the date from the experiments. This deviation can be caused as a result of many factors that act individually or interactively to produce these deviations. These factors are: the randomization level of the natural fibers within the matrix; the random orientation and complex geometry of the short natural fibers within the matrix; and the error due to the accumulative approximation taking place during the nonlinear regression process used to evaluate the parameters of the developed model.

4.6 CONCLUSIONS

In this study, the effect of the strain rate ($\dot{\varepsilon}$) on the mechanical properties, maximum tensile stress (σ_{ut}) and its corresponding strain (ε_{ut}) along with Young's modulus (E), of short-hemp-fiber-reinforced HDPE was experimentally investigated and modeled under normal and wet conditions.

Both unreinforced HDPE and hemp-HDPE composites showed a strain rate hardening behaviour as $\dot{\varepsilon}$ increased.

A generalized power law model was developed to simulate the relationship of σ_{ut}, ε_{ut} and E with $\dot{\varepsilon}$. The results from the developed model had a very good match with the experiments for both the unreinforced HDPE and the hemp-HDPE composites. As the developed model is validated for different types of polymer/fiber combinations as well as different loading conditions, this model will enable the effect of $\dot{\varepsilon}$ and v_f as well as moisture absorption to be incorporated into other empirical or physics-based models to predict monotonic or cyclic behaviours of these type of composites. In this way, new products of natural-fiber-reinforced composites can be selected appropriately for reliable product design.

CHAPTER 5: UNIAXIAL TENSILE BEHAVIOUR MODELING OF NATURAL-FIBER-REINFORCED POLYMER USING NORMALIZED STRESS-STRAIN CURVES[§]

ABSTRACT

The monotonic uniaxial tensile behavior of hemp-fiber-reinforced High Density Polyethylene (HDPE) was investigated at different values of hemp fiber volume fraction (v_f) and strain rate ($\dot{\varepsilon}$). A normalized stress-strain family of curves was generated. An exponential normalized monotonic model was developed. A general uniaxial monotonic model was developed from the normalized model to simulate the stress-strain relationship at different values of $\dot{\varepsilon}$ and v_f. A modified Harris mechanistic model and a linear model were proposed to incorporate the effect of v_f and the absorbed moisture into the developed model.

KEYWORDS

Natural Fiber Composites, Normalized Stress-Strain, Strain Rate, Monotonic Modeling, Fiber Volume Fraction, Moisture Effect.

[§] This chapter is a modified version of a paper that was published as Ahmed Fotouh, J. D. Wolodko, M. Lipsett, "Uniaxial Tensile Behaviour Modeling of Natural-Fiber-Reinforced Viscoplastic Polymer Using Normalize Stress-Strain Curves", Journal of Material Composites , Aug. 21st, 2014, DOI: 10.1177/0021998314547427.

5.1 INTRODUCTION

Natural-Fiber-Reinforced Polymer (NFRP) has a very promising industrial future, especially because of the many advantages that natural fibers have over synthetic fibers [1-5]. However, in order to ensure the commercial viability of NFRP, engineering models simulating its mechanical behaviour need to be developed and validated. Additionally, the effect of moisture absorption forms another potential challenge to the expansion of NFRP applications [5-13]. Therefore, in order to permit this expansion, more research should be undertaken to study and model the mechanical behaviour of NFRP under normal and different environmental conditions.

In this study, a generalized monotonic semi-analytical model is developed to simulate the uniaxial tensile behaviour of hemp-fiber-reinforced HDPE using normalized engineering stress-strain curves to eliminate the effect of strain rate ($\dot{\varepsilon}$). Later, the effect of $\dot{\varepsilon}$ is reintroduced to the model using different power models that represent the proposed relationships between $\dot{\varepsilon}$ and the maximum engineering tensile strength (σ_{ut}) as well as the corresponding strain (ε_{ut}). As a result, a generalized semi-analytical stress-strain model is developed to simulate the monotonic behaviour of NFRP. The new developed model takes into consideration the effect of: (1) strain rate, $\dot{\varepsilon}$; (2) natural fiber volume fraction, v_f; and (3) absorbed moisture on the monotonic behaviour of NFRPs. The developed model can serve as an engineering design tool that designers can use to incorporate NFRPs into reliable and well designed products.

5.2 TESTING PROCEDURES AND MODELING CRITERIA

5.2.1 Testing Materials and Procedures

The short hemp bast fibers and High Density Polyethylene (HDPE HD306) were compounded using a Haake Rheomix PTW 24/40 twin screw extruder at two

fiber weight percentages of 20% and 40%, corresponding to fiber volume fractions (v_f) of 13.5% and 30.1%, respectively. Table 5.1 represents the physical and mechanical properties of the HDPE used as a matrix.

Table 5.1 Physical and mechanical properties of the HDPE matrix material:

Property	HDPE	Test Method
Density	0.943 ±0.02 g/cm^3 (5 tested samples)	ASTM D1505
Melt mass flow rate (from manufacturer table) (190^{o}C/2.16kg)	7.5 g/10min	ASTM D1238
Tensile strength at yield (50mm/min)	24 ±0.26 MPa (3 tested samples)	ASTM D638
Stiffness (Young's modulus) (50mm/min)	1.8 ±0.143 GPa (3 tested samples)	ASTM D638
Elongation at yield (50mm/min)	9 ±0.43 % (3 tested samples)	ASTM D638

Tensile test specimens were designed according to ASTM D638 Type 1 with 3 mm thickness and 50 mm gauge length, as shown in Figure 5.1. These specimens were manufactured using an injection moulding process. Tensile tests were carried out at different engineering strain rates ($\dot{\varepsilon}$) of 0.13, 0.50, 1.00, 2.00, 6.00, 8.00, 10.00 and 14.00 min^{-1}, corresponding to 6.5, 25, 50, 100, 300, 400, 500 and 700 mm/min of elongation speeds, respectively. An extensometer with a gage length of 50 mm was attached to the test specimen during the tensile tests to measure the strain that developed during the tests. Figure 5.2 shows the loading set for one of the uniaxial tensile test experiments. Three samples were used for each tensile test of the unreinforced HDPE; however; five samples were used for each tensile test of HDPE biocomposites. The moisture effect on the mechanical behaviour was investigated using 20% hemp-HDPE test specimens that were immersed in water for 35 days.

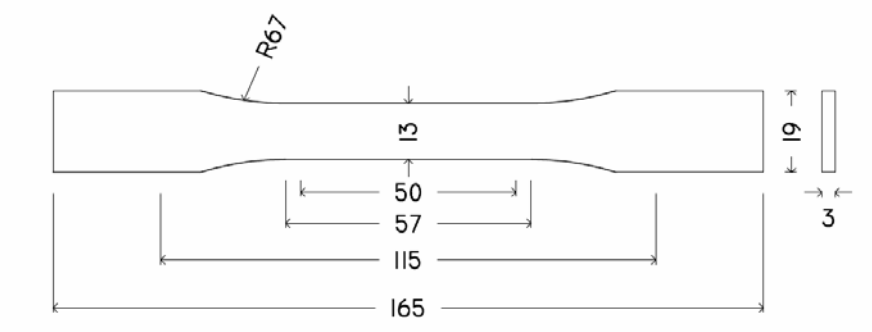

Fig. 5.1 Schematic diagram of the tensile test specimen configurations.

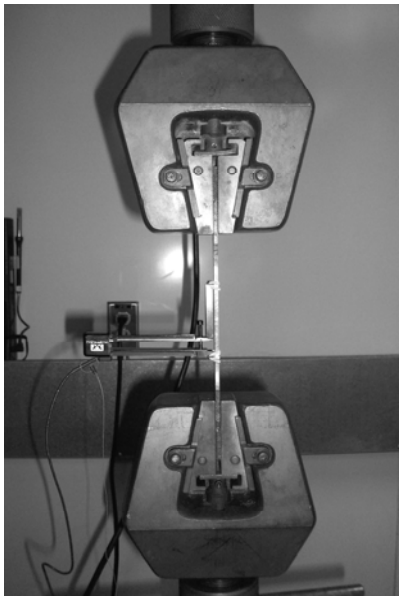

Fig. 5.2 Loading set for a uniaxial tensile test showing the extensometer mounted on the tensile test specimen.

5.2.2 Failure and Modeling Criteria

The failure criteria were chosen based on observed behaviour. For unreinforced HDPE, which failed in a ductile manner, the selected failure criterion was the point of necking, and the maximum engineering tensile strength (σ_{ut}) and its corresponding strain (ε_{ut}) were measured at this necking point, as shown in Figure 5.3-a.

However, for the 20% and 40% hemp-HDPE, the failure criterion was fracture, and σ_{ut} and ε_{ut} were measured at the pint with maximum stress before fracture, as shown in Figure 5.4-a. For investigation and modeling purposes, the whole engineering stress-strain curves in Figures 5.3-a and 5.4-a were reduced to the simulation zones only, as shown in Figures 5.3-b and 5.4-b, respectively. These stress-strain simulation zones were the zones that were analyzed and modeled in this study. The tangent Young's modulus (E) was evaluated using the tangent linear elastic modulus, and it was considered the stiffness measure of the tested materials.

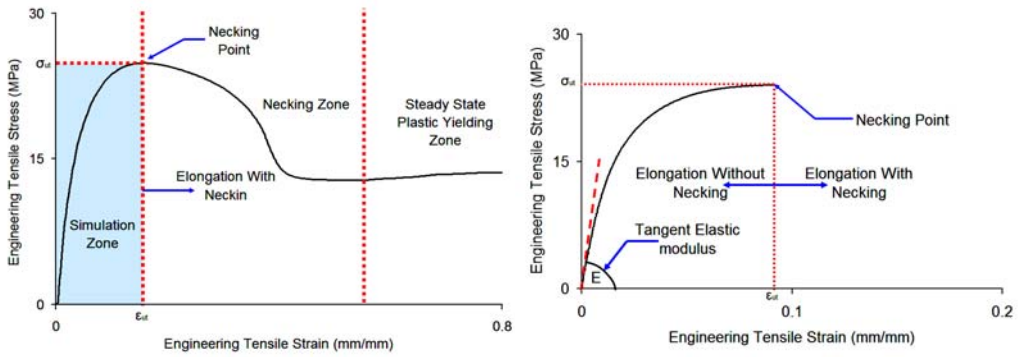

(a) **(b)**

Fig. 5.3 (a) A part of typical engineering stress-strain diagram and (b) its reduced simulation zone for unreinforced HDPE at an elongation rate of 1 min^{-1}.

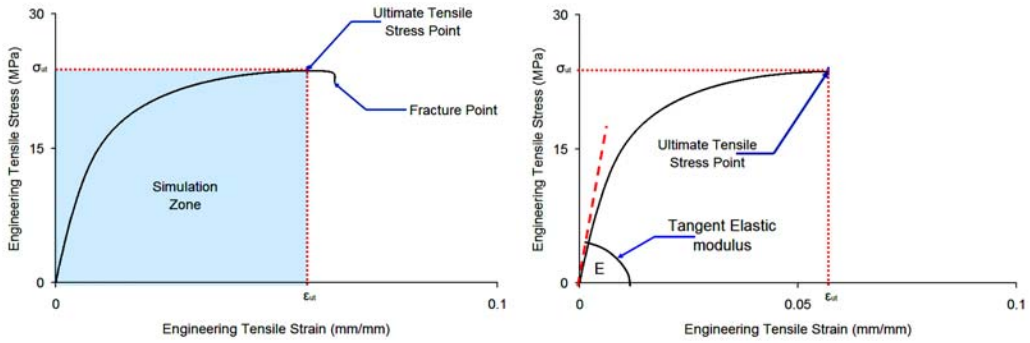

(a) **(b)**

Fig. 5.4 (a) A typical engineering stress-strain diagram and (b) its reduced simulation zone for 20% hemp-HDPE at an elongation rate of 1 min^{-1}.

5.3 NORMALIZED UNIAXIAL STRESS-STRAIN BEHAVIOUR

Form the conducted monotonic tensile tests, and according the failure criteria stated previously, Table 5.2 illustrates the measured values of σ_{ut}, ε_{ut} and E of the tested materials at different values of strain rate ($\dot{\varepsilon}$) for the unreinforced HDPE, 20% hemp-HDPE, 40% hemp HDPE and 20% hemp-HDPE immersed in water for 35 days. The results in Table 5.2 show that adding hemp fibers increased the values of σ_{ut} and E, while the over all values of ε_{ut} was decreased; on the other hand, the moisture absorption reduced the values of σ_{ut} as a result of the weakening effect of the absorbed moisture on the reinforcing hemp fibers [14].

By normalizing the curves in Figure 5.5 (i.e. dividing each point in the stress-strain curve by its σ_{ut} and its corresponding ε_{ut}), all curves were combined in one normalized curve (shown in Figure 5.6). Therefore, it can be concluded that the matrix material is homogeneous, and the effect of strain rate can be eliminated through the normalization of stress-strain curves. In Figure 5.5, the strength (σ_{ut}) and the stiffness (E) (i.e. Young's modulus) of the unreinforced HDPE were

increased consistently by increasing the tensile strain rate ($\dot{\varepsilon}$); by contrast, a consistent decrease in the maximum tensile strain (ε_{ut}) was produced by increasing the tensile strain rate ($\dot{\varepsilon}$). The same phenomenon was recorded for 20% hemp-HDPE, 40% hemp-HDPE and 20% hemp-HDPE immersed in water for 35 days, as shown in Figures 5.7, 5.8 and 5.9, respectively. This phenomenon is known as the strain rate hardening process; in it, the strength and the stiffness are increased by increasing $\dot{\varepsilon}$ [14, 15].

The normalized curves formed a range of curves, as shown in Figures 5.10, 5.11 and 5.12 for 20% hemp-HDPE, 40% hemp-HDPE and 20% hemp-HDPE immersed in water for 35 days, respectively. This can be attributed to the reduced homogeneity in the tested samples as a result of introducing the hemp fibers to the matrix during the manufacturing process.

The normalized curves of 20% hemp-HDPE immersed in water for 35 days (in Figure 5.12) converge more closely than the normalized stress-strain curves of the dry 20% hemp-HDPE shown in Figure 5.10. This can be attributed to the weakening effect of moisture absorption on the natural fibers within the matrix, as a result of the hydrophilic nature of natural fibers [5-9]. The strength of natural fibers is weakened due to the moisture absorption; additionally, the fibers swell which increases the interfacial matrix/fiber stress [5, 6, 9]. Therefore, the effect of natural fibers was reduced after moisture absorption, causing the normalized stress-strain curves to converge, as shown in Figure 5.12.

Table 5.2 Measured σ_{ut}, ε_{ut} and E for the Tested Unreinforced HDPE and Other Composites:

Material	$\dot{\varepsilon}$ (min^{-1})	Average σ_{ut} (MPa)	Standard Error of σ_{ut}	Average ε_{ut} (mm/mm)	Standard Error of ε_{ut}	Average E (GPa)	Standard Error of E
Unreinforced HDPE	0.5	22.31	0.175	0.0996	0.0020	1.440	0.020
	1	23.61	0.174	0.0963	0.0029	1.590	0.096
	2	25.19	0.227	0.0885	0.0003	1.520	0.117
	6	26.25	0.109	0.0873	0.0017	1.730	0.176
	8	27.11	0.104	0.0870	0.0003	1.910	0.053
	10	27.54	0.192	0.0857	0.0012	1.970	0.224
	14	28.32	0.147	0.0836	0.0018	2.080	0.146
20% Hemp-HDPE	0.5	22.53	0.057	0.0639	0.0024	2.140	0.108
	1	23.91	0.080	0.0602	0.0026	2.450	0.061
	2	25.65	0.155	0.0563	0.0005	2.490	0.120
	6	26.64	0.131	0.0556	0.0009	2.570	0.034
	8	27.38	0.103	0.0537	0.0004	2.760	0.061
	10	27.86	0.099	0.0502	0.0011	2.940	0.080
	14	29.54	0.180	0.0464	0.0020	3.110	0.096
40% Hemp-HDPE	0.13	23.13	0.113	0.0260	0.0011	3.920	0.036
	0.5	24.58	0.129	0.0248	0.0001	4.050	0.061
	2	26.53	0.167	0.0235	0.0003	4.320	0.005
	6	28.47	0.133	0.0203	0.0005	4.610	0.016
	8	29.35	0.150	0.0204	0.0015	4.830	0.052
	14	30.18	0.173	0.0230	0.0001	5.140	0.075
20% Hemp-HDPE immersed in water for 35 days	1	23.01	0.084	0.0703	0.0015	2.380	0.115
	2	24.67	0.235	0.0675	0.0033	2.590	0.101
	6	25.33	0.243	0.0609	0.0026	2.640	0.166
	10	26.45	0.117	0.0595	0.0014	2.920	0.072
	14	27.36	0.182	0.0565	0.0013	2.970	0.101

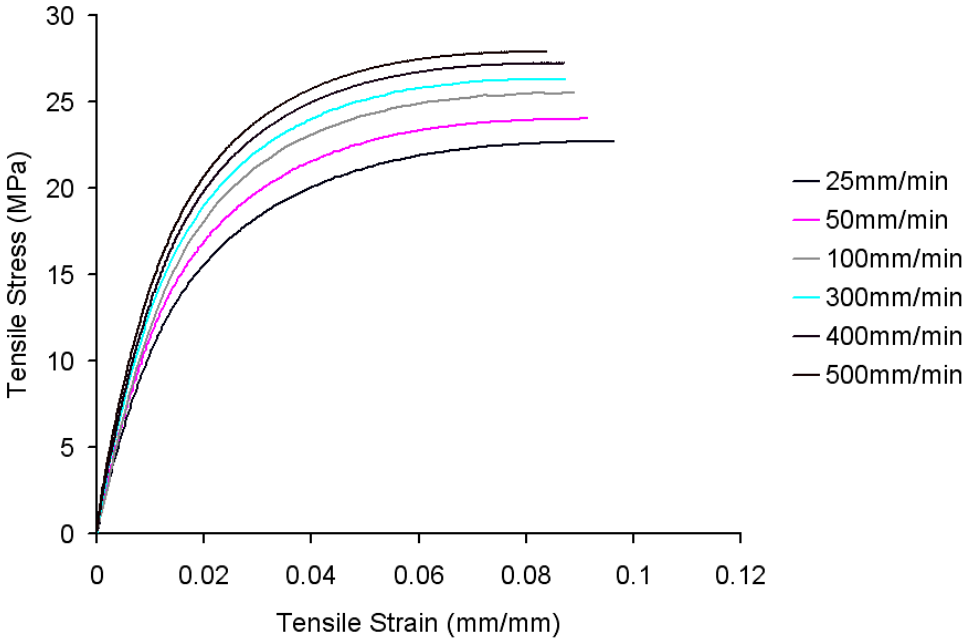

Fig. 5.5 Stress-strain curves for HDPE, generated at different $\dot{\varepsilon}$.

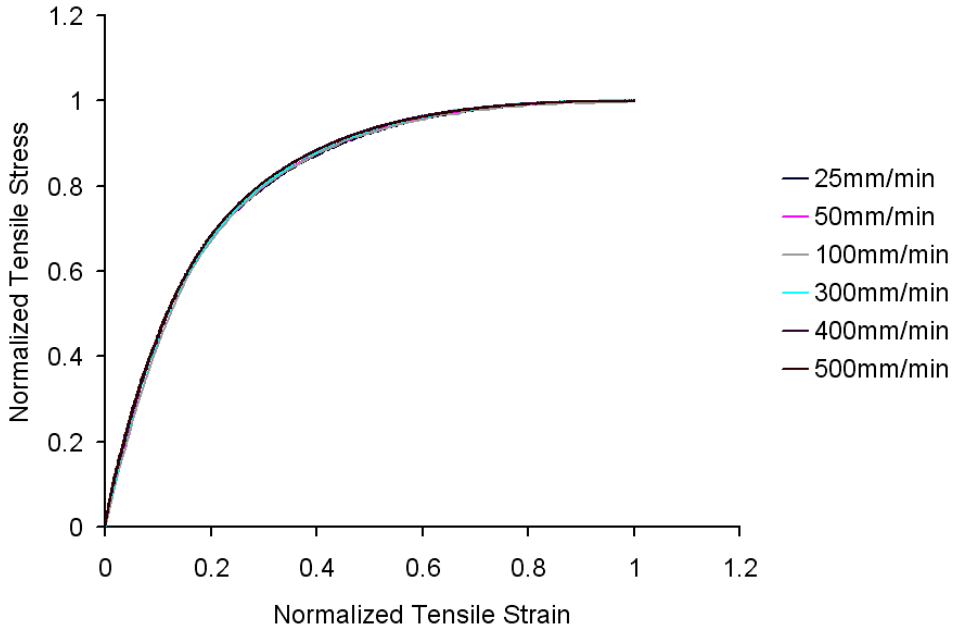

Fig. 5.6 Normalized stress-strain curves for HDPE, generated at different $\dot{\varepsilon}$.

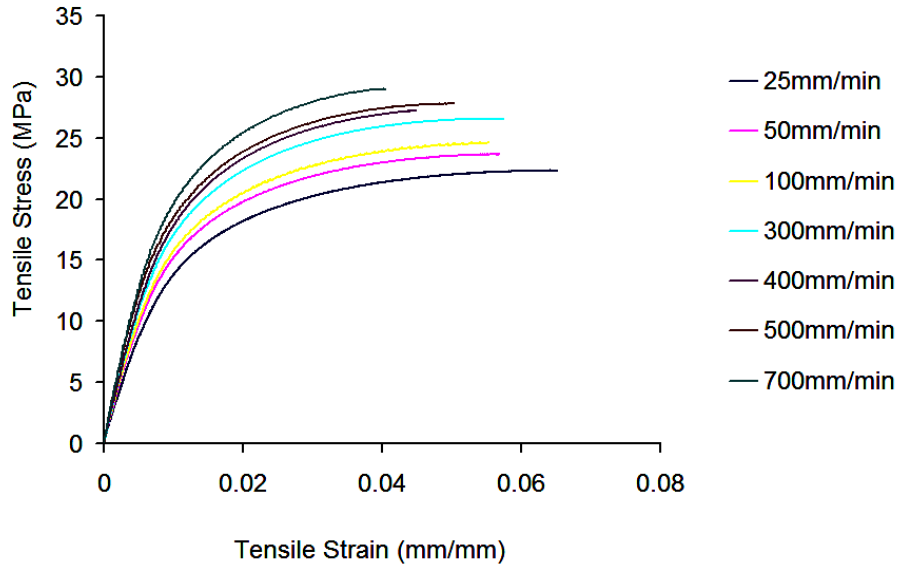

Fig. 5.7 Stress-strain curves for 20% hemp-HDPE, generated at different $\dot{\varepsilon}$.

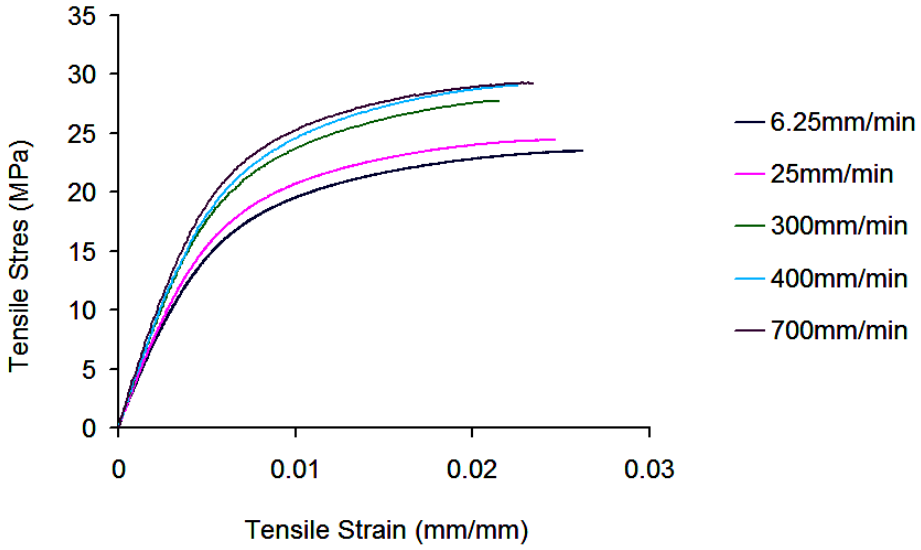

Fig. 5.8 Stress-strain curves for 40% hemp-HDPE, generated at different $\dot{\varepsilon}$.

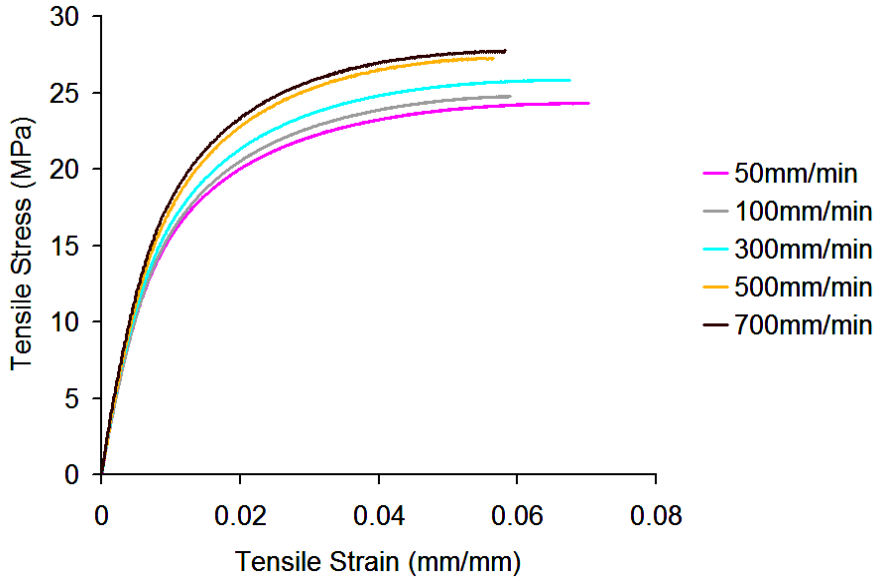

Fig. 5.9 Stress-strain curves at different $\dot{\varepsilon}$ for 20% hemp-HDPE immersed in water for 35 days.

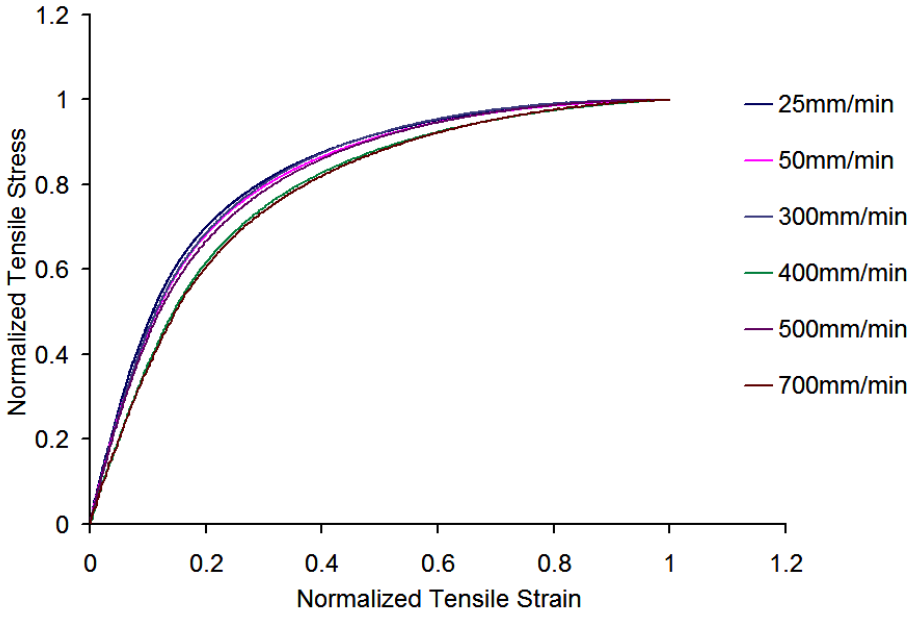

Fig. 5.10 Normalized stress-strain curves for 20% hemp-HDPE, generated at different $\dot{\varepsilon}$.

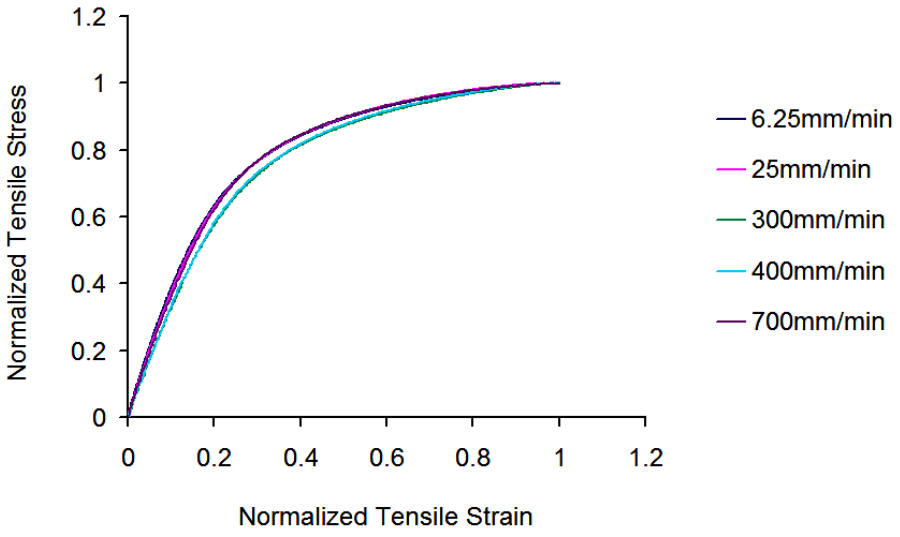

Fig. 5.11 Normalized stress-strain curves for 40% hemp-HDPE, generated at different $\dot{\varepsilon}$.

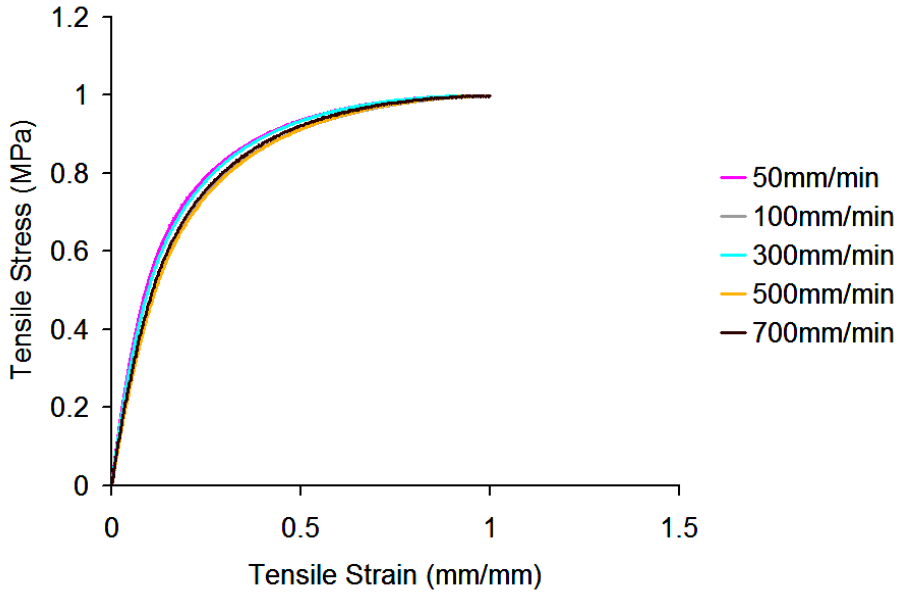

Fig. 5.12 Normalized stress-strain curves at different $\dot{\varepsilon}$ for 20% hemp-HDPE immersed in water for 35 days.

The normalized stress-strain curves of the unreinforced HDPE and the normalized stress-strain curves of 40% hemp-HDPE were plotted together, as shown in Figure 5.13, while the average of the normalized curves in Figures 5.6, 5.10 and 5.11 were plotted together in Figure 5.14. As shown in Figures 5.13 and 5.14, adding more natural fibers shifted the normalized stress-strain curve downward (i.e. the normalized elastic modulus, E_{norm}, was reduced); this means that at the same applied stress, the resulting strain decreases by adding natural fibers, from which it can be concluded that when the amount of the natural fibers is increased, the elongation decreases, while the strength and stiffness increase, as recorded previously in Table 5.2.

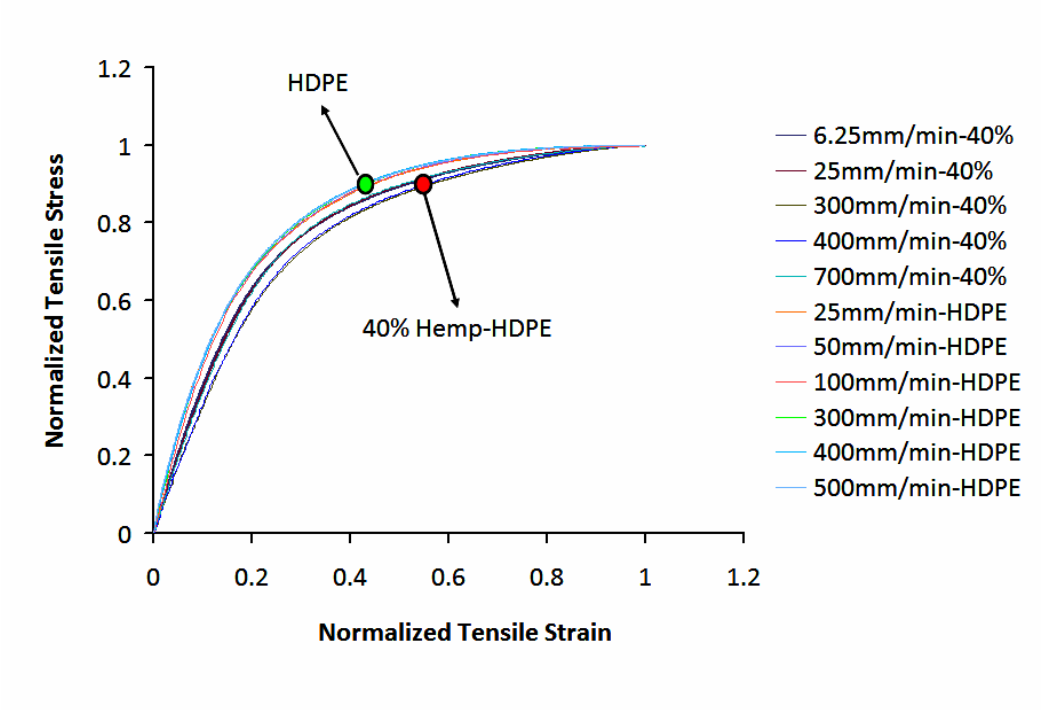

Fig. 5.13 Normalized stress-strain curves of unreinforced HDPE and 40% Hemp-HDPE, generated at different $\dot{\varepsilon}$.

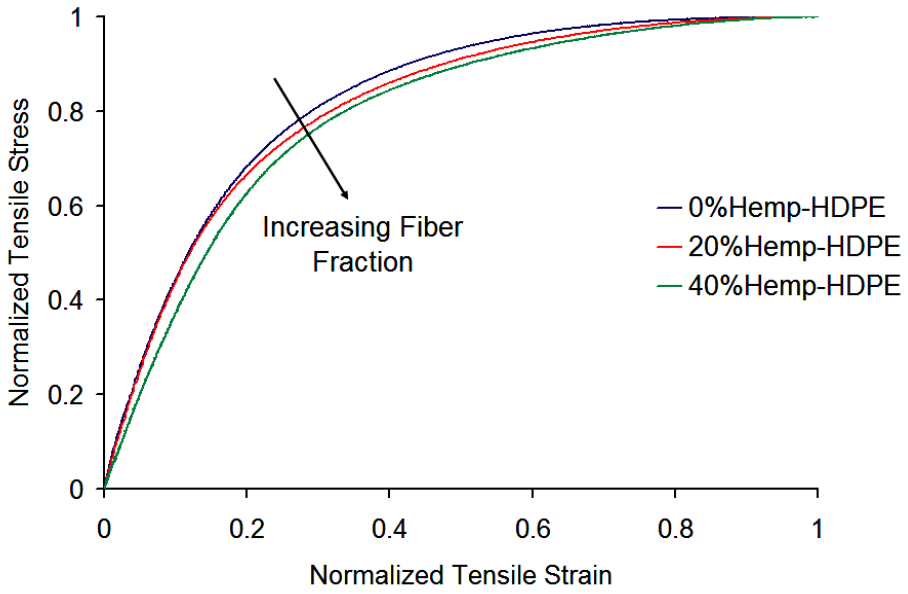

Fig. 5.14 Normalized stress-strain curves of unreinforced HDPE, 20% and 40% Hemp-HDPE, generated at different $\dot{\varepsilon}$.

To understand the effect of moisture absorption on normalized stress-strain behaviour, the average of the normalized curves in Figures 5.6, 5.10 and 5.12 are represented in Figure 5.15. Figure 5.15 shows that the normalized elastic modulus (E_{norm}) of 20% hemp-HDPE increased as a result of absorbing moisture. This means that the generated strain is increased under a certain amount of stress due to the weakening effect of the absorbed moisture.

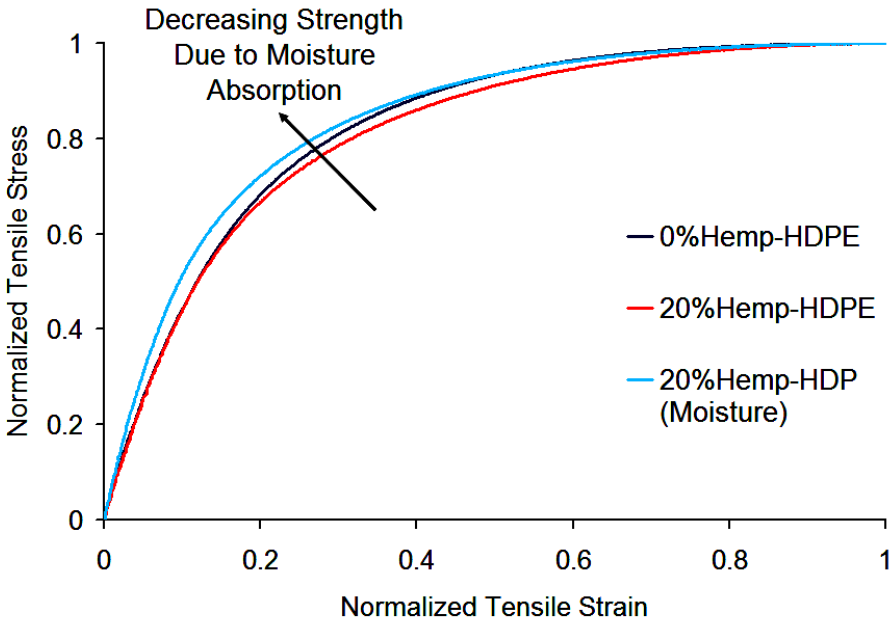

Fig. 5.15 Normalized stress-strain curves generated at different $\dot{\varepsilon}$ for unreinforced HDPE, 20% Hemp-HDPE and 20% hemp-HDPE immersed in water for 35 days.

5.4 MODELING THE UNIAXIAL STRESS-STRAIN BEHAVIOUR OF NFRP

5.4.1 Modeling the Normalized Monotonic Tensile Behaviour of NFRP

As demonstrated in Figures 5.6, 5.10, 5.11 and 5.12, the developed normalized strain (ε_{norm}) can be assumed to be growing exponentially with the applied normalized uniaxial stress (σ_{norm}). This exponential relationship can be simulated using an exponential differential equation as follows:

$$\frac{d\sigma_{norm}}{d\varepsilon_{norm}} = \xi c e^{-c\varepsilon_{norm}} \quad \text{..... 5.1.}$$

where c and ξ are dimensionless constants, σ_{norm} is the normalized monotonic stress (i.e. $\sigma_{norm}= \sigma/\sigma_{ut}$) (which is dimensionless), and ε_{norm} is the corresponding dimensionless normalized monotonic strain (i.e. $\varepsilon_{norm}= \varepsilon/\varepsilon_{ut}$).

A normalized stress-strain exponential model can be developed by solving the differential equation 5.1 as follows:

$$\sigma_{norm}=\xi\left[b-e^{-c\varepsilon_{norm}}\right] \quad \textbf{5.2}$$

where ξ,c and b are dimensionless constants, σ_{norm} is the dimensionless normalized monotonic stress, and ε_{norm} is the corresponding dimensionless normalized monotonic strain.

By applying the boundary conditions in Figures 5.6, 5.10, 5.11 and 5.12, equation 5.2 can be represented as follows:

$$\sigma_{norm}=\frac{1}{1-e^{-c}}\left[1-e^{-c\varepsilon_{norm}}\right] \quad \textbf{5.3}$$

where c is a dimensionless constant, σ_{norm} is the dimensionless normalized monotonic stress , and ε_{norm} is the dimensionless normalized monotonic strain.

The value of the tangent modulus of the normalized stress-strain curve at the zero point (E_{norm}) can be calculated by differentiating the model in equation 5.3, creating a model to calculate E_{norm} as follows:

$$E_{norm}=\frac{c}{1-e^{-c}} \quad \textbf{5.4}$$

where E_{norm} is the dimensionless tangent modulus of the normalized stress-strain curve at zero point, and c is a dimensionless constant.

As it was assumed previously that the effect of strain rate ($\dot{\varepsilon}$) can be eliminated by using the normalization of stress-strain curves, it can be concluded that the only effect remaining is the effect of the fiber volume fraction (v_f). Therefore, the parameter c in equation 5.3 can be assumed to be a function of the fiber volume fraction (v_f). To simulate this relationship, a modified Harris yield mechanistic model was proposed. The Harris model, a more simplified version of Holiday's yield model, is considered to be one of the most important parametric approaches for yield relationships [16, 17]. Additionally, the Harris model is highly suited as mechanistic to simulate the effect of v_f on the monotonic and the cyclic behaviour of NFRP [18, 19]. The Harris model was modified in order to give a more physical meaning to the parameters, as follows:

$$Y=\frac{a}{1+a\ b\ (v_f)^z} \quad \text{.....} \quad \textbf{5.5}$$

where v_f is the hemp fiber volume fraction, a is the value of the arbitrary variable "Y" at v_f equal zero, and b and z are matrix parameters.

As it was mentioned previously that moisture was absorbed as a result of adding natural fibre to the matrix, the effect of moisture absorption can be represented as a factor that affect the v_f; therefore, equation 5.5 can be reformulated as follows:

$$Y=\frac{a}{1+a\ b\ \omega\ (v_f)^z} \quad \text{.....} \quad \textbf{5.6}$$

where ω is a moisture absorption coefficient.

Using the modified harries model in equation 5.6, the c-v_f relationship can be represented as follows:

$$c=\frac{c_o}{1+\ c_o\beta_c\omega_c(v_f)^{\Psi_c}} \quad \text{.....} \quad \textbf{5.7}$$

where c_o is c for the unreinforced matrix polymer (which is dimensionless), β_c and ψ_c are dimensionless matrix-dependent parameters, and ω_c is another dimensionless parameter that has been added to the Harris model as a moisture absorption coefficient to incorporate the effect of moisture absorption. The estimated values for the parameters in equation 5.7 can be evaluated using the Levenberg-Marquaredt method, which is a modified version of the Gauss-Newton method [16]. The values of the parameters in equation 5.7 are represented in Table 5.3.

Table 5.3 Values for parameters c_o, β_c, ψ_c and ω_c in equation 5.7:

Parameter	Parameter Value
c_o	5.624 (dimensionless)
β_c	0.215 (dimensionless)
ψ_c	1.455 (dimensionless)
ω_c (for dry conditions)	1.000 (dimensionless)
ω_c (20% hemp immersed In water for 35 days)	-1.790 (dimensionless)

To simplify and reduce the number of parameters in Harris model, another linearized model was proposed to simulate the relationship of c-v_f. The simplified linear model can be represented as follows:

$$c=c_o(1+a_c w_c v_f) \quad \textbf{5.8}$$

where c_o is c for the unreinforced matrix polymer, v_f is the hemp fiber volume fraction, a_c is a dimensionless matrix-dependent parameter, and w_c is a dimensionless parameter added to the linear model as a moisture absorption coefficient in order to incorporate the effect of moisture absorption. The values for the parameters c_o, a_c and w_c in equation 5.8 are represented in Table 5.4.

As c_o in equation 5.7 and 5.8 represents the value of parameter c in equation 5.3 for an unreinforced matrix polymer, the values of c_o, derived from both the modified Harris model and the linear model, are extremely close to each other, as shown in Tables 5.3 and 5.4, respectively. The values of c_o in Tables 5.3 and 5.4 are very close to the experimental value of c_o, which is 5.624; however, the values of c_o derived from the modified Harris model are exactly the same as the experimental value for c_o.

Table 4 Calculated values of parameters c_o, a_c and w_c in equation 5.8:

Parameter	Parameter Value
c_o	5.657 (dimensionless)
a_c	-0.578 (dimensionless)
ω_c (for dry conditions)	1.000 (dimensionless)
ω_c (20% hemp immersed In water for 35 days)	-1.617 (dimensionless)

5.4.2 Mathematical representation of strain rate effect on σ_{ut} and ε_{ut}

From the data in Table 5.2, and as it was mentioned previously, the material strength is increased (i.e. it is resistance to deformation is increased) by increasing $\dot{\varepsilon}$, which is known by strain rate hardening phenomenon [14, 15]. For viscoplastic matrix such as HDPE [20], the strain hardening phenomenon can be represented using the non-linear one-dimensional form of Norton-Hoff rheology model for viscoplastic material [14, 19, 21-25] as follows:

$$\sigma_{ut} = k_\sigma(\dot{\varepsilon})^{m_\sigma} \quad \text{..... 5.9}$$

where σ_{ut} is the maximum tensile stress (MPa) produced by a strain rate $\dot{\varepsilon}$ (min^{-1}) at a constant temperature, k_σ is a material constant ($MPa.min^{m_\sigma}$), and m_σ is a behaviour index for σ_{ut} (dimensionless).

Similar to the previous equations developed for parameter "c" as a function of the fibre volume fraction (v_f), parameters in equation 5.9 can be assumed to be functions of v_f as well; using the modified Harris mechanistic model, equations 5.10 and 5.11 can represent k_σ and m_σ, respectively [14, 26].

$$k_\sigma = \frac{k_{\sigma o}}{1 - k_{\sigma o}\beta_{k_\sigma}\omega_{k_\sigma}(v_f)^{\psi_{k_\sigma}}} \quad \text{..... 5.10}$$

where $k_{\sigma o}$ is k_σ for the unreinforced matrix polymer ($MPa.\min^{m_\sigma}$), v_f is the hemp fibre volume fraction, β_{k_σ} is a matrix dependent parameters ($MPa^{-1}.\min^{-m_\sigma}$), ψ_{k_σ} is a dimensionless matrix dependent parameter, and ω_{k_σ} a dimensionless moisture absorption coefficient; and

$$m_\sigma = \frac{m_{\sigma o}}{1 + m_{\sigma o}\beta_{m_\sigma}\omega_{m_\sigma}(v_f)^{\psi_{m_\sigma}}} \quad \text{..... 5.11}$$

where $m_{\sigma o}$ is m_σ for the matrix polymer (dimensionless), β_{m_σ} and ψ_{m_σ} are dimensionless matrix dependent parameters, and ω_{m_σ} is a dimensionless moisture absorption coefficient.

Using the data measured in Table 5.2, the estimated values for parameters in equation 5.10 are represented in Table 5.5, while the values for the parameters in equation 5.11 are tabulated in Table 5.6.

Using the simplified linearized model, the parameters in equation 5.9 can be also represented as in equations 5.12 and 5.13 [14].

$$k_\sigma = k_{\sigma o}(1 + a_{k_\sigma} w_{k_\sigma} v_f) \quad \text{..... 5.12}$$

where a_{k_σ} is a dimensionless matrix dependent parameter, and w_{k_σ} is a moisture absorption coefficient; the values for parameters in equation 5.12 are represented in Table 5.1.

Table 5.5 Calculated values of the parameters $k_{\sigma o}$, β_{k_σ}, ψ_{k_σ} and ω_{k_σ} in equation 5.10:

Parameter	Parameter Value
$k_{\sigma o}$	23.588 (MPa. $\min^{m_\sigma}$)
β_{k_σ}	0.060 (MPa^{-1}. $\min^{-m_\sigma}$)
ψ_{k_σ}	2.422 (dimensionless)
ω_{k_σ} (for dry conditions)	1.000 (dimensionless)
ω_{k_σ} (20% hemp soaked In water for 35 days)	-1.790 (dimensionless)

$$m_\sigma = m_{\sigma o}(1 + a_{m_\sigma} w_{m_\sigma} v_f) \quad \text{..... 5.13}$$

where a_{m_σ} is a matrix dependent parameter, and w_{m_σ} a moisture absorption coefficient; Table 5.2 represents that values for parameters in equation 5.13.

A power law, similar to the one used to represent the relationship of σ_{ut}- $\dot{\varepsilon}$, can be used to simulate the relationship between the tensile strain (ε_{ut}) and $\dot{\varepsilon}$, as follows [14, 19]:

$$\varepsilon_{ut} = k_\varepsilon (\dot{\varepsilon})^{m_\varepsilon} \quad \text{..... 5.14}$$

where ε_{ut} is the dimensionless strain corresponding to σ_{ut} developed by strain rate $\dot{\varepsilon}$ ($\min^{-1}$) at constant temperature, k_ε is a material constant ($\min^{m_\varepsilon}$), and m_ε is the dimensionless power law index for ε_{ut}.

Table 5.6 Calculated values of the parameters $m_{\sigma o}$, β_{m_σ}, ψ_{m_σ} and ω_{m_σ} in equation 5.11:

Parameter	Parameter Value
$m_{\sigma o}$	0.068 (dimensionless)
β_{m_σ}	-29.706 (dimensionless)
ψ_{m_σ}	1.954 (dimensionless)
ω_{m_σ} (for dry conditions)	1.000 (dimensionless)
ω_{m_σ} (20% hemp soaked in water for 35 days)	-7.303 (dimensionless)

Table 5.7 Calculated values of the parameters $k_{\sigma o}$, a_{k_σ} and w_{k_σ} in equation 5.12:

Parameter	Parameter Value
$k_{\sigma o}$	23.588 ($MPa.\min^{m_\sigma}$)
a_{k_σ}	0.287 (dimensionless)
w_{k_σ} (for dry conditions)	1.000 (dimensionless)
w_{k_σ} (20% hemp soaked in water for 35 days)	-0.114 (dimensionless)

Similar to k_σ and m_σ, parameters k_ε and m_ε in equation 5.9 can be assumed to be functions of fibre volume fraction (v_f), and they can be modeled using the modified Harris model as in equations 5.15 and 5.16, respectively [14, 26].

$$k_\varepsilon = \frac{k_{\varepsilon o}}{1 + k_{\varepsilon o}\beta_{k_\varepsilon}\omega_{k_\varepsilon}(v_f)^{\psi_{k_\varepsilon}}} \quad \text{..... 5.15}$$

Table 5.8 Calculated values of the parameters $m_{\sigma o}$, a_{m_σ} and w_{m_σ} in equation 5.13:

Parameter	Parameter Value
$m_{\sigma o}$	0.066 (dimensionless)
a_{m_σ}	0.822 (dimensionless)
w_{m_σ} (for dry conditions)	1.000 (dimensionless)
w_{k_σ} (20% hemp soaked In water for 35 days)	-1.881 (dimensionless)

where $k_{\varepsilon o}$ is k_ε for the matrix polymer $(\min^{m_\varepsilon}), \beta_{k_\varepsilon}$ is a matrix dependent parameter $(\min^{-m_\varepsilon})$, ψ_{k_ε} is a dimensionless matrix dependent parameter, and ω_{k_ε} is a dimensionless moisture absorption coefficient; and

$$m_\varepsilon = \frac{m_{\varepsilon o}}{1+m_{\varepsilon o}\beta_{m_\varepsilon}\omega_{m_\varepsilon}(v_f)^{\psi_{m_\varepsilon}}} \quad \textbf{5.16}$$

where $m_{\varepsilon o}$ is m_ε for the matrix polymer, β_{m_ε} and ψ_{m_ε} are matrix dependent parameters, and ω_{m_ε} is a moisture absorption coefficient.

The values for parameters in equation 5.15 and 5.16 were estimated using Levenberg-Marquaredt method as tabulated Tables 5.9 and 5.10, respectively.

By using the simplified linear model, the parameters k_ε and m_ε in equation 5.9 can be also modeled as follows [14]:

$$k_\varepsilon = k_{\varepsilon o}(1+a_{k_\varepsilon} w_{k_\varepsilon} v_f) \quad \textbf{5.17}$$

where a_{k_ε} is a matrix dependent parameter, and w_{k_ε} is a moisture absorption coefficient; Table 5.5 represents the estimated parameters' values;

Table 5.9 Values for parameters $k_{\varepsilon o}$, β_{k_ε}, ψ_{k_ε} and ω_{k_ε} in equation 5.15:

Parameter	Parameter Value
$k_{\varepsilon o}$	0.095 ($\min^{m_\varepsilon}$)
β_{k_ε}	379.094 ($\min^{-m_\varepsilon}$)
ψ_{k_ε}	2.082 (dimensionless)
ω_{k_ε} (for dry conditions)	1.000 (dimensionless)
ω_{k_ε} (20% hemp soaked In water for 35 days)	0.616 (dimensionless)

$$m_\varepsilon = m_{\varepsilon o}(1 + a_{m_\varepsilon} w_{m_\varepsilon} v_f) \quad \text{..... 5.18}$$

where a_{m_ε} is a matrix dependent parameter, and w_{m_ε} is a moisture absorption coefficient. The estimated parameters' values are shown in Table 5.6.

Table 5.10 Calculated values of the parameters $m_{\varepsilon o}$, β_{m_ε}, ψ_{m_ε} and ω_{m_ε} in equation 5.16:

Parameter	Parameter Value
$m_{\varepsilon o}$	-0.036 (dimensionless)
β_{m_ε}	11.449 (dimensionless)
ψ_{m_ε}	0.029 (dimensionless)
ω_{m_ε} (for dry conditions)	1.000 (dimensionless)
ω_{m_ε} (20% hemp soaked In water for 35 days)	1.384 (dimensionless)

Table 5.11 Calculated values of the parameters $k_{\varepsilon o}$, a_{k_ε} and w_{k_ε} in equation 5.17:

Parameter	Parameter Value
$k_{\varepsilon o}$	0.094 (min^{m_ε})
a_{k_ε}	-2.499 (dimensionless)
w_{k_ε} (for dry conditions)	1.000 (dimensionless)
w_{k_ε} (20% hemp soaked In water for 35 days)	0.739 (dimensionless)

Table 5.12 Calculated values of the parameters $m_{\varepsilon o}$, a_{m_ε} and w_{m_ε} in equation 5.18:

Parameter	Parameter Value
$m_{\varepsilon o}$	-0.060 (dimensionless)
a_{m_ε}	-0.278 (dimensionless)
w_{m_ε} (for dry conditions)	1.000 (dimensionless)
w_{m_ε} (20% hemp soaked In water for 35 days)	-9.338 (dimensionless)

5.4.3 Generalized Modeling of Monotonic Uniaxial Tensile Behaviour of NFRP

Taking into consideration the fact that $\sigma_{norm}= \sigma/\sigma_{ut}$ and $\varepsilon_{norm}= \varepsilon/\varepsilon_{ut}$, equation 5.3 can be represented as follows:

$$\sigma=\frac{\sigma_{ut}}{1-e^{-c}}\left[1-e^{-\frac{c\,\varepsilon}{\varepsilon_{ut}}}\right] \quad \text{..... 5.19}$$

where, σ is the applied tensile stress (MPa), ε is the corresponding tensile strain (mm/mm, dimensionless), c is a dimensionless constant (function in v_f), σ_{ut} is the maximum or ultimate tensile strength (MPa), and ε_{ut} is the tensile strain corresponding to σ_{ut} (mm/mm, dimensionless).

By using the previously developed equations 5.9 and 5.9, the developed model in equation 5.19 can be represented as follows:

$$\sigma = \frac{k_\sigma (\dot{\varepsilon})^{m_\sigma}}{1-e^{-c}} \left[1-e^{-\frac{c\varepsilon}{k_\varepsilon (\dot{\varepsilon})^{m_\varepsilon}}} \right] \quad \textbf{5.20}$$

Figures 5.16-a, 5.17-a, 5.18-a and 5.19-a depict the experimental stress-strain behaviours versus the simulation results produced by the model in equation 5.20 at different values of applied strain rate ($\dot{\varepsilon}$); the modified Harris model was used to express the relationship between the parameters of the model and the natural fiber volume fraction (v_f), including the moisture absorption effect. On the other hand, in Figures 5.16-b, 5.17-b, 5.18-b and 5.19-b, the linear model was used as a function that ties the model parameters to v_f. Whether using the modified Harris mode or the linear model, the simulated stress-strain behaviour produced by the model in equation 5.20 shows a very close match to stress-strain behaviour resulting from experiments, as shown in Figures 5.16, 5.17, 5.18 and 5.19 for unreinforced HDPE, 20% hemp-HDPE, 40% hemp-HDPE and 20% hemp HDPE immersed in water for 35 days at different values of $\dot{\varepsilon}$, respectively.

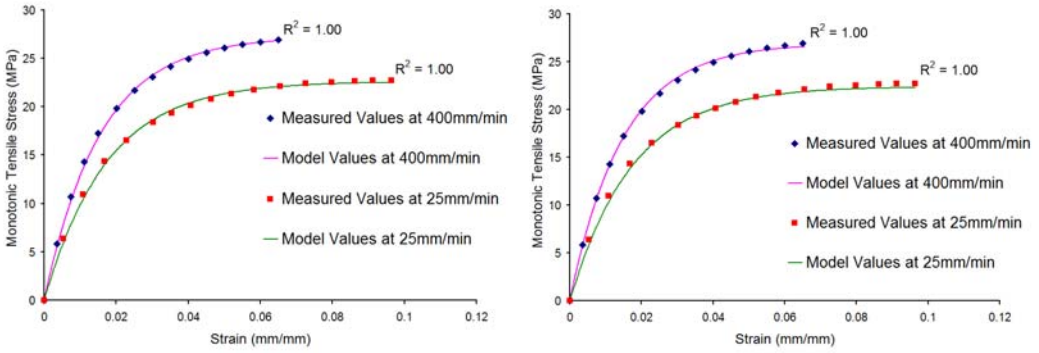

(a) **(b)**

Fig. 5.16 Measured and model stress-strain curves for unreinforced HDPE (a) using the modified Harris model and (b) using the linear model, at 400mm/min and 25mm/min.

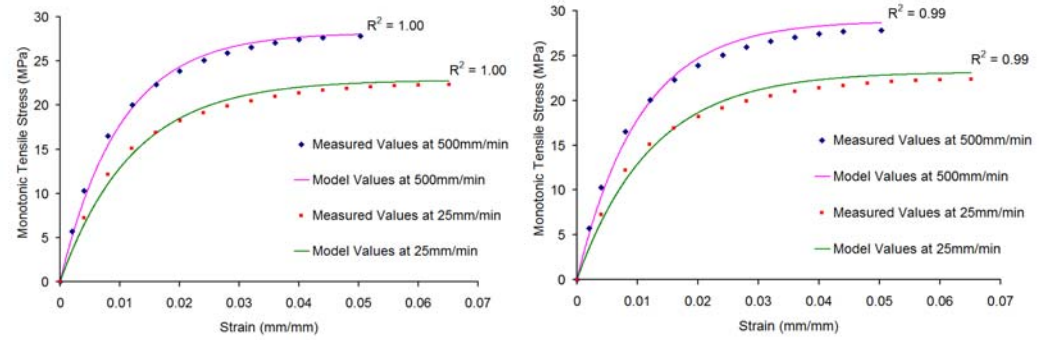

(a) **(b)**

Fig. 5.17 Measured and model stress-strain curves for 20% hemp-HDPE (a) using the modified Harris model and (b) using the linear model, at 500mm/min and 25mm/min.

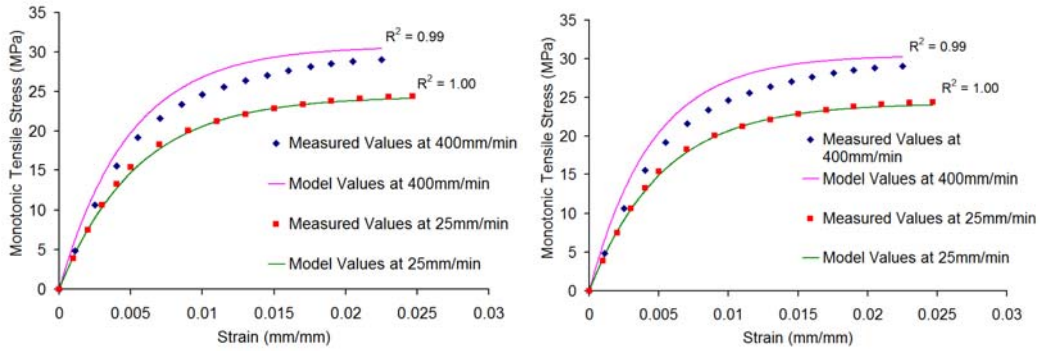

(a) **(b)**

Fig. 5.18 Measured and model stress-strain curves for 40% hemp- HDPE (a) using the modified Harris model and (b) using the linear model, at 400mm/min and 25mm/min.

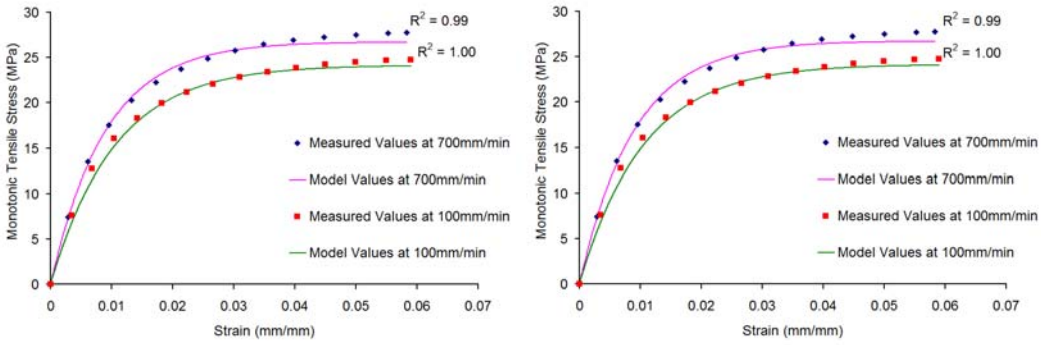

(a) **(b)**

Fig. 5.19 Measured and model stress-strain curves at 700mm/min and 100mm/min for 20% hemp-HDPE immersed in water for 35 days (a) using the modified Harris model and (b) using the linear model.

5.4.4 Generalized Stiffness Model

From equation 5.20, the tangent stiffness modulus (E) of the engineering stress-strain curve can be represented using the flowing model:

$$E=\left(\frac{c}{1-e^{-c}}\right)\frac{k_\sigma}{k_\varepsilon}\dot{\varepsilon}^{(m_\sigma-m_\varepsilon)} \quad \text{..... 5.21}$$

where E is the tangent stiffness modulus (MPa), $\dot{\varepsilon}$ is the applied strain rate (min^{-1}), k_σ is a material constant ($MPa.min^{m_\sigma}$), m_σ is a behaviour index for σ_{ut} (dimensionless), k_ε is a material constant (min^{m_ε}), m_ε is the power law index for ε_{ut} (dimensionless), and c is a parameter from the normalized monotonic model (dimensionless).

Using equation 5.4, the stiffness model in equation 5.21 can also be represented as follows:

$$E=E_{norm}\frac{k_\sigma}{k_\varepsilon}\dot{\varepsilon}^{(m_\sigma-m_\varepsilon)} \quad \text{..... 5.22}$$

The form developed in equation 5.22 can be represented in a general power law form as follows:

$$E=k_E\dot{\varepsilon}^{m_E} \quad \text{..... 23}$$

where $k_E = E_{norm}\frac{k_\sigma}{k_\varepsilon} = \left(\frac{c}{1-e^{-c}}\right)\frac{k_\sigma}{k_\varepsilon}$, and $m_E = m_\sigma - m_\varepsilon$.

Figures 5.20, 5.21, 5.22 and 5.23 depict the values of E resulting from experiments and produced by the stiffness model developed in equation 5.21 at different values of applied strain rate ($\dot{\varepsilon}$) and fiber volume fractions (v_f). As

previously shown, the parameters of the stiffness model in equation 5.21 (i.e. k_σ, m_σ, k_ε, m_ε, and c) have been represented as functions of v_f once by using the modified Harris mode and another time by using the linear model. Whether the modified Harris model or the linear model is used, the simulation results from the stiffness model in equation 5.21 show a close match with the experimental results, as shown in Figures 5.20, 5.21, 5.22 and 5.23 for unreinforced HDPE, 20% hemp-HDPE, 40% hemp-HDPE and 20% hemp HDPE immersed in water for 35 days, respectively. However, for 40% hemp-HDPE, the developed stiffness model predicted a slightly higher stiffness than the stiffness measured in experiments at higher values of $\dot{\varepsilon}$, as shown in Figure 5.22. This can be attributed to the accumulative approximation during the nonlinear regression process used to evaluate the parameters equation 5.21 for 40% hemp-HDPE samples.

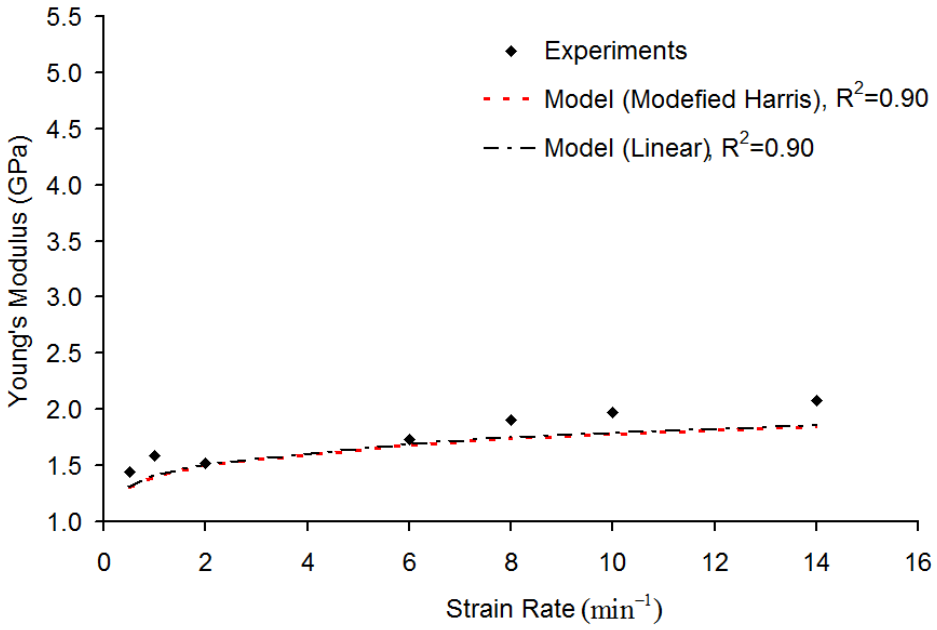

Fig. 5.20 The tangent stiffness modulus (E) resulting from experiments and from the stiffness model for unreinforced HDPE.

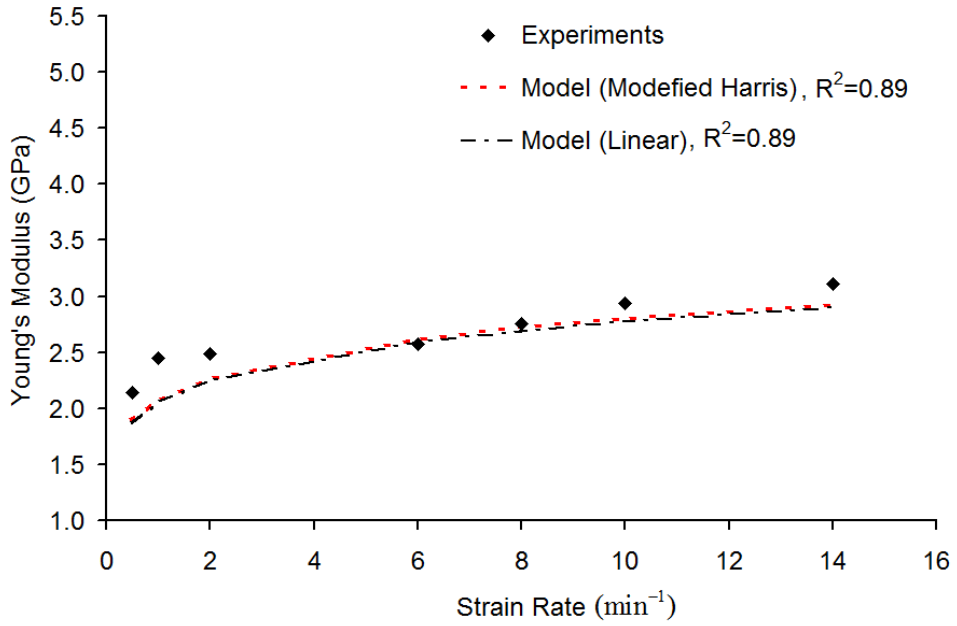

Fig. 5.21 The tangent stiffness modulus (E) resulting from experiments and from the stiffness model for 20% hemp-HDPE.

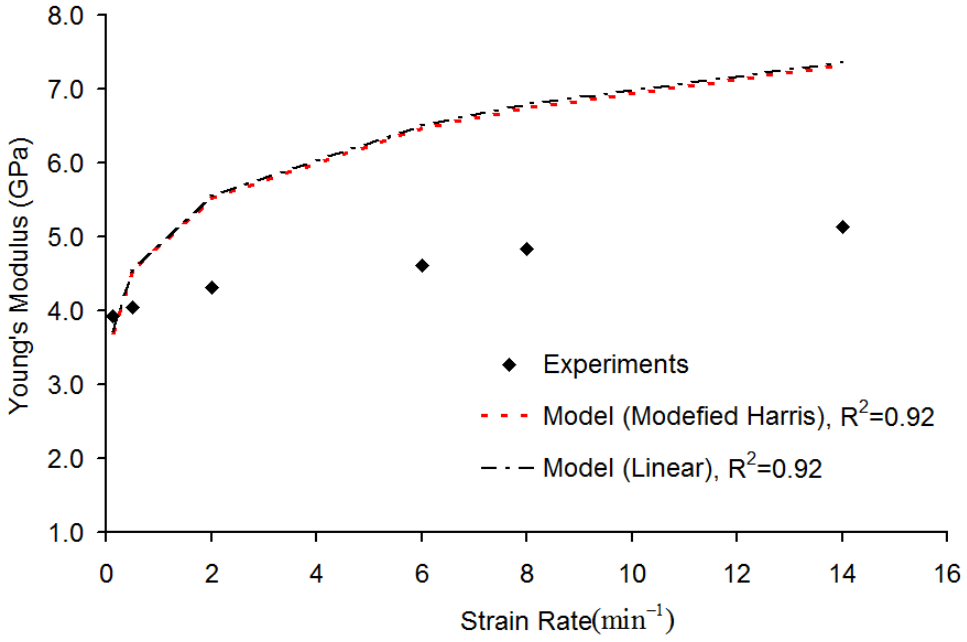

Fig. 5.22 The tangent stiffness modulus (E) resulting from experiments and from the stiffness model for 40% hemp-HDPE.

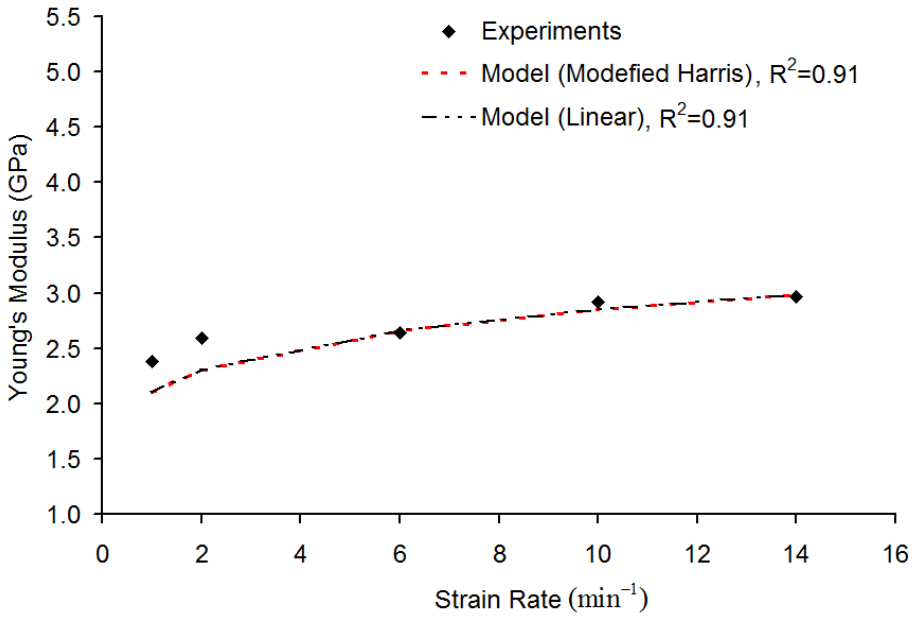

Fig. 5.23 The tangent stiffness modulus (E) resulting from experiments and from the stiffness model for 20% hemp-HDPE immersed in water for 35 days.

5.5 CONCLUSIONS

Normalized Engineering stress-strain curves were developed and analyzed in order to demonstrate the effect on the monotonic tensile behaviour of NFRPs of adding short hemp natural fibers and moisture absorption. The normalized stress-strain curves were capable of eliminating the effect of the applied strain rate ($\dot{\varepsilon}$).An exponential model was proposed to simulate the normalized stress-strain behaviour of NFRPs.

The new developed semi-analytical monotonic model was successful in simulating the engineering stress-strain behaviour of NFRPs at different values of strain rate ($\dot{\varepsilon}$) and short fiber volume fraction (v_f); additionally, the developed generalized model was successfully capable of taking into consideration the effect of moisture absorption due to the hydrophilic nature of the natural fibers.

A generalized stiffness model was developed to simulate the tangent stiffness modulus of the stress-strain curve (i.e. Young's modulus (E)) of NFRPs. The model showed a good match with the experimental values, taking into consideration the effect of applied strain rate ($\dot{\varepsilon}$), short fiber volume fraction (v_f) and moisture absorption.

CHAPTER 6: FATIGUE OF NATURAL FIBER THERMOPLASTIC COMPOSITES[**]

ABSTRACT

The fatigue behavior of hemp-fiber-reinforced High Density Polyethylene (HDPE) composites is investigated using fatigue-life (S-N) curves at different fiber volume fractions. For this purpose, a new modified stress level is proposed to normalize the developed S-N curves into one normalized S-N curve. A generalized fatigue behaviour model is developed to simulate the fatigue-life response of these composites. It is demonstrated that the developed model is capable of predicting the fatigue behaviour of the natural fiber composites at different fiber fractions and fatigue stress ratios, and is also capable of accounting for the effect of moisture absorption.

KEYWORDS

Natural Fiber Composites; Fatigue; Mechanical Testing; Analytical Modeling; Fractography.

6.1 INTRODUCTION

Composites are an important category of materials for engineering applications. They form an essential part in the design process in many sectors, including the automotive, marine and aircraft industries. Over the past decade,

---

[**] This chapter is a modified version of a paper that was published as Ahmed Fotouh, J. D. Wolodko, M. Lipsett, "Fatigue of Natural Fiber Thermoplastic Composites", Journal of Composites Part B: Engineering, Vol. 62, pp. 175-192, Jun. 20th, 2014.

there has been an increased demand for “green” or natural-fiber-reinforced composites. Natural fibers provide many advantages over synthetic fibers, including low density (light weight), reasonable mechanical properties, and environmental benefits (including sustainability and a lower carbon footprint) [1-4]. However, the range of applications involving natural fiber composites in engineering design is still limited due, partly, to a lack of understanding of the long-term behavior of these materials especially under cyclic (fatigue) loading. Like all composites, this can be attributed to the complex nature of how these materials fail. Unlike monolithic materials (such as metals or polymers) where failure is associated with the initiation and propagation of a dominant fracture event, failure in composites is characterized by accumulation of multiple damage modes including [5-10]: 1) debonding between the reinforcing fibers and the polymer matrix; 2) fiber failure; and 3) matrix failure. These damage mechanisms take place independently or, more commonly, in a synergistic manner [11, 12]. Natural fibers further complicate this behaviour due to variation in properties and surface characteristics [13, 14].

Furthermore, natural fibers have a tendency to absorb moisture from air or direct contact with water or other liquids due to their hydrophilic nature. Natural fibers are mainly composed of three constituents: cellulose, hemicellulose and lignin [14]. Cellulose, a semi-crystalline polysaccharide, is the main constituent of most natural fibers, and is also the component responsible for its excellent structural properties. Cellulose is also hydrophilic, and is the main cause of water uptake in natural fibers. Hemicellulose is an amorphous polysaccharide, and is partially soluble in water. Finally, lignin is a complex polymer which acts as a binder for the other components (cellulose, hemicellulose and others) in natural fibers. Lignin is mainly hydrophobic in nature. Studies on natural fibre composites have shown that absorbed moisture weakens fibers and the bonding between the fiber-matrix interface, resulting in an overall reduction in mechanical properties [15-17].

The fatigue behavior of fiber reinforced composites has been studied extensively over the past four decades [5, 9, 10, 18, 19]. A majority of these studies, however, are related to long-fiber composites made with glass, carbon and aramid fibers. A smaller subset of studies has focused on the cyclic performance of short fiber reinforced composites made from synthetic fibers such as glass and carbon. Mandell *et al.* [18] conducted a comprehensive investigation of the fatigue response of a variety of reinforced thermoplastics with both chopped glass and carbon fibers. The authors showed that the fatigue behavior of the composite was a function of the matrix properties (in particular, ductility), fiber type, and the quality of the fiber/matrix interface. The response of carbon fiber composites tended to be matrix and interface dominated, while glass fiber composites exhibited more fiber dominated behaviors. Lavengood and Gulbransen [19] studied the cyclic response of short fiber boron/epoxy composites and found that fatigue life increased with increasing fiber aspect ratio (to a maximum). Harris *et al.* [20] compared the fatigue life behavior of long versus short random fiber composites with the same carbon/epoxy constituents. It was found that the long fiber composites had better overall fatigue life properties than their short fiber counterparts, but the fatigue sensitivity was greater (steeper decline over the fatigue-life curve).

For natural fiber based composites, there has been a great deal of work focused on determining static mechanical properties [21-25], but very limited studies related to fatigue. Towo and Ansell [26] investigated the cyclic behavior of sisal fiber reinforced thermoset composites under both tension-tension fatigue and fully reversed loading. This study found that alkali treated fiber composites had better fatigue performance due to improved fiber-matrix adhesion. Yang *et al.* [30] studied the flexural fatigue behavior of wood flour reinforced high density polyethylene. In their study, a statistical model using a Weibull distribution was developed to predict the fatigue behavior of these materials. Belaadi *et al.* [27] studied the fatigue behavior of unreinforced sisal natural fibers, and found that

conventional empirical fatigue-life models worked well to correlate fatigue response.

In this current study, experiments were performed on natural-fiber-reinforced thermoplastic composites under cyclic loading, and a new model was developed which predicts the fatigue behaviour of these materials. This model predicts the fatigue life of these materials as a function of loading condition, fiber fraction, and moisture absorption. Fatigue stress-life (S-N) curves were used as a tool to study and to model the fatigue behaviour of natural fiber composites.

6.2 EXPERIMENTAL BEHAVIOUR OF HEMP-REINFORCED COMPOSITES UNDER MONOTONIC AND CYCLIC LOADING

6.2.1 Materials and Methodology

In this study, a series of monotonic and cyclic tests were performed on test specimens made from natural-fiber-reinforced thermoplastic composites. High Density Polyethylene (HDPE) was used as the polymer matrix, and chopped hemp bast fibers (<5 mm length) were used as the reinforcement. The HDPE polymer (HD360) was supplied by M. Holland Company, and the hemp fibers were grown and processed at Alberta Innovates – Technology Futures' (AITF) research facilities in Alberta, Canada. The bast fibers were extracted from hemp stalks using a custom built, short fiber decortication system. Chopped bast fibers used in this study were not modified or chemically treated. Table 6.1 shows the mechanical and physical properties of the HDPE. The hemp fibers and HDPE were mixed at two fiber fractions (weight percentages of 20% and 40%) using a PTW 24/40 Thermo-Fisher-Scientific twin-screw extruder/compounder. The density of the hemp bast fiber was 1.475 g/cm^3 as measured using the Archimedes' method, modified for natural fiber applications [32]. This measured density was found to be very close to values reported in the literature [33]. Based

on the hemp fiber density, the estimated volume fiber fractions (v_f) were calculated to be 13.5% and 30.1% for the 20% and 40% weight fractions, respectively. Test specimens, for both monotonic and fatigue tests, were manufactured using a Battenfield 100 injection moulding machine according to ASTM D 638-03 (Type I test specimen with 3 mm thickness and 50 mm gage length – see Figure 6.1). All mechanical tests (monotonic and cyclic) were performed using an Instron 8501 universal testing machine under controlled ambient conditions (23°C and 50% relative humidity environment). Elongation (up to 50%) was measured using an extensometer (50 mm gage length) attached to the test specimen.

Table 6.1 Mechanical and physical properties of HDPE:

Property	HDPE	Test Method
Density	0.943 ±0.02 g/cm^3 (3 tested samples)	ASTM D1505
Tensile strength at yield (50mm/min)	24 ±0.26 MPa (3 tested samples)	ASTM D638
Stiffness (Young's modulus) (50mm/min)	1.8 ±0.143 GPa (3 tested samples)	ASTM D638
Elongation at yield (50mm/min)	9 ±0.43 % (3 tested samples)	ASTM D638
Melt mass flow rate (from manufacturer table) (190^{o}C/2.16kg)	7.5 g/10min	ASTM D1238

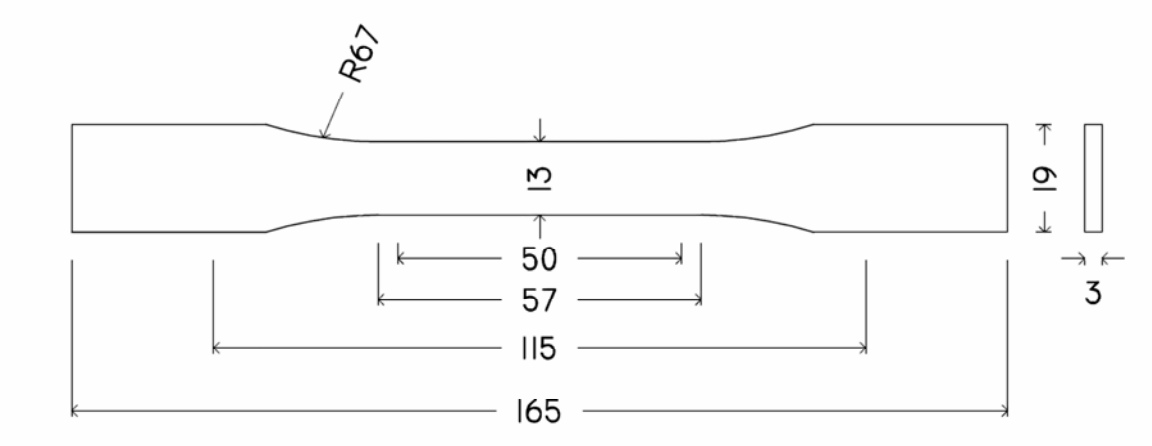

Fig. 6.1 A schematic diagram of the specimen used in fatigue and monotonic tests (all dimension in mm).

To investigate the effect of moisture absorption, 20% hemp-HDPE and unreinforced HDPE specimens were immersed in water for 35 days, prior to mechanical testing. After 35 days, the 20% hemp-HDPE specimens absorbed approximately 2.4% of its original weight, while the unreinforced HDPE specimen did not absorb any measurable amount of moisture. This demonstrates that moisture uptake in these composites is entirely due to the presence of the natural fibers.

Fatigue tests were conducted under tensile-tensile cyclic loading at two different fatigue-stress ratios (R = min. fatigue load/max. fatigue load) of 0.1 and 0.8. All fatigue tests were conducted under load (stress) control at a maximum frequency (f) of 3 Hz (tests conducted at frequencies above 3 Hz had significant self-heating or autogenous temperature effects. The fatigue stress levels used in the cyclic tests were chosen based on percentages of the monotonic strength, and are follows: 80%, 70%,, 65%, 60%, 55% and 40% for unreinforced HDPE; and 85%, 80%, 75%,70%,65%,60%,55%, 50% and 40% for 20% hemp-HDPE; and 80%, 75%, 70%, 65%, 60%, 55%, and 40% for 40% hemp-HDPE; and 80%, 70%, 65%, 55%, 45% for 20% hemp-HDPE with moisture. Fatigue tests were repeated three times at each stress.

In addition to the cyclic tests, a series of monotonic tensile tests were also performed at a various strain rates to simulate the loading ramps under fatigue conditions. The resulting monotonic data was used to develop the fatigue model in subsequent sections. Initial attempts were made to conduct the monotonic tests under stress control, but control problems were encountered at the high rates of loading. As such, monotonic tests were subsequently performed under strain controlled conditions to ensure repeatable and controllable responses. Based on the stress and strain at failure from these strain based tests, an effective (approximate) stress rate was calculated for each strain rate condition. Using this method, the monotonic results from strain controlled tests were used to approximately correlate the fatigue loading ramps under stress control (see Sections 6.3.1 and 6.3.3). Strain controlled tests were conducted at engineering strain rates ($\dot{\varepsilon}$) of 0.13, 0.50, 1.00, 2.00, 6.00, 8.00, 10.00 and 14.00 min^{-1}, which correspond to elongation speeds of 6.5, 25, 50, 100, 300, 400, 500 and 700 mm/min, respectively. Similar to the cyclic tests, all monotonic tests were repeated at least three times with the final results being averaged.

For monotonic and fatigue tests, the failure criterion was defined based on the observed failure modes. For unreinforced HDPE, the failure mode was found to be ductile failure (with necking). As such, the point of necking was selected as the failure criterion for monotonic tensile tests. The maximum engineering tensile stress at necking was taken as the ultimate tensile strength (σ_{ut}), and its corresponding engineering strain was considered to be the ultimate tensile strain (ε_{ut}). Similarly, the failure mode for cyclic loading of the unreinforced HDPE was also necking measured at a 15% reduction in the fatigue stress amplitude during the test. On other hand, the failure mode for the hemp-HDPE composites was brittle for all of the hemp fiber fractions. As a result, the failure criterion for the monotonic tensile tests was the maximum engineering tensile stress before brittle fracture (instantaneous separation of specimen). This was considered the ultimate tensile strength (σ_{ut}), while its corresponding engineering strain was considered as

the ultimate tensile strain (ε_{ut}). The failure mode of the hemp-HDPE composites during cyclic tests was the number of cycles to brittle fracture.

6.2.2 Experimental Results

The fatigue-life (S-N) curves of the various materials and conditions tested are shown in Figure 6.2. It can be seen that increasing the hemp fiber content (20% to 40% weight fraction) results in a slight increase in the fatigue strength, while exposure to moisture (for 20% weight fraction hemp) reduces the overall composite fatigue strength. The latter is most likely due to the degradation of the fiber-matrix interfacial strength and the fiber itself due to absorbed moisture [15-17]. The fatigue-life response of the unreinforced HDPE, however, is observed to somewhat intersect (cross) the curve of 20% hemp-HDPE after a fatigue life of N=10,000 cycles. At this point, the observed material failure pattern of the unreinforced HDPE changed from a ductile failure mode to a brittle one. This type of observed fatigue behaviour can be attributed to crazing, and it is known as a “ductile-brittle” fatigue failure system [18]. The fatigue-life response of 20% hemp composite immersed in water (for 35 days) was lower than all of other specimens tested. For all hemp-reinforced composites, the failure mode was consistently brittle in nature, irrespective of fiber fraction or environment (wet or dry). Also in Figure 6.2, the cyclic data shows good repeatability between individual tests. In particular, there appears to be no effect of the noted failure mode change on the repeatability of the results for the unreinforced HDPE.

It can also be observed that the fatigue sensitivity (i.e. the slope of S-N curve) is relatively constant for all materials tested, implying that the behavior is "matrix dominated" [11, 18]. This suggests that any model developed for these materials must account for this mechanistic behavior.

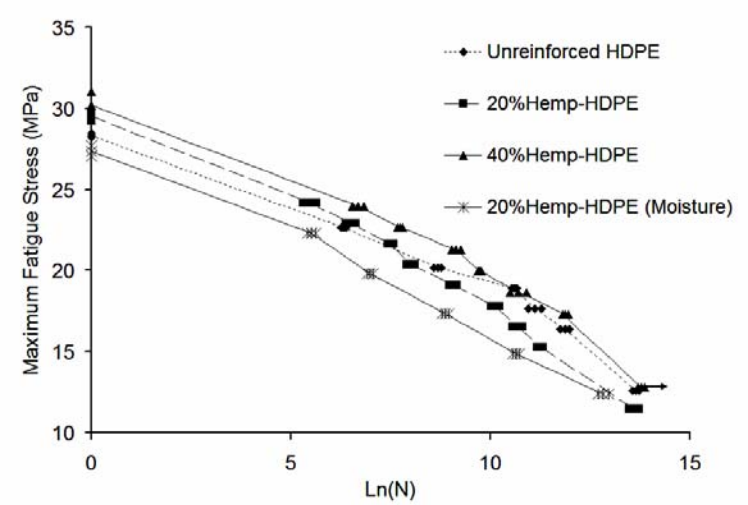

Fig. 6.2 Fatigue-life (S-N) curves for unreinforced HDPE, 20%, 40% Hemp-HDPE and 20%Hemp-HDPE immersed in water for 35 days. R=0.1 and fatigue frequency=3 Hz.

Figures 6.3-a and 6.3-b show two Scanning Electron Microscope (SEM) images from the fracture surfaces of 20% hemp-HDPE (tested at a max. applied stress of 19 MPa., stress ratio of 0.1 and frequency of 3.0 Hz) . The fracture surfaces demonstrate a number of failure mechanisms including fiber failure (FF), matrix failure (MF) and interfacial separation (IS) between fibers and matrix. The images also highlight the variability in fiber distribution and orientation which is expected of compounded composites. Conversely, the fracture surface of 20% hemp-HDPE immersed in water for 35 days is shown in Figure 6.4. Most of the reinforcing fibers were separated from the matrix, which can be attributed to the weakening of the fiber-matrix interfacial strength as a result of moisture absorption.

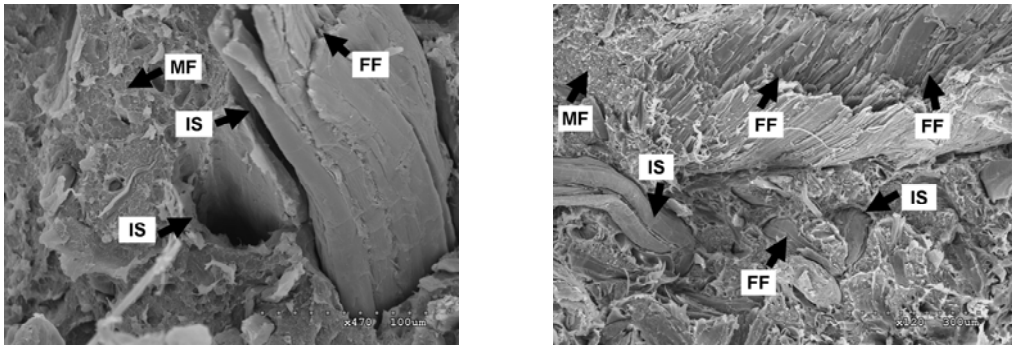

(a) **(b)**

Fig. 6.3 Scanning Electron Microscope (SEM) images of fracture surfaces of two fatigue samples for 20% hemp-HDPE at different magnifications: a) 470X and b) 120X. Both samples were tested at maximum applied fatigue stress (σ_{max}) of 19 MPa. Different types of failure mechanisms are shown: fibre failure (FF); matrix failure (MF); and interfacial separation between fibres and matrix (IS).

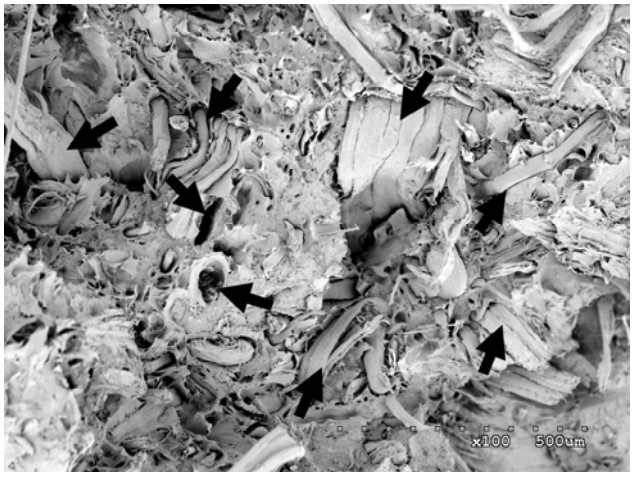

Fig. 6.4 Scanning Electron Microscope (SEM) image of 20% hemp-HDPE sample fatigue fracture surface immersed in water for 35 days under maximum applied fatigue stress (σ_{max}) of 19.8 MPa. Interfacial separation is noted by arrows.

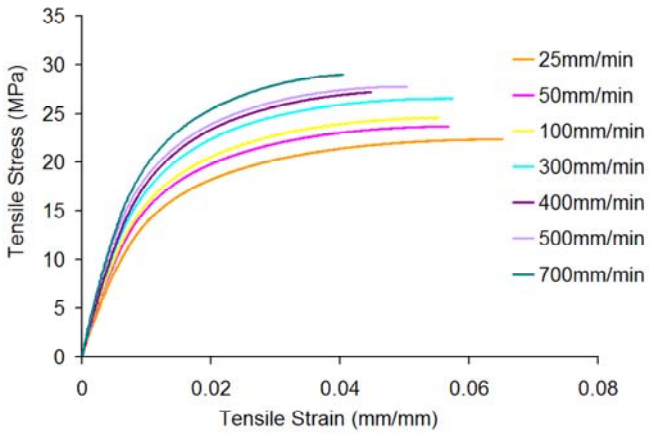

Fig. 6.5 Typical stress-strain responses of 20% hemp-HDPE composite for various strain rates.

In addition to the cyclic testing data, monotonic stress-strain curves were generated for the various materials at a number of strain rates. A typical plot is shown in Figure 6.5 for 20% hemp-HDPE composites. It can be seen that increasing the strain rate ($\dot{\varepsilon}$) results in a general trend of increasing stress with decreasing elongation at failure. For unreinforced HDPE, the failure mode was observed to be ductile, while for all reinforced HDPS composites (wet or dry), the failure mode tended to be brittle.

6.3 DEVELOPMENT OF A FATIGUE MODEL FOR NATURAL-FIBER-REINFORCED THERMOPLASTIC COMPOSITES

6.3.1 Mathematical Strain Rate Relationships for Monotonic Uniaxial Tensile Loading

As mentioned in Section 6.2.1, monotonic tests were conducted to approximate the loading ramps under cyclic loading. The results from these monotonic tests (conducted under strain control) will be incorporated into the

developed fatigue modeling through an approximate expression that will be developed later in Section 6.3.3. As such, to incorporate the monotonic tensile test results into the developed fatigue model, the relationship between the monotonic engineering ultimate tensile stress (σ_{ut}) and strain rates ($\dot{\varepsilon}$), as well as the engineering ultimate tensile strain (ε_{ut}) and strain rates ($\dot{\varepsilon}$), were characterized at different rates. These values were extracted from the stress-strain responses previously discussed (see typical plot in Figure 6.5).

For unreinforced HDPE, 20% hemp-HDPE, 40% hemp HDPE and 20% hemp-HDPE immersed in water for 35 days, Table 6.2 summarizes the following properties from the monotonic tensile tests: 1) the maximum engineering stress (i.e., ultimate tensile strength) (σ_{ut}); 2) the corresponding engineering strain to σ_{ut} (i.e., ultimate tensile strain) (ε_{ut}); and 3) the tangent elastic modulus of the engineering stress-strain curve (i.e., Young's modulus) (E).

For short-fiber-reinforced thermoplastic composites, the mathematical relationship of the σ_{ut}-$\dot{\varepsilon}$ curve can be represented using the non-linear one-dimensional interpretation of the Norton-Hoff rheology model for viscoplastic material, which can be represented as follows [28-30]:

$$\sigma_{ut} = k_{\sigma}(\dot{\varepsilon})^{m_{\sigma}} \quad \text{.....} \quad \textbf{6.1}$$

where σ_{ut} is the maximum tensile stress (MPa) produced by a strain rate $\dot{\varepsilon}$ (min^{-1}), k_{σ} is a material constant ($MPa.min^{m_{\sigma}}$), and m_{σ} is a behaviour index for σ_{ut} (dimensionless).

Table 6.2 Different measured values of σ_{ut}, ε_{ut} and E for the tested materials:

Material	$\dot{\varepsilon}$ (min^{-1})	Average σ_{ut} (MPa)	Standard Error of σ_{ut}	Average ε_{ut} (mm/mm)	Standard Error of ε_{ut}	Average E (GPa)	Standard Error of E
Unreinforced HDPE	0.5	22.31	0.175	0.0996	0.0020	1.440	0.020
	1	23.61	0.174	0.0963	0.0029	1.590	0.096
	2	25.19	0.227	0.0885	0.0003	1.520	0.117
	6	26.25	0.109	0.0873	0.0017	1.730	0.176
	8	27.11	0.104	0.0870	0.0003	1.910	0.053
	10	27.54	0.192	0.0857	0.0012	1.970	0.224
	14	28.32	0.147	0.0836	0.0018	2.080	0.146
20% Hemp-HDPE	0.5	22.53	0.057	0.0639	0.0024	2.140	0.108
	1	23.91	0.080	0.0602	0.0026	2.450	0.061
	2	25.65	0.155	0.0563	0.0005	2.490	0.120
	6	26.64	0.131	0.0556	0.0009	2.570	0.034
	8	27.38	0.103	0.0537	0.0004	2.760	0.061
	10	27.86	0.099	0.0502	0.0011	2.940	0.080
	14	29.54	0.180	0.0464	0.0020	3.110	0.096
40% Hemp-HDPE	0.13	23.13	0.113	0.0260	0.0011	3.920	0.036
	0.5	24.58	0.129	0.0248	0.0001	4.050	0.061
	2	26.53	0.167	0.0235	0.0003	4.320	0.005
	6	28.47	0.133	0.0203	0.0005	4.610	0.016
	8	29.35	0.150	0.0204	0.0015	4.830	0.052
	14	30.18	0.173	0.0230	0.0001	5.140	0.075
20% Hemp-HDPE immersed in water for 35 days	1	23.01	0.084	0.0703	0.0015	2.380	0.115
	2	24.67	0.235	0.0675	0.0033	2.590	0.101
	6	25.33	0.243	0.0609	0.0026	2.640	0.166
	10	26.45	0.117	0.0595	0.0014	2.920	0.072
	14	27.36	0.182	0.0565	0.0013	2.970	0.101

The relationship between ε_{ut} and $\dot{\varepsilon}$ can also be represented by a power law as follows [31, 32]:

$$\varepsilon_{ut} = k_{\varepsilon}(\dot{\varepsilon})^{m_{\varepsilon}} \quad \text{..... 6.2}$$

where ε_{ut} is the strain (dimensionless) corresponding to σ_{ut} for an applied strain rate $\dot{\varepsilon}$ (min^{-1}), k_{ε} is material constant ($min^{m_{\varepsilon}}$), and m_{ε} is the power law index for ε_{ut} (dimensionless).

Parameters k_{σ} and m_{σ} in equation 6.1, and k_{ε} and m_{ε} in equation 6.2, can be represented as functions of fiber volume fraction (v_f) using the Harris mechanistic yield model, which is a simplified version of Holiday's yield model [31, 33, 34], as follows:

$$k_{\sigma} = \frac{k_{\sigma o}}{1 - k_{\sigma o}\beta_{k_{\sigma}}\omega_{k_{\sigma}}(v_f)^{\psi_{k\sigma}}} \quad \text{..... 6.3}$$

where $k_{\sigma o}$ is k_{σ} for the unreinforced matrix polymer, v_f is the hemp fiber volume fraction, $\beta_{k_{\sigma}}$ is a matrix-dependent parameter, $\psi_{k_{\sigma}}$ is a matrix-dependent parameter, and $\omega_{k_{\sigma}}$ is a moisture-absorption coefficient; and

$$X\big|_{X=m_{\sigma},\, k_{\varepsilon},\, m_{\varepsilon}} = \frac{X_o}{1 + X_o\beta_X\omega_X(v_f)^{\psi_X}} \quad \text{..... 6.4}$$

where X_o is the variable X for the unreinforced matrix polymer (variable X can be m_{σ}, k_{ε} or m_{ε}), β_X is a matrix-dependent parameter for variable X, ψ_X is a matrix-dependent parameter for variable X, and ω_X is a term added to the Harris model as a moisture absorption coefficient to include the effect of moisture absorption for variable X.

Using the monotonic data in Table 6.2, the material constants (k_{σ} and m_{σ} in equation 6.1 and k_{ε} and m_{ε} in equation 6.2) were estimated using the non linear regression method of Levenberg-Marquardt which is a modified version of the

Gauss-Newton method [33]. This non-linear regressions analysis was performed using the commercial package MATLAB (version R2013a). These materials constants were then used, with the associated values of fiber volume fractions (v_f), to estimate the values of parameters in equations 6.3 and 6.4. These are shown in Tables 6.5, 6.4, 6.5 and 6.6 for k_σ, m_σ, k_ε and m_ε, respectively.

Table 6.3 Calculated parameters for k_σ in equation 6.3:

For Parameter k_σ in equation 3	Value	Units
$k_{\sigma o}$	23.588	$MPa.\min^{m_\sigma}$
β_{k_σ}	0.060	$MPa^{-1}.\min^{-m_\sigma}$
ψ_{k_σ}	2.422	Dimensionless
ω_{k_σ}	1.000	Dimensionless
ω_{k_σ} (For 20% hemp immersed in water for 35 days)	-1.790	Dimensionless

Table 6.4 Calculated parameters for m_σ in equation 6.4:

For Parameter X= m_σ in equation 4	Value	Units
$m_{\sigma o}$	0.068	Dimensionless
β_{m_σ}	-29.706	Dimensionless
ψ_{m_σ}	1.954	Dimensionless
ω_{m_σ}	1.000	Dimensionless
ω_{m_σ} (For 20% hemp immersed in water for 35 days)	-7.303	Dimensionless

Table 6.5 Calculated parameters for k_ε in equation 6.4:

For Parameter X= k_ε in equation 4	Value	Units
$k_{\varepsilon o}$	0.095	min^{m_ε}
β_{k_ε}	379.094	min^{-m_ε}
ψ_{k_ε}	2.082	Dimensionless
ω_{k_ε}	1.000	Dimensionless
ω_{k_ε} (For 20% hemp immersed in water for 35 days)	0.616	Dimensionless

Table 6.6 Calculated parameters for m_ε in equation 6.4:

For Parameter X= m_ε in equation 4	Value	Units
$m_{\varepsilon o}$	-0.036	Dimensionless
β_{m_ε}	11.449	Dimensionless
ψ_{m_ε}	0.029	Dimensionless
ω_{m_ε}	1.000	Dimensionless
ω_{m_ε} (For 20% hemp immersed in water for 35 days)	1.384	Dimensionless

6.3.2 Fatigue Life Relationships

As a consequence of the "matrix-dominated" behaviour in Figure 6.2, a single model can be developed to represent the fatigue behaviour of both unreinforced and reinforced materials. Assuming a linear fit for curves in Figure 6.2, the proposed relationship between maximum fatigue stress (σ_{max}) and cyclic fatigue life (N) for each S-N curve can be expressed as follows:

$$\sigma_{max} = \theta - \vartheta \ln(N) \quad \text{..... 6.5}$$

where σ_{max} is maximum fatigue stress, N is the number of fatigue life cycles to failure, and θ and ϑ are material parameters which are functions of fiber volume fraction (v_f) and fatigue loading conditions and fatigue stress ratio (R).

The fatigue-life (S-N) curves in Figure 6.2 can be normalized by dividing the maximum applied stress by the maximum stress for a one cycle lifetime (i.e. the fatigue strength of one cycle). This latter value can be estimated by the monotonic ultimate tensile stress (σ_{ut}) from a monotonic test that approximately produces a stress rate similar to the fatigue stress loading rate [35-37] (see Section 6.3.1). Since the fatigue-life curves in Figure 6.2 are seen to be parallel, the normalized fatigue-life curves will form one curve which represents the whole family of curves shown in Figure 6.2. For 20% hemp-HDPE, 40% hemp-HDPE and 20% hemp-HDPE immersed in water for 35 days, the relationship between the normalized maximum fatigue stress (stress level) and the corresponding function of the number of cycles to failure (N) is shown in Figure 6.6, where the stress level (q) can be represented as follows:

$$q=\frac{\sigma_{max}}{\sigma_{max1}}=\frac{\sigma_{max}}{\sigma_{ut}} \quad \textbf{6.6}$$

where, σ_{max} is the maximum applied fatigue stress at N cycle fatigue-life, and σ_{max1} is the fatigue strength at one cycle fatigue-life. For this analysis, it is assumed that σ_{max1} can be approximated by the ultimate monotonic strength, σ_{ut}, determined at a loading rate similar to the fatigue stress loading rate.

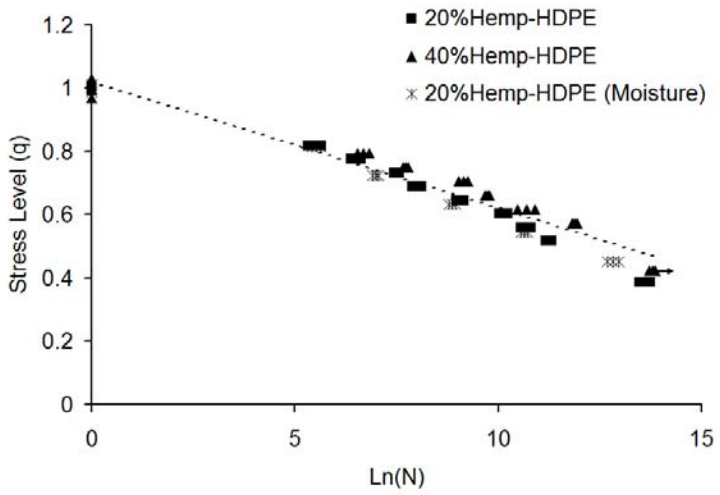

Fig. 6.6 The relationship between the stress level (q) and number of cycles to failure (N) for 20%, 40% Hemp-HDPE and 20% Hemp-HDPE immersed in water for 35 days. R=0.1 and fatigue frequency=3 Hz (bands on data represent the max/min limits).

Using the stress level (q) in equation 6.6 to plot the q-N relationship in Figure 6.6, the linear model in equation 6.5 can be rewritten to simulate the relationship between the stress level (q) and the cyclic fatigue life (N) in Figure 6.6 for all tested natural fiber composites, as follows:

$$q = \alpha - \kappa \ln(N) \quad \text{..... 6.7}$$

where q is the stress level at which the fatigue life cycle equals N, and α and κ are material parameters which are functions of fatigue-loading conditions (i.e. frequency, f, and the fatigue stress ratio, R).

Given the boundary conditions of the data points of normalized curves in Figure 6.6, α in equation 6.7 is assumed to be equal to 1.0 (i.e. the maximum stress at a life of one fatigue cycle is approximately equivalent to the monotonic stress), and κ is a material parameter that can be assumed to be a function of the fatigue stress ratio (R) [37]. Therefore, equation 6.7 can be re-written as follows:

$$q = 1 - \kappa \ln(N) \quad \text{..... 6.8}$$

where q is the stress level, and κ is a material parameter which is a function of fatigue loading and the fatigue stress ratio (R).

Based on equation 6.8 and the experimental data in Figure 6.6, the material parameter (κ) was found to be 0.0379 using best-fit linear regression. The resulting coefficient of determination (R^2-value) was 0.99, demonstrating a good fit to the data.

In order to fully define equation 6.8, a large number of experiments are required to characterize how the parameter κ changes with the fatigue loading conditions, such as the stress ratio (R) and the mean stress (σ_m). However, to eliminate the need to conduct further experiments, the effect of the fatigue loading conditions can be introduced into the stress level (q) [37]. Based on this, a new modified stress level (S_m), incorporating the effect of the fatigue loading conditions, can be developed through the following derivation.

6.3.3 The Modified Stress Level and the Fatigue Model

Assuming that the fatigue stress (σ_{max}) at one cycle fatigue-life can be approximated using the monotonic tensile strength (σ_{ut}) [35-37], the fatigue stress ratio ($R = \frac{\text{Min. fatigue stress}}{\text{Max. fatigue stress}} = \frac{\sigma_{min}}{\sigma_{max}}$) has a value of zero and σ_{max} will be equal to σ_{ut}; hence, the following relationship can be developed:

$$\sigma_m = \sigma_{max} - \sigma_a = \sigma_{ut} - \sigma_a \quad \text{..... 6.9}$$

where σ_a is the fatigue stress amplitude, and σ_m is the mean stress. This equation can be re-written in the following form:

$$\frac{\sigma_m}{\sigma_{ut}-\sigma_a}=1 \quad \text{..... 6.10}$$

The expression in equation 6.10 is the normalization of the fatigue strength at one cycle fatigue-life. This equation can now be generalized to form a new modified stress parameter, as follows:

$$S_m=\frac{\sigma_m}{\sigma_{ut}-\sigma_a}=\frac{(\sigma_{max}+\sigma_{min})/2}{\sigma_{ut}-(\sigma_{max}-\sigma_{min})/2}=\frac{(1+R)q}{2-(1-R)q} \quad \text{..... 6.11}$$

where S_m is the new modified stress level, σ_a is the fatigue stress amplitude [$\sigma_a=(\sigma_{max}-\sigma_{min})/2$], σ_{max} is the maximum applied fatigue stress, σ_{min} is the minimum applied fatigue stress, σ_{ut} is the monotonic ultimate tensile strength (i.e. fatigue strength at one cycle), σ_m is the mean stress [$\sigma_m=(\sigma_{max}+\sigma_{min})/2$], R is the fatigue stress ratio, and q is the fatigue stress level ($q=\sigma_{max}/\sigma_{ut}$).

By using the new modified stress level (S_m) in equation 6.11, the fatigue-life curves in Figure 6.2 can be normalized as shown in Figure 6.7. From Figure 6.7, a new linear model can be proposed, as follows:

$$S_m=\gamma - \eta \ln(N) \quad \text{..... 6.12}$$

where S_m is the new modified stress level at which the fatigue life cycle equals N, and γ and η are fitting parameters.

Since the effect of fatigue-loading conditions has been introduced to S_m in equation 6.11, forming one normalized S-N curve, the parameter η in equation 6.12 can be assumed to be constant for all loading conditions. η is the slope, which can be assumed to be a constant, and can also be referred to as a "fatigue sensitivity index" for this specific polymer matrix. In addition, the new modified stress level (S_m) in equation 6.11 is equal to one for a fatigue life of one cycle (i.e. for q is equal to one); therefore, for the normalized curves in Figure 6.7, γ in

equation 6.12 is equal to one. Therefore, the linear model in equation 6.12 can be represented as follows:

$$S_m = 1 - \eta \ln(N) \quad \text{..... 6.13}$$

Based on equation 6.13 and the experimental data in Figure 6.7, the fatigue sensitivity index (η) was found to be 0.0517 using best-fit linear regression. The resulting coefficient of determination (R^2-value) was 0.99, demonstrating a good fit to the data.

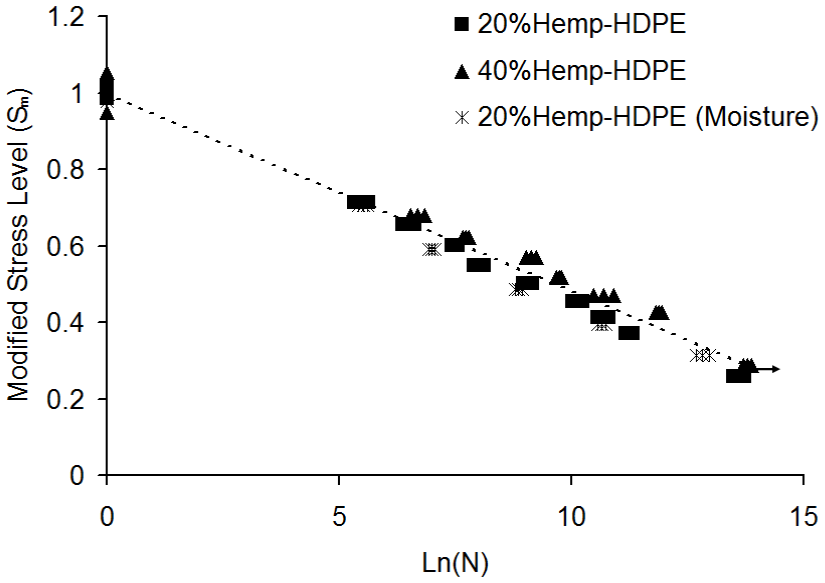

Fig. 6.7 The relationship between the new modified stress level (S_m) and number of cycles to failure (N) for 20, 40% Hemp-HDPE and 20% Hemp-HDPE immersed in water for 35 days. R=0.1 and fatigue frequency=3 Hz (bands on data represent the max/min limits).

Using equations 6.1, 6.5, 6.6, 6.11 and 6.13, a model can be developed to calculate the maximum fatigue stress (σ_{max}) as follows:

$$\sigma_{max} = \frac{\left[2k_{\sigma}\dot{\varepsilon}^{m_{\sigma}}\left(\eta \ln(N)-1\right)\right]}{\left[\eta(1-R)\ln(N)-2\right]} \quad \text{..... 6.14}$$

Equation 6.14 can be inverted to determine the fatigue life to failure (N) for given loading conditions:

$$\ln(N) = \frac{\left[k_{\sigma}\dot{\varepsilon}^{m_{\sigma}} - \sigma_{max}\right]}{\eta\left[k_{\sigma}\dot{\varepsilon}^{m_{\sigma}} - \sigma_{a}\right]} \quad \text{..... 6.15}$$

To incorporate the fatigue frequency (f), a relationship must be developed between the monotonic tensile strain rate ($\dot{\varepsilon}$) and the fatigue frequency. For a monotonic tensile test under strain control, an approximate stress rate ($\dot{\sigma}$) expression can be assumed to be a function of strain rate ($\dot{\varepsilon}$) as follows:

$$\dot{\sigma} \approx \frac{\sigma_{ut}}{t} = \sigma_{ut}\frac{\dot{\varepsilon}}{\varepsilon_{ut}} \quad \text{..... 6.16}$$

where t is the time needed to reach σ_{ut} under strain-controlled monotonic loading conditions.

For fatigue cyclic loading, the stress ramping rate ($\dot{\sigma}$) can be represented at a given fatigue frequency (f) and stress ratio (R) by the following expression:

$$\dot{\sigma} = 4f\sigma_{a} = 2f\sigma_{max}(1-R) \quad \text{..... 6.17}$$

As mentioned in Section 6.3.1, the monotonic tensile strength (σ_{ut}), measured under stress rates similar to those developed in the fatigue test, was assumed to approximate the fatigue strength (σ_{max}) at one cycle fatigue-life. Based on this assumption, R in equation 6.17 will have a value of zero, and σ_{max} will be σ_{ut}. By equating equation 6.16 and equation 6.17, and using equation 6.2, the following

expression can be assumed to approximately represent the monotonic strain rate ($\dot{\varepsilon}$) in the terms of stress controlled fatigue loading conditions:

$$\dot{\varepsilon} \approx \left(2k_{\varepsilon} f\right)^{\frac{1}{1-m_{\varepsilon}}} \quad \text{..... 6.18}$$

where $\dot{\varepsilon}$ is the monotonic strain rate that is approximately corresponding to fatigue frequency, f.

By using equation 6.18, the generalized fatigue model in equation 6.14 can be represented as follows:

$$\sigma_{max} = \frac{\left[2k_{\sigma}\left(2k_{\varepsilon} f\right)^{\frac{m_{\sigma}}{1-m_{\varepsilon}}}\left(\eta \ln\left(N\right)-1\right)\right]}{\left[\eta\left(1-R\right)\ln\left(N\right)-2\right]} \quad \text{..... 6.19}$$

Furthermore, by using equation 6.18, the fatigue stress life (N) model in equation 6.15 can be re-arranged as follows:

$$\ln(N) = \frac{\left[k_{\sigma}\left(2k_{\varepsilon} f\right)^{\frac{m_{\sigma}}{1-m_{\varepsilon}}} - \sigma_{max}\right]}{\eta\left[k_{\sigma}\left(2k_{\varepsilon} f\right)^{\frac{m_{\sigma}}{1-m_{\varepsilon}}} - \sigma_{a}\right]} \quad \text{..... 6.20}$$

6.3.4 Comparison of the Model with Experiments

In comparing the experimental results to the derived fatigue-life model, a series of plots are provided. For clarity, the effect of fiber volume fraction, moisture condition and fatigue loading condition (R value) are each plotted separately from Figure 6.8 to Figure 6.11.

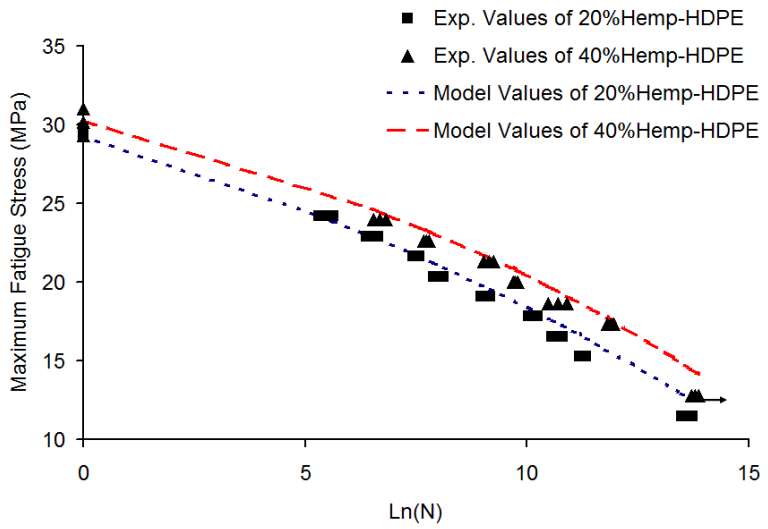

Fig. 6.8 Measured and predicted fatigue-life (S-N) curves for 20% and 40% hemp-reinforced HDPE at R= 0.1 and f = 3.0 Hz.

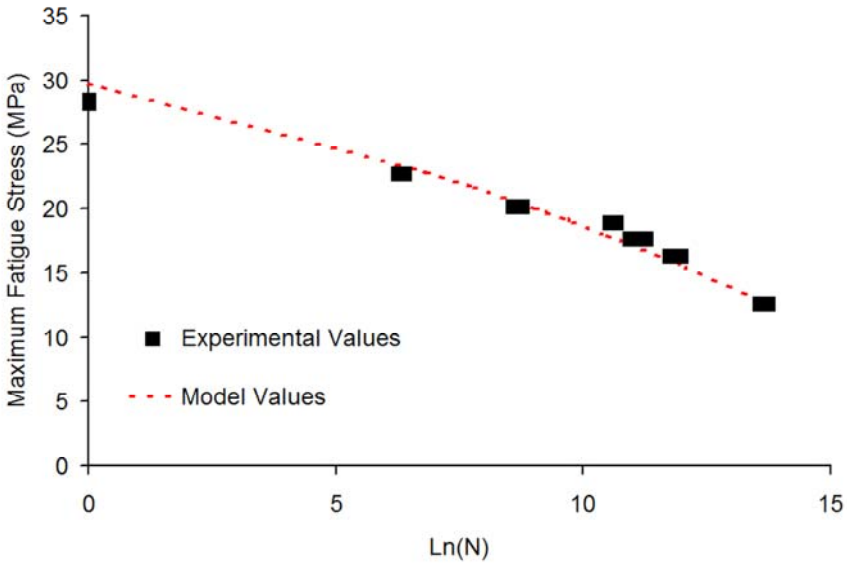

Fig. 6.9 Measured and predicted fatigue-life (S-N) curve for unreinforced HDPE at R= 0.1 and f = 3.0 Hz.

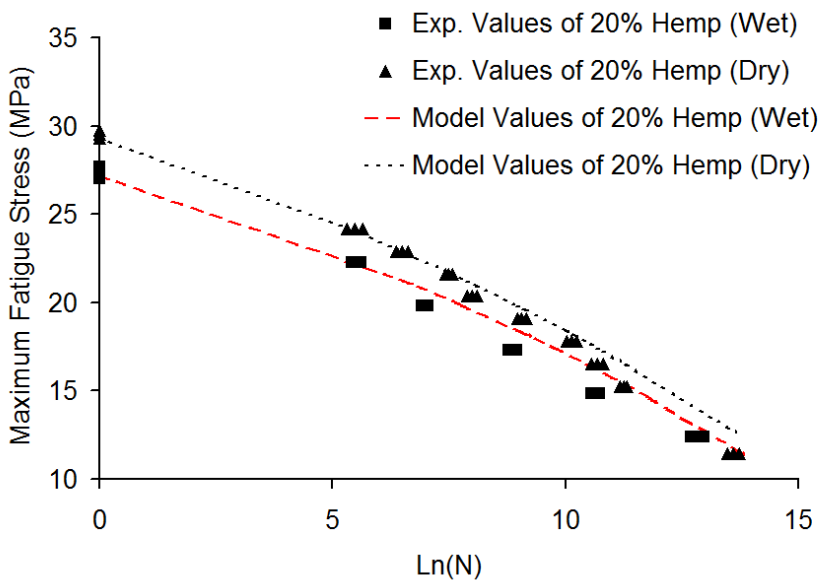

Fig. 6.10 Measured and predicted fatigue-life (S-N) curves for 20% hemp-HDPE without and without moisture at R= 0.1 and f = 3.0 Hz.

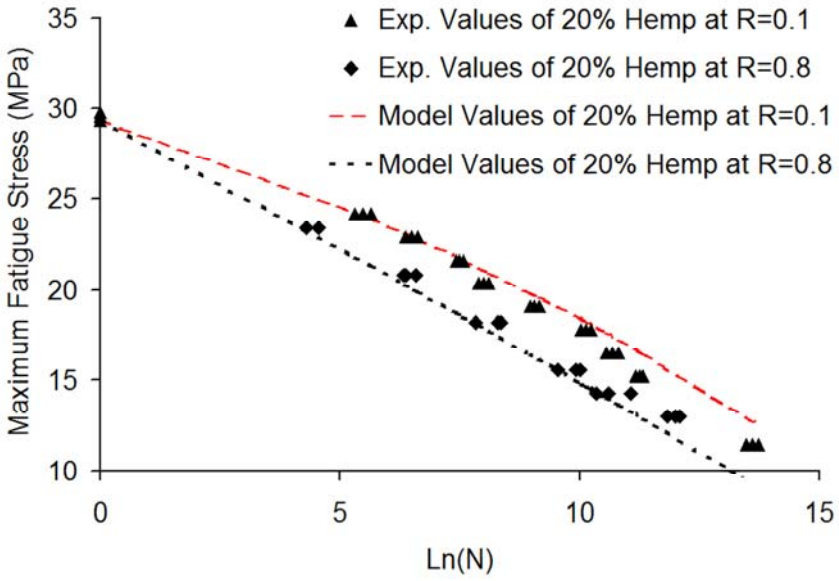

Fig. 6.11 Measured and predicted fatigue-life (S-N) curves for 20% hemp-reinforced HDPE at two stress ratios (R=0.1 and 0.8) and f = 3.0 Hz.

Figure 6.8 shows the comparison between the experimental data and the model for both 20% and 40% hemp-HDPE composites. It can be seen that there is a good correlation between the measured fatigue life behaviour and the values predicted by the model in equation 6.19. Similarly, for unreinforced HDPE, the experimental versus predicted values of the fatigue-life response shows good correlation as shown in Figure 6.9. While the model does a good job representing the general trend, it does not capture the slight change in slope observed at approximately 10,000 cycles (observed change in failure mode).

For the hemp-HDPE composites with and without absorbed moisture (wet vs. dry), the model again shows a reasonable fit to the experimental data, as shown in Figure 6.10. The model is seen to capture the convergence of the wet and dry data sets with increasing fatigue-life. It is clear that exposure to moisture and the resulting degradation of the natural fibers is more detrimental in the low cycle regime (i.e. at higher stress conditions) than it is at longer lives. This also demonstrates the increased contribution of fiber loading at higher stress levels. At longer fatigue-lives, the behavior becomes dominated by the properties of the matrix. Further work, however, is necessary to better understand the root cause of these damaging mechanisms.

Finally, the developed fatigue model in equation 6.19 was also used to predict the fatigue behaviour of hemp-fiber-reinforced HDPE at two different stress ratios (R=0.1 and 0.8). As shown in Figure 6.11, the model predict for both stress ratios quite well, and captures the increase in the fatigue sensitivity (i.e the curve become more steep) with increasing of the stress ratio (R) from 0.1 to 0.8. This is the expected behaviour since the fatigue mean stress should increase with increasing stress ratio.

6.4 CONCLUSIONS

In this study, the fatigue behaviour of hemp-reinforced HDPE was investigated. Overall, the addition of hemp fibers slightly improved the fatigue strength of the polymer matrix, however, adding hemp fibers did not change the sensitivity of the developed fatigue life curves. The observed fatigue failures varied from a ductile-brittle behaviour for the unreinforced HDPE, to a consistent brittle failure system for the reinforced composites. The fatigue strength after water absorption was also found to be lower than the fatigue strength of both the unreinforced matrix polymer and the dry hemp-HDPE composites. This was attributed to the hydrophilic nature of the natural fibers which resulted in a reduction of fiber and interfacial strength between the fibers and the matrix.

A new model was developed to predict the fatigue life of these natural fiber composites. This model incorporates a new modified stress level (S_m), which was used to normalize all fatigue life curves for different fatigue loading and environmental conditions. The new fatigue model was developed using these normalized fatigue life curves. In general, the developed fatigue model was capable of predicting the fatigue behavior of the tested natural fiber composites at different values of the fiber volume fraction (v_f) and stress ratio (R), as well as taking into consideration the effect of moisture absorption.

CHAPTER 7: CONCLUSIONS

7.1 RESEARCH CONCLUSIONS

The moisture absorption of natural-fiber-reinforced polymer was investigated using high density polyethylene (HDPE) and low density polyethylene (LDPE) with different matrix crystallinity. The moisture absorption rate was found to be affected by two factors: 1) the matrix crystallinity; and 2) natural fiber volume fraction (v_f). The maximum absorbed moisture was found to be affected by the matrix stiffness and its contraction along with v_f. The dominating moisture diffusion mechanism was found to be Fickian diffusion; therefore, the flux of the diffused moisture mass can be assumed to be proportional to the moisture concentration gradient in the diffusion direction. The diffusion mechanism was found to shift toward pseudo-Fickian when the v_f was decreased in the LDPE composites. On the other hand, the diffusion mechanism shifted towards anomalous diffusion by increasing v_f in the HDPE composites. The diffusivity of the tested composites was also investigated. The Diffusivity increased by increasing hemp volume fractions. In 40% hemp, it was found that the diffusivity increased considerably by using HDPE as a matrix; this can be attributed to: 1) the slightly larger amount of hemp fibers included in 40% hemp-HDPE; 2) the increasing effect of the negative pressure voids as a result of increasing the crystallinity and the decompaction forces.

Uniaxial monotonic tensile tests under both normal and wet conditions were conducted on unreinforced HDPE and HDPE reinforced with short hemp bast fibers forming 20% and 40% of the total weight. In general, the addition of hemp fiber reinforcement results in a slight increase in HDPE strength, compared to a significant increase in stiffness. Exposure to moisture, however, results in a decrease in strength relative to dry conditions. The effect of the strain rate ($\dot{\varepsilon}$) on the mechanical properties, maximum tensile stress (σ_{ut}) and its corresponding strain (ε_{ut}) along with Young's modulus (E), was investigated. Both unreinforced

HDPE and hemp-HDPE composites showed a strain rate hardening behaviour as $\dot{\varepsilon}$ increased. The results of the tested composites showed that for short natural fiber reinforced polymer, the mechanical behaviour is dominated by the matrix. The effect of $\dot{\varepsilon}$ on the mechanical properties was successfully modeled under normal and wet conditions. Normalized Engineering stress-strain curves were developed and analyzed in order to: 1) eliminate the effect of $\dot{\varepsilon}$; and 2) demonstrate the individual effect of adding short hemp natural fibers and moisture absorption. Generalized empirical and semi-analytical model were successfully developed to simulate the monotonic behaviour of the tested Natural-Fiber-Reinforced Polymers (NFRPs) at different values of $\dot{\varepsilon}$ and v_f. The developed generalized models were successfully capable to simulate the effect of moisture absorption on the monotonic behaviour of NFRPs. Different stiffness model forms were developed to simulate the tangent stiffness modulus of the stress-strain curve (i.e. Young's modulus,E) of NFRPs; all models showed a good match with the experimental values, taking into consideration the effect of applied strain rate ($\dot{\varepsilon}$), short fiber volume fraction (v_f) and moisture absorption.

Fatigue tests (under both dry and wet conditions) were conducted on the same NFRPs that were tested for the monotonic behaviour investigations. In general, the addition of hemp fiber reinforcement resulted in an increase in HDPE fatigue strength; however, adding hemp fibers did not change the slopes of the fatigue life (S-N) curves, as they were shown to be parallel for all hemp reinforced material tested, suggesting that the fatigue behavior is matrix dominated under both dry or wet conditions. Exposure to moisture, however, results in a decrease in fatigue strength relative to the fatigue strength of both the unreinforced matrix polymer and the dry hemp-HDPE composites. A new comprehensive fatigue model was developed to predict the fatigue life of these natural fiber composites. This model incorporates a new modified stress level (S_m), used to normalize fatigue-life curves for different fatigue loading and environmental conditions (i.e. dry and wet conditions). The developed fatigue model was capable of predicting the fatigue behavior of the tested natural fiber composites at different values of the fiber

volume fraction (v_f) and stress ratio (R), as well as considering the effect of moisture absorption.

7.2 RESEARCH CONTRIBUTION

The investigations and the models developed in this study form one step forward toward building a better engineering understanding of these new NFRP products, and this will enable these products to be incorporated in the engineering design process in a more reliable approach. This was achieved through the following steps:

- Unique experimental monotonic and fatigue results of natural fibre composites.

- Better understanding and modeling of the moisture absorption in NFRPs including the effect of matrix crystallinity on the absorption kinetic behaviour at different fiber volume fractious.

- A comprehensive power law model representing the effect of strain rate ($\dot{\varepsilon}$), short fiber volume fraction (v_f) and moisture absorption on the mechanical properties of NFRPs.

- Comprehensive empirical and semi-analytical monotonic models that were successfully developed to simulate the stress-strain behaviour of NFRPs.

- Comprehensive fatigue life prediction model that was developed to simulate the fatigue-life behaviour at different loading and environmental (wet and dry) conditions.

7.3 FUTURE WORK

This research can be expanded in the future to investigate the following points:

- Investigating and modeling the effect of fiber length and distribution on the mechanical behaviour of NFRP.

- Investigating and modeling the effect chemical treatment and coupling agent on the mechanical behaviour, monotonic and cyclic behaviour of NFRP.

- Better understanding of moisture absorption mechanisms in NFRP, including the possible effect of shrinkage micro-voids and injection/extrusion pressure.

- Expand the range of experiments to validate the developed model as predictive models.

- Expand the range of the experiments under wet conditions to better define the moisture absorption factor developed in the models.

- Further experiments are to be conduct to determine whether or not there is an effect for extrusion pressure on the mechanical properties of the extruded unreinforced polymer.

- Studying the monotonic and cyclic behaviour using other reinforcing natural fibre types such as :
  i. Cereal straws (e.g. wheat, Triticale,…..etc.).
  ii. Wood (dust, fibre and pulp).

- Investigating the effect of micro fibres (e.g. delivered from pulps) or Micro Crystalline Cellulose (MCC) on the mechanical behaviour of NFRP. Preliminary SEM photos from this current study have shown that micro-fibres might have improved bonding and distribution in the matrix. Further experiments are required to validate this observation.

- Investigating the effect of using other types of fibre processing and/or chemical treatments on the mechanical behaviour of NFRPs.

BIBLIOGRAPHY

CHAPTER 1 REFERENCES

1. Holbery, J. and D. Houston, *Natural-fiber-reinforced polymer composites in automotive applications.* JOM, 2006. **58**(11): p. 80-6.

2. Panthapulakkal, S. and M. Sain, *Studies on the water absorption properties of short hemp-glass fiber hybrid polypropylene composites.* Journal of Composite Materials, 2007. **41**(15): p. 1871-1883.

3. Drzal, L.T., M. Misra, and A.K. Mohanty, *Natural fibers, biopolymers, and biocomposites*. 2005, Boca Raton, FL: Taylor & Francis. 875 p.

4. Hargitai, H., I. Racz, and R. Anandjiwala, *Development of hemp fibre - PP nonwoven composites.* Macromolecular Symposia, 2006. **239**: p. 201-208.

CHAPTER 2 REFERENCES

1. Holbery, J. and D. Houston, *Natural-fiber-reinforced polymer composites in automotive applications.* JOM, 2006. **58**(11): p. 80-6.

2. Panthapulakkal, S. and M. Sain, *Studies on the water absorption properties of short hemp-glass fiber hybrid polypropylene composites.* Journal of Composite Materials, 2007. **41**(15): p. 1871-1883.

3. ASM-International., *ASM Handbook Volume 21:Composites*, in *ASM Handbook*, S.L.D. D.B. Miracle, Editor. 2001, ASM International: USA.

4. Hargitai, H., I. Racz, and R. Anandjiwala, *Development of hemp fibre - PP nonwoven composites.* Macromolecular Symposia, 2006. **239**: p. 201-208.

5. Drzal, L.T., M. Misra, and A.K. Mohanty, *Natural fibers, biopolymers, and biocomposites*. 2005, Boca Raton, FL: Taylor & Francis. 875 p.

6. Friedrich, K., *Mesoscopic aspects of polymer composites: processing, structure and properties.* Journal of Materials Science, 1998. **33**(23): p. 5535-56.

7. Wolodko, J., J. Vidmar, J. Slaski, W. Chute, L. Mcliveen, and M. Hopkins, *Polymer Biocomposites from Alberta Feedstock – Hemp Reinforced Polyethylene*. 2008, Alberta Research Council: Edmonton, Canada.

8. Li, X., L. Tabil, and S. Panigrahi, *Chemical treatments of natural fiber for use in natural fiber-reinforced composites: A review.* Journal of Polymers and the Environment, 2007. **15**(1): p. 25-33.

9. Espert, A., F. Vilaplana, and S. Karlsson, *Comparison of water absorption in natural cellulosic fibres from wood and one-year crops in polypropylene composites and its influence on their mechanical properties.* Composites Part A: Applied Science and Manufacturing, 2004. **35**(Compendex): p. 1267-1276.

10. Crank, J., *The mathematics of diffusion*. 2d ed. 1975, Oxford, [Eng]: Clarendon Press. viii, 414 p.

11. Comyn, J., *Polymer permeability*. 1985, London: Elsevier Applied Science. vii, 383 p.

12. Westman, M.P., S.G. Laddha, L.S. Fifield, T.A. Kafentzis, and K.L. Simmons, *Natural fiber composites: A review*. 2010, Pacific Northwest National Laboratory Richland, Washington.

13. Gtridhar, J. and R. Rao, *Moisture absorption characteristics of natural fibre composites.* Journal of Reinforced Plastics and Composites, 1986. **5**(2): p. 141-150.

14. Bharath, K.N. and A.M. Rajesh, *Moisture absorption characteristics of Areca/Maize reinforced hybrid polymer composites.* International Journal of Advanced Engineering & Application, 2010. **1**: p. 207-211.

15. Dhakal, H., Z. Zhang, and M. Richardson, *Effect of water absorption on the mechanical properties of hemp fibre reinforced unsaturated polyester composites.* Composites Science and Technology, 2006. **67**(7-8).

16. Saheb, D. and J.P. Jog, *Natural fiber polymer composites: A review.* Advances in Polymer Technology, 1999. **18**(Compendex): p. 351-363.

17. Bledzki, K. and J. Gassan, *Composites reinforced with cellulose based fibres.* Progress in Polymer Science (Oxford), 1999. **24**(Compendex): p. 221-274.

18. Baillie, C., *Green composites : polymer composites and the environment*. 2004, Boca Raton,Cambridge, England: CRC Press ; Woodhead Pub. xii, 308 p.

19. Li, H., *Smart hydrogel modeling*. 1st ed. 2009, Heidelberg ; New York: Springer. 359.

20. Cooper, S.L., A.S. Hoffman, T. Tsuruta, and C.H. Bamford, *Polymer biomaterials in solution, as interfaces and as solids : festschrift honoring the 60th birthday of Dr. Allan S. Hoffman*. 1995, Utrecht: VSP. 1134p.

21. Reid, D.S., *Water properties in food, health, pharmaceutical and biological systems : ISOPOW 10*. 2010, Ames, Iowa, USA: Wiley-Blackwell. 771 p.

22. Neogi, P., *Diffusion in polymers*. Plastics engineering ;. 1996, New York: Marcel Dekker. ix, 309 p.

23. Li-Chan, E., J.M. Chalmers, and P.R. Griffiths, *Applications of vibrational spectroscopy in food science*. 2010, Chichester: Wiley.

24. Silva, L.D., A. Ochsner, and R. Adams, *Handbook of adhesion technology*, ed. A.O. Lucas Da Silva, Robert Adams. 2011, New York: Springer.

25. Cronier, D., B. Monties, and B. Chabbert, *Structure and chemical composition of bast fibers isolated from developing hemp stem.* Journal of Agricultural and Food Chemistry, 2005. **53**(21): p. 8279-8289.

26. Mussig, J. and C. Stevens, *Industrial application of natural fibres : structure, properties, and technical applications*. Wiley series in renewable resources. 2010, Chichester: Wiley. xxi, 538 p.

27. Rowell, R.M., R.A. Young, and J.K. Rowell, *Paper and composites from agro-based resources*. 1997, Boca Raton: CRC/Lewis Publishers. 446 p.

28. Alvarez, V.A., R.A. Ruscekaite, and A. Vazquez, *Mechanical properties and water absorption behavior of composites made from a biodegradable matrix and alkaline-treated sisal fibers.* Journal of Composite Materials, 2003. **37**(Compendex): p. 1575-1588.

29. Wallenberger, P.F.T. and N.E. Weston, *Natural fibers, plastics and composites* 2003, NY, USA: Springer. 392.

30. Williams, P.A., ed. *Handbook of industrial water soluble polymers*. 2007, Blackwell Pub.: Ames, Iowa. 344

31. Giles, H.F., J.R. Wagner, and E.M. Mount, *Extrusion the definitive processing guide and handbook*. Second ed. PDL handbook series. 2005, Norwich, N.Y.: William Andrew Inc.

32. Vasile, C. and M. Pascu, *Practical guide to polyethylene*. 2005, Shrewsbury, UK: Rapra Technology Limited.

33. Aguado Villalba, J., D.P. Serrano, and Royal Society of Chemistry (Great Britain), *Feedstock recycling of plastic wastes*. RSC clean technology monographs. 1999, Cambridge: Royal Society of Chemistry. xi-192.

34. Fotouh, A., J. Wolodko, and M. Lipsett, *Isotherm moisture absorption kinetics in natural-fiber-reinforced polymer under immersion conditions.* Journal of Composite Materials, 2014.

35. Anandjiwala, R.D., *Textiles for sustainable development*. 2007, New York: Nova Science Publishers, Inc. x, 435 p.

36. Fotouh, A., J. Wolodko, and M. Lipsett, *Fatigue of natural fiber thermoplastic composites.* Composites Part B 2014.

37. Fotouh, A., J. Wolodko, and M. Lipsett, *Characterization and modeling of strain rate hardening in natural-fiber-reinforced viscoplastic polymer.* Polymer Composites 2014.

38. Fotouh, A. and J. Wolodko, *Fatigue Behavior of Natural Fiber Reinforced Thermoplastic Composites in Dry and Wet Environments*, in *International Mechanical Engineering Congress & Exposition (IMECE)*. 2011, ASME: Denver, Colorado, USA.

39. Facca, A.G., M.T. Kortschot, and N. Yan, *Predicting the elastic modulus of natural fibre reinforced thermoplastics.* Composites Part A: Applied Science and Manufacturing, 2006. **37**(10): p. 1660-1671.

40. Pickering, K.L., G.W. Beckermann, S.N. Alam, and N.J. Foreman, *Optimising industrial hemp fibre for composites.* Composites Part A (Applied Science and Manufacturing), 2007. **38**(2): p. 461-8.

41. Ganan, P. and I. Mondragon, *Effect of fiber treatments on mechanical behavior of short fique fiber-reinforced polyacetal composites.* Journal of Composite Materials, 2005. **39**(7): p. 633-646.

42. Ruihua, H. and M. Jae-Kyoo Ll, *Fabrication and mechanical properties of completely biodegradable hemp fiber reinforced polylactic acid composites.* Journal of Composite Materials, 2007. **41**(13): p. 123-137.

43. Gassan, J., *A study of fibre and interface parameters affecting the fatigue behaviour of natural fibre composites.* Composites - Part A: Applied Science and Manufacturing, 2002. **33**(3): p. 369-374.

44. Van de Weyenberg, I., J. Ivens, A. De Coster, B. Kino, E. Baetens, and I. Verpoest, *Influence of processing and chemical treatment of flax fibres on their composites.* Composites Science and Technology, 2003. **63**(9): p. 1241-1246.

45. Agrawal, R., N.S. Saxena, K.B. Sharma, S. Thomas, and M.S. Sreekala, *Activation energy and crystallization kinetics of untreaded and treated oil palm fibre reinforced phenol formaldehyde composites.* Materials Science and Engineering A, 2000. **277**(1-2): p. 77-82.

46. Valadez-Gonzalez, A., J.M. Cervantes-Uc, R. Olayo, and P.J. Herrera-Franco, *Effect of fiber surface treatment on the fiber-matrix bond strength of natural fiber reinforced composites.* Composites Part B: Engineering, 1999. **30**(3): p. 309-320.

47. Khalil, H.P.S.A., H.D. Rozman, M.N. Ahmad, and H. Ismail, *Acetylated plant-fiber-reinforced polyester composites: A study of mechanical, hygrothermal, and aging characteristics.* Polymer-Plastics Technology and Engineering, 2000. **39**(4): p. 757-781.

48. Manikandan Nair, K.C., S. Thomas, and G. Groeninckx, *Thermal and dynamic mechanical analysis of polystyrene composites reinforced with short sisal fibres.* Composites Science and Technology, 2001. **61**(16): p. 2519-2529.

49. Nystrom, B., R. Joffe, and R. Langstrom, *Microstructure and strength of injection molded natural fiber composites.* Journal of Reinforced Plastics and Composites, 2007. **26**(6): p. 579-599.

50. Fotouh, A., J. Wolodko, and Z. Xia, *Generalized monotonic modeling of natural fibre composites based on its normalized stress-strain tensile*

behaviour, in *AES-ATEMA' 2011International Conference*. 2011: Montreal, Canada.

51. Venkateshwaran, N., A.E. Perumal, and D. Arunsundaranayagam, *Fiber surface treatment and its effect on mechanical and visco-elastic behaviour of banana/epoxy composite.* Materials & Design, 2013. **47**: p. 151-159.

52. Madsen, B. and E.K. Gamstedt, *Wood versus Plant Fibers: Similarities and Differences in Composite Applications.* Advances in Materials Science and Engineering, 2013.

53. Gurdal, Z., R.T. Haftka, and P. Hajela, *Design and optimization of laminated composite materials*. 1999, New York ; Chichester: Wiley. xiv, 337 p.

54. Facca, A.G., M.T. Kortschot, and N. Yan, *Predicting the tensile strength of natural fibre reinforced thermoplastics.* Composites Science and Technology, 2007. **67**(11-12): p. 2454-2466.

55. Jones, R.M., *Mechanics of composite materials*. 2nd ed. 1999, Philadelphia, PA: Taylor & Francis. xvi, 519 p.

56. Kuriyama, T., M. Mizoguchi, and T. Ogawa, *Effect of injection speed on internal structure and mechanical properties in short glass fibre reinforced polyamide injection mouldings.* Polymers and Polymer Composites, 2004. **12**(5): p. 423-431.

57. Zhou, Y. and P.K. Mallick, *Fatigue performance of an injection-molded short E-glass fiber-reinforced polyamide 6,6. I. Effects of orientation, holes, and weld line.* Polymer Composites, 2006. **27**(2): p. 230-237.

58. Friedrich, K., A.K. Schlarb, and ScienceDirect (Online service), *Tribology of polymeric nanocomposites friction and wear of bulk materials and coatings*, in *Tribology and interface engineering series,*. 2008, Elsevier: Oxford. p. xvi, 551 p.

59. Harris, B., *Fatigue in composites : science and technology of the fatigue response of fibre-reinforced plastics*. 2003, Boca Raton Cambridge: CRC ;Woodhead. xxi, 742 p.

60. Huston, R.J., *Fatigue life prediction in composites.* International Journal of Pressure Vessels and Piping, 1994. **59**(1-3).

61. Lee, C.S. and W. Hwang, *Fatigue life prediction of matrix dominated polymer composite materials.* Polymer Composites, 2000. **21**(5): p. 798-805.

62. Mandell, J.F., F.J. McGarry, D.D. Huang, and C.G. Li, *Some effects of matrix and interface properties on the fatigue of short fiber-reinforced thermoplastics.* Polymer Composites, 1983. **4**(1): p. 32-39.

63. Mori, K.C., *Simulation of materials processing : theory, methods and applications : proceedings of the 7th International Conference on Numerical Methods in Industrial Forming Processes--NUMIFORM 2001, Toyohashi, Japan, 18-20 June 2001*. 2001, Lisse ; Exton (PA): A.A. Balkema. xxi, 1134 p.

64. Rappaz, M., M. Bellet, and M.O. Deville, *Numerical modeling in materials science and engineering*. Springer series in computational mathematics,. 2003, Berlin ; New York: Springer-Verlag. xi, 540 p.

65. Wyrzykowski, R., *Parallel processing and applied mathematics 6th international conference, PPAM 2005, Poznań, Poland, September 11-14, 2005 : revised selected papers*, in *Lecture notes in computer science,*. 2006, Springer: Berlin ; New York. p. xxiii, 1126 p.

66. Murty, K.L., D. Frear, and E.P. Simonen. *Characterization of Strain Rate Sensitivity of Sb-5%Sb Solder using ABI Testing*. in *Microstructures and Mechanical Properties of Aging Materials II*. 1995. Las Vegas: Minerals, Metals & Materials Society.

67. Toderas, M., *From Rheology to Plasticity and Viscoplasticity*, in *Annual of the University Of Mining and Geology "ST. Ivan Rilski", Mining and Mineral processing*. 2007: Sofia, Bulgaria.

68. Bathias, C., *An engineering point of view about fatigue of polymer matrix composite materials.* International Journal of Fatigue, 2006. **28**(10): p. 1094-9.

69. Nisitani, H., H. Noguchi, and Y.H. Kim, *Evaluation of fatigue strength of plain and notched specimens of short carbon-fiber reinforced polyetheretherketone in comparison with polyetheretherketone.* Engineering Fracture Mechanics, 1992. **43**(5): p. 685-705.

70. Matthews, F.L., *Finite element modelling of composite materials and structures*. 2000, Boca Raton, FL: CRC Press. x, 214 p.

71. Noda, K., A. Takahara, and T. Kajiyama, *Fatigue failure mechanisms of short glass-fiber reinforced nylon 66 based on nonlinear dynamic viscoelastic measurement.* Polymer, 2001. **42**(13): p. 5803-5811.

72. ASM International., *Characterization and failure analysis of plastics*. 2003, Materials Park, OH: ASM International. vi, 482 p.

73. Natarajan, V., H.V.S. GangaRao, and V. Shekar, *Fatigue response of fabric-reinforced polymeric composites.* Journal of Composite Materials, 2005. **39**(17): p. 1541-1559.

74. Varvani-Farahani, A., H. Haftchenari, and M. Panbechi, *An energy-based fatigue damage parameter for off-axis unidirectional FRP composites.* Composite Structures, 2007. **79**(3): p. 381-389.

75. Zhang, G. and R.A. Latorur, *FRP composite compressive strength and its dependence upon interfacial bond strength, fiber misalignment, and matrix nonlinearity.* Journal of Thermoplastic Composite Materials, 1993. **6**(4): p. 298-311.

76. Belaadi, A., A. Bezazi, M. Bourchak, and F. Scarpa, *Tensile static and fatigue behaviour of sisal fibres.* Materials & Design, 2013. **46**: p. 76-83.

77. Kawai, M., *A phenomenological model for off-axis fatigue behavior of unidirectional polymer matrix composites under different stress ratios.* Composites Part A (Applied Science and Manufacturing), 2004. **35A**(7-8): p. 955-63.

78. *ASM Handbook Volume 19: Fatigue and Fracture*, in *ASM Handbook*, S.R. Lampman, Editor. 1997, ASM International.

79. American Society for Testing Materials., *Manual on low cycle fatigue testing*. 1969, Philadelphia. ix, 193 p.

80. Collins, J.A., *Failure of materials in mechanical design : analysis, prediction, prevention*. 1981, New York: Wiley. xv, 629 p.

81. Zago, A., G.S. Springer, and M. Quaresimin, *Cumulative damage of short glass fiber reinforced thermoplastics.* Journal of Reinforced Plastics and Composites, 2001. **20**(7): p. 596-605.

82. Hodgkinson, J.M., ed. *Mechanical testing of advanced fibre composites*. 2000, Woodhead Publishing: Boca Raton, FL, Cambridge, England. 362.

83. Jessen, S.M. and A. Plumtree, *Continuum damage mechanics applied to cyclic behaviour of a glass fibre composite pultrusion.* Composites, 1991. **22**(3): p. 181-190.

84. Wang, Y.H., Z.D. Wang, and X.X. Zhao. *Prediction of the fatigue life based on stiffness degradation concept*. 2008. Urumqi, China: Trans Tech Publications.

85. Hwang, W. and K.S. Han, *Interlaminar fracture behavior and fiber bridging of glass-epoxy composite under Mode I static and cyclic loadings.* Journal of Composite Materials, 1989. **23**(4): p. 396-430.

86. Hwang, W., C.S. Lee, H.C. Park, and K.S. Han, *Single- and multi-stress level fatigue life prediction of glass/epoxy composites.* Journal of Advanced Materials, 1995. **26**(4): p. 3-9.

87. Zhang, Y., A.P. Vassilopoulos, and T. Keller, *Stiffness degradation and fatigue life prediction of adhesively-bonded joints for fiber-reinforced polymer composites.* International Journal of Fatigue, 2008. **30**(10-11): p. 1813-1820.

88. Degrieck, J. and W.V. Paepegem, *Fatigue damage modeling of fibre-reinforced composite materials: Review.* Appl. Mech. Rev, 2001. **Volume 54**(Issue 4).

89. Yang, J.N., L.J. Lee, and D.Y. Sheu, *Modulus reduction and fatigue damage of matrix dominated composite laminates.* Composite Structures, 1992. **21**(2): p. 91-100.

90. Lemaitre, J. and A. Plumtree, *Application of damage concepts to predict creep-fatigue failures.* American Society of Mechanical Engineers (Paper), 1978(78-PVP-26): p. 10.

91. Nicholas, T., *High cycle fatigue a mechanics of materials perspective*. 2006, Elsevier: Oxford. p. xiv, 641 p.

92. Sadowski, T., *Lecture notes on composite materials*. 2008, New York, NY: Springer Dordrecht.

93. Xia, Z., D. Kujawski, and F. Ellyin, *Effect of mean stress and ratcheting strain on fatigue life of steel.* International Journal of Fatigue, 1996. **18**(5): p. 335-341.

94. Tchankov, D.S. and K.V. Vesselinov, *Fatigue life prediction under random loading using total hysteresis energy.* International Journal of Pressure Vessels and Piping, 1998. **75**(13): p. 955-60.

95. Seber, G.F. and C.J. Wild, *Nonlinear regression*. 1989, New York: Wiley. xx, 768.

CHAPTER 3 REFERENCES

1. Westman, M.P., S.G. Laddha, L.S. Fifield, T.A. Kafentzis, and K.L. Simmons, *Natural fiber composites: A review*. 2010, Pacific Northwest National Laboratory Richland, Washington.

2. Gtridhar, J. and R. Rao, *Moisture absorption characteristics of natural fibre composites.* Journal of Reinforced Plastics and Composites, 1986. **5**(2): p. 141-150.

3. Panthapulakkal, S. and M. Sain, *Studies on the water absorption properties of short hemp-glass fiber hybrid polypropylene composites.* Journal of Composite Materials, 2007. **41**(15): p. 1871-1883.

4. Bharath, K.N. and A.M. Rajesh, *Moisture absorption characteristics of Areca/Maize reinforced hybrid polymer composites.* International Journal of Advanced Engineering & Application, 2010. **1**: p. 207-211.

5. Dhakal, H., Z. Zhang, and M. Richardson, *Effect of water absorption on the mechanical properties of hemp fibre reinforced unsaturated polyester composites.* Composites Science and Technology, 2006. **67**(7-8).

6. Saheb, D. and J.P. Jog, *Natural fiber polymer composites: A review.* Advances in Polymer Technology, 1999. **18**(Compendex): p. 351-363.

7. Li, X., L. Tabil, and S. Panigrahi, *Chemical treatments of natural fiber for use in natural fiber-reinforced composites: A review.* Journal of Polymers and the Environment, 2007. **15**(1): p. 25-33.

8. Bledzki, K. and J. Gassan, *Composites reinforced with cellulose based fibres.* Progress in Polymer Science (Oxford), 1999. **24**(Compendex): p. 221-274.

9. Baillie, C., *Green composites : polymer composites and the environment*. 2004, Boca Raton,Cambridge, England: CRC Press ; Woodhead Pub. xii, 308 p.

10. Fotouh, A., J.D. Wolodko, and M.G. Lipsett, *A Review of Aspects Affecting Performance and Modeling of Short-Natural-Fiber-Reinforced Polymers under Monotonic and Cyclic Loading Conditions*. Accepted in Press, Journal of Polymer Composites, 14 - Febraury, 2014.

11. Rowell, R.M., R.A. Young, and J.K. Rowell, *Paper and composites from agro-based resources*. 1997, Boca Raton: CRC/Lewis Publishers. 446 p.

12. Alvarez, V.A., R.A. Ruscekaite, and A. Vazquez, *Mechanical properties and water absorption behavior of composites made from a biodegradable matrix and alkaline-treated sisal fibers.* Journal of Composite Materials, 2003. **37**(Compendex): p. 1575-1588.

13. Wallenberger, P.F.T. and N.E. Weston, *Natural fibers, plastics and composites* 2003, NY, USA: Springer. 392.

14. Williams, P.A., ed. *Handbook of industrial water soluble polymers*. 2007, Blackwell Pub.: Ames, Iowa. 344

15. Anandjiwala, R.D., *Textiles for sustainable development*. 2007, New York: Nova Science Publishers, Inc. x, 435 p.

16. Giles, H.F., J.R. Wagner, and E.M. Mount, *Extrusion the definitive processing guide and handbook*. Second ed. PDL handbook series. 2005, Norwich, N.Y.: William Andrew Inc.

17. Aguado Villalba, J., D.P. Serrano, and Royal Society of Chemistry (Great Britain), *Feedstock recycling of plastic wastes*. RSC clean technology monographs. 1999, Cambridge: Royal Society of Chemistry. xi-192.

18. Friedrich, K., *Mesoscopic aspects of polymer composites: processing, structure and properties.* Journal of Materials Science, 1998. **33**(23): p. 5535-56.

19. Wolodko, J., J. Vidmar, J. Slaski, W. Chute, L. Mcliveen, and M. Hopkins, *Polymer Biocomposites from Alberta Feedstock – Hemp Reinforced Polyethylene*. 2008, Alberta Research Council: Edmonton, Canada.

20. Holbery, J. and D. Houston, *Natural-fiber-reinforced polymer composites in automotive applications*. JOM, 2006. **58**(11): p. 80-6.

21. Cronier, D., B. Monties, and B. Chabbert, *Structure and chemical composition of bast fibers isolated from developing hemp stem*. Journal of Agricultural and Food Chemistry, 2005. **53**(21): p. 8279-8289.

22. Mussig, J. and C. Stevens, *Industrial application of natural fibres : structure, properties, and technical applications*. Wiley series in renewable resources. 2010, Chichester: Wiley. xxi, 538 p.

23. Troung, M., *Establishment of Protocol for Natural Fibre Density Measurements*. 2007, University of Manitoba, and Composites Innovation Center Manitoba Inc. (CIC), and Department of Agriculture and Agri-Food Canada: Manitoba, Canada.

24. Pickering, K.L., G.W. Beckermann, S.N. Alam, and N.J. Foreman, *Optimising industrial hemp fibre for composites*. Composites Part A (Applied Science and Manufacturing), 2007. **38**(2): p. 461-8.

25. Facca, A.G., M.T. Kortschot, and N. Yan, *Predicting the elastic modulus of natural fibre reinforced thermoplastics*. Composites Part A: Applied Science and Manufacturing, 2006. **37**(10): p. 1660-1671.

26. Vasile, C. and M. Pascu, *Practical guide to polyethylene*. 2005, Shrewsbury, UK: Rapra Technology Limited.

27. Ho, T.N. and A.D. Ngo, *Sorption of Water in Hemp and Coir Fibers*, in *8th International Conference on Woodfiber-Plastic Composites* 2005: Wisconsin, USA

28. Craver, C.D. and C.E. Carraher, *Applied polymer science : 21st century*. 2000, Amsterdam ; London: Elsevier. xiv, 1072 p.

29. Srivastava, A.K. and P.C. Gope, *Strength Of Materials*. 2007, New Delhi: Prentice-Hall of India.

30. Huston, R.L. and H. Josephs, *Practical Stress Analysis in Engineering Design*. Third ed. 2009, NY, USA: CRC PressINC.

31. Leandro José da Silva, T.H.P., André Luis Christoforo, Luís Miguel Pereira Durão, Francisco Antonio Rocco Lahr, *Numerical and*

experimental analyses of biocomposites reinforced with natural fibres. International Journal of Materials Engineering 2012. **2**(4): p. 7.

32. Scheirs, J., *A Guide to Polymeric Geomembranes: A Practical Approach*. 2009, Chichester, West Sussex, U.K.: Wiley.

33. Ashby, M.F., *Materials and the Environment: Eco-Informed Material Choice*. 2012: Elsevier Limited, Oxford.

34. Throne, J.L., *Technology of Thermoforming*. 1996, Munich, Germany: Carl Hanser Verlag.

35. Carraher, C.E., Jr. and R.B. Seymour, *Seymour/Carraher's polymer chemistry*. 7th edition / Charles E. Carraher, Jr. ed. 2008, Boca Raton, Fla.: CRC ; London : Taylor & Francis [distributor].

36. Cunha, A.M. and S. Fakirov, eds. *Structure Development During Polymer Processing*. Series E: Applied Science. Vol. 370. 2000, Springer: Dordrecht, Netherland.

37. Dissado, L.A. and J.C. Fothergill, *Electrical degradation and breakdown in polymers*. IEE materials and devices series. 1992, London: P. Peregrinus. xix, 601 p.

38. Long, A.C., *Design and manufacture of textile composites*. 2005, Cambridge: Woodhead.

39. Michler, G.H. and F.J.B. Calleja, *Mechanical Properties Of Polymers Based On Nanostructure And Morphology*. 2005, Weinheim, Germany: Taylor & Francis Group.

40. Galeski, A., E. Piorkowska, L. Koenczoel, and E. Baer, *Acoustic emission during crystallization of polymers.* Journal of Polymer Science, Part B: Polymer Physics, 1990. **28**(7): p. 1171-1186.

41. Pawlak, A. and E. Piorkowska, *Effect of negative pressure on melting behavior of spherulites in thin films of several crystalline polymers.* Journal of Applied Polymer Science, 1999. **74**(6): p. 1380-1385.

42. Nowacki, R., J. Kolasinska, and E. Piorkowska, *Cavitation during isothermal crystallization of isotactic polypropylene.* Journal of Applied Polymer Science, 2001. **79**(13): p. 2439-2448.

43. Ezrin, M., *Plastics Failure Guide: Cause and Prevention*. 1996, Munich, Germany: Hanser Pub.

44. Utracki, L.A. and A.M. Jamieson, *Polymer Physics: From Suspensions to Nanocomposites and Beyond*. 2011, Hoboken, New Jersey: Wiley.

45. Friedrich, K., S. Fakirov, and Z. Zhang, *Polymer Composites: From Nano- to Macro-Scale*. 2005, NY, USA: Springer.

46. Wood, J.R. and M.G. Bader, *Void control for polymer-matrix composites (2): experimental evaluation of a diffusion model for the growth and collapse of gas bubbles.* Composites manufacturing, 1994. **5**(3): p. 149-158.

47. Bagheri, R. and R.A. Pearson, *The use of microvoids to toughen polymers.* Polymer, 1995. **36**(25): p. 4883-5.

48. Espert, A., F. Vilaplana, and S. Karlsson, *Comparison of water absorption in natural cellulosic fibres from wood and one-year crops in polypropylene composites and its influence on their mechanical properties.* Composites Part A: Applied Science and Manufacturing, 2004. **35**(Compendex): p. 1267-1276.

49. Crank, J., *The mathematics of diffusion*. 2d ed. 1975, Oxford, [Eng]: Clarendon Press. viii, 414 p.

50. Comyn, J., *Polymer permeability*. 1985, London: Elsevier Applied Science. vii, 383 p.

51. Cooper, S.L., A.S. Hoffman, T. Tsuruta, and C.H. Bamford, *Polymer biomaterials in solution, as interfaces and as solids : festschrift honoring the 60th birthday of Dr. Allan S. Hoffman*. 1995, Utrecht: VSP. 1134p.

52. Li, H., *Smart hydrogel modeling*. 1st ed. 2009, Heidelberg ; New York: Springer. 359.

53. Neogi, P., *Diffusion in polymers*. Plastics engineering ;. 1996, New York: Marcel Dekker. ix, 309 p.

54. Liu, C.P.A. and P. Neogi, *Sorption of methylene chloride in semicrystalline polyethylene terephthalate.* Journal of Macromolecular Science - Physics, 1992. **B31**(Compendex): p. 265-279.

55. Reid, D.S., *Water properties in food, health, pharmaceutical and biological systems : ISOPOW 10*. 2010, Ames, Iowa, USA: Wiley-Blackwell. 771 p.

56. Hodgkinson, J.M., ed. *Mechanical testing of advanced fibre composites*. 2000, Woodhead Publishing: Boca Raton, FL, Cambridge, England. 362.

57. Dhoot, G. and M.S. University, *Estimation of Eugenol Diffusion Coefficient in LLDPE Using FTIR-ATR Flow Cell and HPLC Techniques*. 2008: Michigan State University.

58. Li-Chan, E., J.M. Chalmers, and P.R. Griffiths, *Applications of vibrational spectroscopy in food science*. 2010, Chichester: Wiley.

59. Silva, L.D., A. Ochsner, and R. Adams, *Handbook of adhesion technology*, ed. A.O. Lucas Da Silva, Robert Adams. 2011, New York: Springer.

60. Steel, R.G.D. and J.H. Torrie, *Principles and procedures of statistics, with special reference to the biological sciences*. 1960, New York,: McGraw-Hill. xvi, 481 p. illus.

CHAPTER 4 REFERENCES

1. Holbery, J. and D. Houston, *Natural-fiber-reinforced polymer composites in automotive applications.* JOM, 2006. **58**(11): p. 80-6.

2. Panthapulakkal, S. and M. Sain, *Studies on the water absorption properties of short hemp-glass fiber hybrid polypropylene composites.* Journal of Composite Materials, 2007. **41**(15): p. 1871-1883.

3. ASM-International., *ASM Handbook Volume 21:Composites*, in *ASM Handbook*, S.L.D. D.B. Miracle, Editor. 2001, ASM International: USA.

4. Drzal, L.T., M. Misra, and A.K. Mohanty, *Natural fibers, biopolymers, and biocomposites*. 2005, Boca Raton, FL: Taylor & Francis. 875 p.

5. Hargitai, H., I. Racz, and R. Anandjiwala, *Development of hemp fibre - PP nonwoven composites.* Macromolecular Symposia, 2006. **239**: p. 201-208.

6. Mandell, J.F., F.J. McGarry, D.D. Huang, and C.G. Li, *Some effects of matrix and interface properties on the fatigue of short fiber-reinforced thermoplastics.* Polymer Composites, 1983. **4**(1): p. 32-39.

7. Fotouh, A. and J. Wolodko, *Fatigue Behavior of Natural Fiber Reinforced Thermoplastic Composites in Dry and Wet Environments*, in *International Mechanical Engineering Congress & Exposition (IMECE)*. 2011, ASME: Denver, Colorado, USA.

8. Fotouh, A., J. Wolodko, and Z. Xia, *Generalized monotonic modeling of natural fibre composites based on its normalized stress-strain tensile behaviour*, in *AES-ATEMA' 2011International Conference*. 2011: Montreal, Canada.

9. Emmens, W.C., *Formability A Review of Parameters and Processes that Control, Limit or Enhance the Formability of Sheet Metal*, in *SpringerBriefs in Applied Sciences and Technology Ser.* 2011, Springer: New York. p. ix, 112 p.

10. Westman, M.P., S.G. Laddha, L.S. Fifield, T.A. Kafentzis, and K.L. Simmons, *Natural fiber composites: A review*. 2010, Pacific Northwest National Laboratory Richland, Washington.

11. Gtridhar, J. and R. Rao, *Moisture absorption characteristics of natural fibre composites.* Journal of Reinforced Plastics and Composites, 1986. **5**(2): p. 141-150.

12. Bharath, K.N. and A.M. Rajesh, *Moisture absorption characteristics of Areca/Maize reinforced hybrid polymer composites.* International Journal of Advanced Engineering & Application, 2010. **1**: p. 207-211.

13. Dhakal, H., Z. Zhang, and M. Richardson, *Effect of water absorption on the mechanical properties of hemp fibre reinforced unsaturated polyester composites.* Composites Science and Technology, 2006. **67**(7-8).

14. Mori, K.C., *Simulation of materials processing : theory, methods and applications : proceedings of the 7th International Conference on Numerical Methods in Industrial Forming Processes--NUMIFORM 2001, Toyohashi, Japan, 18-20 June 2001*. 2001, Lisse ; Exton (PA): A.A. Balkema. xxi, 1134 p.

15. Rappaz, M., M. Bellet, and M.O. Deville, *Numerical modeling in materials science and engineering*. Springer series in computational mathematics,. 2003, Berlin ; New York: Springer-Verlag. xi, 540 p.

16. Wyrzykowski, R., *Parallel processing and applied mathematics 6th international conference, PPAM 2005, Poznań, Poland, September 11-14, 2005 : revised selected papers*, in *Lecture notes in computer science,*. 2006, Springer: Berlin ; New York. p. xxiii, 1126 p.

17. Murty, K.L., D. Frear, and E.P. Simonen. *Characterization of Strain Rate Sensitivity of Sb-5%Sb Solder using ABI Testing*. in *Microstructures and Mechanical Properties of Aging Materials II*. 1995. Las Vegas: Minerals, Metals & Materials Society.

18. Toderas, M., *From Rheology to Plasticity and Viscoplasticity*, in *Annual of the University Of Mining and Geology "ST. Ivan Rilski", Mining and Mineral processing*. 2007: Sofia, Bulgaria.

19. Ferhoum, R., M. Aberkane, M. Ould Ouali, and K. Hachour. *The thermal ageing effect on viscoplastic behaviour of high density polyethylene (HDPE)*. in *ASME 2012 11th Biennial Conference on Engineering Systems Design and Analysis, ESDA 2012, July 2, 2012 - July 4, 2012*. 2012. Nantes, France: American Society of Mechanical Engineers.

20. Akbar, A., G.R. Pasha, and M. Aslam, *Yield Density Rapports: A Nonparametric Regression Approach* International Research Journal of Finance and Economics, 2010(43): p. 183-187.

21. Seber, G.F. and C.J. Wild, *Nonlinear regression*. 1989, New York: Wiley. xx, 768.

CHAPTER 5 REFERENCES

1. Holbery, J. and D. Houston, *Natural-fiber-reinforced polymer composites in automotive applications.* JOM, 2006. **58**(11): p. 80-6.

2. Drzal, L.T., M. Misra, and A.K. Mohanty, *Natural fibers, biopolymers, and biocomposites*. 2005, Boca Raton, FL: Taylor & Francis. 875 p.

3. Hargitai, H., I. Racz, and R. Anandjiwala, *Development of hemp fibre - PP nonwoven composites.* Macromolecular Symposia, 2006. **239**: p. 201-208.

4. ASM-International., *ASM Handbook Volume 21:Composites*, in *ASM Handbook*, S.L.D. D.B. Miracle, Editor. 2001, ASM International: USA.

5. Panthapulakkal, S. and M. Sain, *Studies on the water absorption properties of short hemp-glass fiber hybrid polypropylene composites.* Journal of Composite Materials, 2007. **41**(15): p. 1871-1883.

6. Westman, M.P., S.G. Laddha, L.S. Fifield, T.A. Kafentzis, and K.L. Simmons, *Natural fiber composites: A review*. 2010, Pacific Northwest National Laboratory Richland, Washington.

7. Gtridhar, J. and R. Rao, *Moisture absorption characteristics of natural fibre composites.* Journal of Reinforced Plastics and Composites, 1986. **5**(2): p. 141-150.

8. Bharath, K.N. and A.M. Rajesh, *Moisture absorption characteristics of Areca/Maize reinforced hybrid polymer composites.* International Journal of Advanced Engineering & Application, 2010. **1**: p. 207-211.

9. Dhakal, H., Z. Zhang, and M. Richardson, *Effect of water absorption on the mechanical properties of hemp fibre reinforced unsaturated polyester composites.* Composites Science and Technology, 2006. **67**(7-8).

10. Saheb, D. and J.P. Jog, *Natural fiber polymer composites: A review.* Advances in Polymer Technology, 1999. **18**(Compendex): p. 351-363.

11. Li, X., L. Tabil, and S. Panigrahi, *Chemical treatments of natural fiber for use in natural fiber-reinforced composites: A review.* Journal of Polymers and the Environment, 2007. **15**(1): p. 25-33.

12. Bledzki, K. and J. Gassan, *Composites reinforced with cellulose based fibres.* Progress in Polymer Science (Oxford), 1999. **24**(Compendex): p. 221-274.

13. Baillie, C., *Green composites : polymer composites and the environment*. 2004, Boca Raton,Cambridge, England: CRC Press ; Woodhead Pub. xii, 308 p.

14. Fotouh, A., J.D. Wolodko, and M.G. Lipsett, *Characterization and Modeling of Strain rate Hardening in Natural-Fiber-Reinforced Polymer.* Accepted, Polymer Composites, 2014.

15. Emmens, W.C., *Formability A Review of Parameters and Processes that Control, Limit or Enhance the Formability of Sheet Metal*, in *SpringerBriefs in Applied Sciences and Technology Ser.* 2011, Springer: New York. p. ix, 112 p.

16. Seber, G.F. and C.J. Wild, *Nonlinear regression*. 1989, New York: Wiley. xx, 768.

17. Akbar, A., G.R. Pasha, and M. Aslam, *Yield Density Rapports: A Nonparametric Regression Approach* International Research Journal of Finance and Economics, 2010(43): p. 183-187.

18. Fotouh, A., J. Wolodko, and Z. Xia, *Generalized monotonic modeling of natural fibre composites based on its normalized stress-strain tensile behaviour*, in *AES-ATEMA' 2011International Conference*. 2011: Montreal, Canada.

19. Fotouh, A. and J. Wolodko, *Fatigue Behavior of Natural Fiber Reinforced Thermoplastic Composites in Dry and Wet Environments*, in *International Mechanical Engineering Congress & Exposition (IMECE)*. 2011, ASME: Denver, Colorado, USA.

20. Ferhoum, R., M. Aberkane, M. Ould Ouali, and K. Hachour. *The thermal ageing effect on viscoplastic behaviour of high density polyethylene (HDPE)*. in *ASME 2012 11th Biennial Conference on Engineering Systems Design and Analysis, ESDA 2012, July 2, 2012 - July 4, 2012*. 2012. Nantes, France: American Society of Mechanical Engineers.

21. Mori, K.C., *Simulation of materials processing : theory, methods and applications : proceedings of the 7th International Conference on Numerical Methods in Industrial Forming Processes--NUMIFORM 2001, Toyohashi, Japan, 18-20 June 2001*. 2001, Lisse ; Exton (PA): A.A. Balkema. xxi, 1134 p.

22. Rappaz, M., M. Bellet, and M.O. Deville, *Numerical modeling in materials science and engineering*. Springer series in computational mathematics,. 2003, Berlin ; New York: Springer-Verlag. xi, 540 p.

23. Wyrzykowski, R., *Parallel processing and applied mathematics 6th international conference, PPAM 2005, Poznań, Poland, September 11-14, 2005 : revised selected papers*, in *Lecture notes in computer science,*. 2006, Springer: Berlin ; New York. p. xxiii, 1126 p.

24. Murty, K.L., D. Frear, and E.P. Simonen. *Characterization of Strain Rate Sensitivity of Sb-5%Sb Solder using ABI Testing*. in *Microstructures and Mechanical Properties of Aging Materials II*. 1995. Las Vegas: Minerals, Metals & Materials Society.

25. Toderas, M., *From Rheology to Plasticity and Viscoplasticity*, in *Annual of the University Of Mining and Geology "ST. Ivan Rilski", Mining and Mineral processing*. 2007: Sofia, Bulgaria.

26. Fotouh, A., J. Wolodko, and M. Lipsett, *Fatigue of natural fiber thermoplastic composites.* Composites Part B 2014.

CHAPTER 6 REFERENCES

1. ASM-International., *ASM Handbook Volume 21:Composites*, in *ASM Handbook*, S.L.D. D.B. Miracle, Editor. 2001, ASM International: USA.

2. Drzal, L.T., M. Misra, and A.K. Mohanty, *Natural fibers, biopolymers, and biocomposites*. 2005, Boca Raton, FL: Taylor & Francis. 875 p.

3. Hargitai, H., I. Racz, and R. Anandjiwala, *Development of hemp fibre - PP nonwoven composites.* Macromolecular Symposia, 2006. **239**: p. 201-208.

4. Holbery, J. and D. Houston, *Natural-fiber-reinforced polymer composites in automotive applications.* JOM, 2006. **58**(11): p. 80-6.

5. Matthews, F.L., *Finite element modelling of composite materials and structures*. 2000, Boca Raton, FL: CRC Press. x, 214 p.

6. Noda, K., A. Takahara, and T. Kajiyama, *Fatigue failure mechanisms of short glass-fiber reinforced nylon 66 based on nonlinear dynamic viscoelastic measurement.* Polymer, 2001. **42**(13): p. 5803-5811.

7. Natarajan, V., H.V.S. GangaRao, and V. Shekar, *Fatigue response of fabric-reinforced polymeric composites.* Journal of Composite Materials, 2005. **39**(17): p. 1541-1559.

8. Varvani-Farahani, A., H. Haftchenari, and M. Panbechi, *An energy-based fatigue damage parameter for off-axis unidirectional FRP composites.* Composite Structures, 2007. **79**(3): p. 381-389.

9. Talreja, R., *Fatigue of composite materials: damage mechanisms and fatigue-life diagrams.* Proceedings of The Royal Society of London, Series A: Mathematical and Physical Sciences, 1981. **378**(1775): p. 461-475.

10. Nyman, T., *Composite fatigue design methodology: a simplified approach.* Composite Structures, 1996. **35**(2): p. 183-194.

11. Harris, B., *Fatigue in composites : science and technology of the fatigue response of fibre-reinforced plastics*. 2003, Boca Raton Cambridge: CRC ;Woodhead. xxi, 742 p.

12. Bathias, C., *An engineering point of view about fatigue of polymer matrix composite materials.* International Journal of Fatigue, 2006. **28**(10): p. 1094-9.

13. Nisitani, H., H. Noguchi, and Y.H. Kim, *Evaluation of fatigue strength of plain and notched specimens of short carbon-fiber reinforced polyetheretherketone in comparison with polyetheretherketone.* Engineering Fracture Mechanics, 1992. **43**(5): p. 685-705.

14. Madsen, B. and E.K. Gamstedt, *Wood versus Plant Fibers: Similarities and Differences in Composite Applications.* Advances in Materials Science and Engineering, 2013.

15. Panthapulakkal, S. and M. Sain, *Studies on the water absorption properties of short hemp-glass fiber hybrid polypropylene composites.* Journal of Composite Materials, 2007. **41**(15): p. 1871-1883.

16. Dhakal, H., Z. Zhang, and M. Richardson, *Effect of water absorption on the mechanical properties of hemp fibre reinforced unsaturated polyester composites.* Composites Science and Technology, 2006. **67**(7-8).

17. Westman, M.P., et al., *Natural fiber composites: A review*. 2010, Pacific Northwest National Laboratory Richland, Washington.

18. Mandell, J.F., et al., *Some effects of matrix and interface properties on the fatigue of short fiber-reinforced thermoplastics.* Polymer Composites, 1983. **4**(1): p. 32-39.

19. Lavengood, R.E. and L.B. Gulbransen, *Effect of aspect ratio on the fatigue life of short boron fiber reinforced composites.* Polymer Engineering and Science, 1969. **9**(5): p. 365-369.

20. Harris, B., et al., *Fatigue behaviour of carbon fibre reinforced plastics.* Composites, 1990. **21**(3): p. 232-242.

21. Robertson, N., et al., *Mechanical performance and moisture absorption of various natural fiber reinforced thermoplastic composites.* Journal of Applied Polymer Science, 2013. **130**(2): p. 969-980.

22. Xu, Y., et al., *Natural fiber reinforced poly(vinyl chloride) composites: Effect of fiber type and impact modifier.* Journal of Polymers and the Environment, 2008. **16**(4): p. 250-257.

23. Yao, F., et al., *Rice straw fiber-reinforced high-density polyethylene composite: Effect of fiber type and loading.* Industrial Crops and Products, 2008. **28**(1): p. 63-72.

24. Mohanty, A.K., M. Misra, and L.T. Drzal, *Surface modifications of natural fibers and performance of the resulting biocomposites: An overview.* Composite Interfaces, 2001. **8**(5): p. 313-343.

25. Faruk, O., et al., *Biocomposites reinforced with natural fibers: 2000-2010.* Progress in Polymer Science, 2012. **37**(11): p. 1552-1596.

26. Towo, A.N. and M.P. Ansell, *Fatigue of sisal fibre reinforced composites: Constant-life diagrams and hysteresis loop capture.* Composites Science and Technology, 2008. **68**(3-4): p. 915-924.

27. Belaadi, A., et al., *Tensile static and fatigue behaviour of sisal fibres.* Materials & Design, 2013. **46**: p. 76-83.

28. Mori, K.C., *Simulation of materials processing : theory, methods and applications : proceedings of the 7th International Conference on Numerical Methods in Industrial Forming Processes--NUMIFORM 2001, Toyohashi, Japan, 18-20 June 2001*. 2001, Lisse ; Exton (PA): A.A. Balkema. xxi, 1134 p.

29. Rappaz, M., M. Bellet, and M.O. Deville, *Numerical modeling in materials science and engineering*. Springer series in computational mathematics,. 2003, Berlin ; New York: Springer-Verlag. xi, 540 p.

30. Toderas, M., *From Rheology to Plasticity and Viscoplasticity*, in *Annual of the University Of Mining and Geology "ST. Ivan Rilski", Mining and Mineral processing*. 2007: Sofia, Bulgaria.

31. Fotouh, A., J. Wolodko, and Z. Xia, *Generalized monotonic modeling of natural fibre composites based on its normalized stress-strain tensile behaviour*, in *AES-ATEMA' 2011International Conference*. 2011: Montreal, Canada.

32. Fotouh, A. and J. Wolodko, *Fatigue Behavior of Natural Fiber Reinforced Thermoplastic Composites in Dry and Wet Environments*, in *International*

Mechanical Engineering Congress & Exposition (IMECE). 2011, ASME: Denver, Colorado, USA.

33. Seber, G.F. and C.J. Wild, *Nonlinear regression*. 1989, New York: Wiley. xx, 768.

34. Akbar, A., G.R. Pasha, and M. Aslam, *Yield Density Rapports: A Nonparametric Regression Approach* International Research Journal of Finance and Economics, 2010(43): p. 183-187.

35. Lee, C.S. and W. Hwang, *Fatigue life prediction of matrix dominated polymer composite materials.* Polymer Composites, 2000. **21**(5): p. 798-805.

36. Yang, J.N., L.J. Lee, and D.Y. Sheu, *Modulus reduction and fatigue damage of matrix dominated composite laminates.* Composite Structures, 1992. **21**(2): p. 91-100.

37. Kawai, M., *A phenomenological model for off-axis fatigue behavior of unidirectional polymer matrix composites under different stress ratios.* Composites Part A (Applied Science and Manufacturing), 2004. **35A**(7-8): p. 955-63.